2017

Healing Mechanism Investigation of Self-Healing Concrete by Microencapsulated Calcium Nitrate

Gabriel Andres Arce Amador
Louisiana State University and Agricultural and Mechanical College

HEALING MECHANISM INVESTIGATION OF SELF-HEALING CONCRETE BY MICROENCAPSULATED CALCIUM NITRATE

A Dissertation

Submitted to the Graduate Faculty of the
Louisiana State University and
Agricultural and Mechanical College
in partial fulfillment of the
requirements for the degree of
Doctorate of Philosophy

in

The Interdepartmental Program in Engineering Science

by
Gabriel A. Arce
B.S., University of New Orleans, December 2013
M.S., Louisiana State University, May 2016
May 2017

ACKNOWLEDGEMENTS

The author would like to specially thank his major professor, Dr. Marwa Hassan, for her support, invaluable mentoring, and outstanding guidance throughout all phases of this project. Furthermore, the author would also like to acknowledge the time and recommendations provided by supervisory committee members Dr. Charles Berryman, Dr. Sherif Ishak, Dr. Isabelina Nahmens and the Dean's representative Dr. Mark Wilde. The author's gratitude is also expressed to the Department of Construction Management, the Socolofsky Microscopy Center, and the Louisiana Transportation Research Center (LTRC) with special thanks to Dr. Tyson Rupnow.

A special thank is also given to colleagues and friends, including but not limited to Jose Milla, Max Aguirre, Luis Bonilla, and Dr. Clayton Loehn which counseled and supported the author throughout this project. Last and most importantly, the author would like to thank his family for teaching him the value of hard work and providing him with unconditional love and support.

TABLE OF CONTENTS

ABSTRACT

Durability of reinforced concrete structures depends highly on the integrity of the concrete which protects the structure from the environment. However, concrete is a brittle material and as such it is prone to cracking which allows for detrimental agents to penetrate the structure and produce early deterioration. Embedding microcapsules with chemical healing agents in concrete materials for self-healing applications as well as implementing SMAs as reinforcement of concrete structures for self-closing of cracks are both state-of-the-art techniques with enormous potential for enhancement of concrete infrastructure durability. In this work, both techniques are combined as an alternative for superior self-healing of cracks in concrete materials to prevent early deterioration of structures.

The objective of this study was to evaluate the mechanism and effectiveness of microcapsules with encapsulated calcium nitrate on self-healing of unreinforced and reinforced (Steel and SMA) cement mortar. To fulfill this objective, short term healing efficiency (up to 28 days) of unreinforced and reinforced (Steel and SMA) mortar beam specimens with calcium nitrate containing microcapsules were evaluated under different environmental conditions (dry, water submerged, and wet and dry cycles) at different microcapsule dosages. Specimens were cracked by three-point bending test and evaluated during the healing period by light microscopy and Ultrasonic Pulse Velocity (UPV) test. Cracks analyzed ranged from 13 to 387 μm. Water submerged healing conditions yielded the best self-healing results followed by wet and dry cycles. Dry healing conditions did not enable appreciable healing, thereby suggesting the need of external moisture conditions for proper functioning of the self-healing mechanism proposed. Moreover, SMA reinforced specimens (with and without microcapsules) presented an enhanced healing performance at early stages of the healing process likely due to the self-closing effect. Furthermore, the general tendency of healing results suggested that the combination of microcapsules and SMA favored self-healing.

Lastly, the healing products generated in cracks were investigated under ESEM-EDS to assess their chemical nature. The overwhelming majority of healing products were identified as likely calcium carbonate in the form of calcite crystals, and a limited quantity of gel-like healing products of possibly CSH chemical nature were also identified.

CHAPTER 1

INTRODUCTION

Concrete, as the most widely used material in the world, is readily available, has a low cost, and possesses notable mechanical properties, which makes for a formidable construction material. From roads, bridges, and tunnels to water supply systems, sewers, and buildings all over the world, concrete is a key component of the infrastructure on which our societal living conditions depend. Unfortunately, several developed countries in recent years, including Germany, South Korea, and the United States, have experienced an unprecedented deterioration of civil infrastructure to the extent that the annual expenditure for repair and maintenance has surpassed the cost of new infrastructure construction (Li & Hebert 2012). Due to the enormous economic, social, and environmental significance of concrete durability, special attention has been directed to the durability of concrete materials, as well as ways and means to mitigate its deterioration.

Concrete deterioration can occur due to several environmental factors, which can chemically or physically attack the material. Regardless of the nature of the attack, cracks are inevitable in concrete structures, and once cracks occur, they permit detrimental substances to penetrate into the material, thus enhancing the deterioration process. Importantly, novel developments in cementitious materials may lead to the control of cracks in concrete structures and therefore are of immense significance for the future of infrastructure resiliency and sustainability.

Many approaches to control cracking of cementitious materials via self-healing mechanisms were recently proposed in the literature. These approaches may be arranged into five categories: (a) chemical encapsulation; (b) bacterial encapsulation; (c) mineral admixtures; (d) chemicals in glass tubing; and (e) intrinsic self-healing with self- controlled tight crack width (Li & Hebert 2012). These autonomic healing strategies are based on engineered concrete materials, capable of enhancing the well-studied self-healing properties of cementitious materials, or endowing the material with new self-healing mechanisms (Wu et al 2012).

From autonomic healing systems studied in recent years, encapsulation of healing agents is of particular interest, due to three main characteristics of these systems: (a) versatility, which allows the encapsulation of diverse chemicals in a wide range of sizes down to the submicron size; (b) long shelf life capability, which may allow a self-healing mechanism to remain active for prolonged periods of time; and (c) the potential of these systems to endow cementitious materials with self-healing properties, regardless of environmental conditions (Li & Hebert 2012).

Microencapsulation of healing agents for autonomic healing of materials was first introduced by White et al. in polymer composites (White et al. 2001). To date, self-healing technology by microencapsulated healing agents has been primarily developed in polymers and composites. Yet research of an application for cementitious materials has recently started (Wang et al. 2014). The technique of self-healing through microencapsulation of healing agents consists in providing the material with inert microcapsules filled with a reactive healing agent. Once a

cracking event takes place in the vicinity of a microcapsule, the microcapsule will rupture and lead to the release of the healing agent on the crack surface, allowing healing to occur.

There are several elements which are crucial for proper implementation of self-healing through microencapsulation of healing agents: (a) an adequate dosage and distribution of capsules to provide a sufficient amount of healing agent to spread uniformly throughout the material; (b)a sufficient bond strength between the microcapsule external surface and the cementitious matrix, so that rupture can take place in a cracking event; and (c) the crack volume shall not exceed the amount of healing agent available in order for self-healing to be fully successful, thus highlighting the importance of a narrow crack width for this autonomous healing system to be effective (Van Tittelboom et al. 2013).

In order to control crack size in concrete, steel reinforcement is regularly utilized. While this is somehow effective, there are new alternatives, which can provide better crack control. Shape memory alloys (SMA) represent a novel type of material, which can provide concrete with shape memory properties. Upon deformation, SMA recovers its original shape when subjected to heat, thus allowing for crack size reduction. While SMA alone might not be sufficient to absolutely close a crack, this technology can certainly significantly reduce crack size, thus making it a great alternative to work in a combined effect with self-healing microcapsules.

1.1 Problem Statement

Although microencapsulation appears to be a promising technology for addressing durability of concrete, the microencapsulation of healing agents for self-healing cementitious materials application is still at an early development stage. A variety of healing agents have been evaluated in recent years including sodium silicate, polyurethane, epoxy, cyanoacrylates and bacterial spores (Wang et al. 2014; Li et al. 2013; Huang & Ye 2011; Pelletier et al. 2015; Kaes et al. 2014; Van Tittelboom et al. 2011). Dual-component, self-healing systems consisting of a healing agent and a catalyzer, such as methylmethacrylate monomer and triethylborane have also been evaluated (Yang et al. 2011). Nevertheless, while some of these strategies were successful in enhancing self-healing capabilities of cementitious materials, many of these healing agents are expensive and/or require a catalyst to activate the self-healing process. As of today, there are several readily available chemicals with self-healing application potential which have not been explored yet, with one of those being calcium nitrate.

Calcium nitrate has been long utilized as a setting accelerator admixture in concrete industry, due to its hydration enhancing properties. Calcium nitrate hydration accelerating characteristics occur because this admixture possesses the same cations (Ca^{2+}) as the main components of cement, C_2S (dicalcium silicate) and C_3S (tricalcium silicate), which allows for a nucleating action, which boosts the crystallization of hydrates (Karagöl et al. 2013) (Ramachandran 1995). Moreover, calcium hydroxide available in the cementitious matrix can react with calcium nitrate to form calcium hydroxynitrate, which then acts as an initial structural skeleton permitting calcium hydrosilicates to form, thus benefiting the hydration process (Karagöl et al. 2013). These characteristics make calcium nitrate a potential candidate for self-healing agent as it can react with unhydrated cement particles which are present in crack surfaces allowing for an improved autogenous healing action due to further hydration. Moreover, calcium ions (Ca^{2+}), made available by calcium nitrate in the crack, may provide a more favorable

environment for calcium carbonate formation in the crack, which can also serve as a mechanism for self-healing. Therefore, due to its hydration enhancing properties, ready availability and low cost, calcium nitrate is a great candidate for a robust and economic self-healing agent.

The key for robust self-healing through a microencapsulation approach lies greatly in the mechanism by which the healing agent interacts with concrete to produce healing products upon a cracking event. The healing mechanism will therefore define crack healing efficiency over time, as well as the type of healing products generated, thus establishing the reliability and quality of healing. Furthermore, the healing mechanism will determine extant limitations of self-healing, such as dependence to environmental conditions, microcapsule dosage, and crack width. For these reasons, the investigation of healing mechanisms carry a great significance, since findings may allow to optimize a self-healing method, as well as to establish conditions for correct implementation.

1.2 Objectives

In order to address the problem statement, the main goal of this study is to investigate the self-healing mechanism of unreinforced and reinforced mortar specimens with calcium nitrate microcapsules by means of the following objectives:

- Measure short term healing efficiency of unreinforced and reinforced mortar specimens with calcium nitrate microcapsules.
- Characterize healing products of unreinforced and reinforced mortar specimens with calcium nitrate microcapsules.
- Quantify technology limitations of unreinforced and reinforced mortar specimens with calcium nitrate microcapsules.
  a) Evaluate crack size effect on self-healing efficiency.
  b) Evaluate environmental conditions effect on self-healing (wet and dry conditions).
  c) Evaluate microcapsule dosage effect on self-healing efficiency.

1.3 Research Approach

Research will be divided into four phases, addressing each of the research objectives for both unreinforced and reinforced mortar specimens with calcium nitrate microcapsules.

Phase I: Evaluation of Self-Healing Efficiency of Unreinforced Beam Mortar Specimens with Varying Microcapsule Contents under Wet and Dry Conditions.

Objectives addressed:

- Measure of healing efficiency of unreinforced mortar specimens with microcapsules.
- Healing products characterization of unreinforced mortar specimens with microcapsules.
- Evaluation of crack size, microcapsules dosage, and environmental conditions for self-healing of unreinforced mortar specimens with microcapsules.

Task 1: Mortar Beams Production

Prismatic mortar specimens with a 0.48 water to cement ratio (w/c) will be cast with dimensions of 40 mm x 40 mm x 160 mm. The mortar mix will be prepared with Type I Portland Cement, sand, tap water and microcapsules at dosages of 0 (control), 0.5, 1, and 2% by weight of cement. Microcapsule dosage variation will allow gainful insight on

self-healing mechanism dependence on microcapsule content as well as to determine whether there is an optimum microcapsule content. Finally, specimens will be demolded after 24 h of casting and cured for 28 days in a moist room subjected to (23 ± 2°C, > 95% Relative Humidity [RH]). Mix design proportions are detailed on Table 1.

Table 1.1. Mortar Mix Proportions

Material Description	**Proportions (kg/m^3)**
Sand	1375
Cement, Type I	500
Water	242
Water Cement Ratio (W/C) = 0.48	

Task 2: Mortar Testing

Specimens will be tested by a three-point bending test (ASTM C348), in order to induce cracks for a self-healing evaluation of mortar specimens. Crack width will be controlled through a strain-controlled load application at a rate of 0.01 mm/min to keep cracks in the micro range, where effective self-healing can take place.

Task 3: Evaluation of Healing Efficiency over Time

In order to quantify crack healing efficiency over time, a digital image analysis of light microscopy images will be utilized. The area of the cracks will be measured from images taken right after flexural testing (day 0) and throughout the healing period at 3, 7, 14, and 28 days. This will allow for quantifying self-healing efficiency, as the ratio of healed crack area over initial crack area. To promote self-healing after cracking, test specimens will be exposed to dry and wet conditions. Dry conditions will be set at 50 ± 4% relative humidity and a controlled temperature of 23 ± 2 °C. On the other hand, wet conditions will be water-submerged at a controlled temperature of 23 ± 2 °C. Sealed containers will be utilized to reduce carbonation due to dissolution of CO_2 into the water; water will be replaced at days 3, 7, 14 and 28 of the healing period. Wet and dry conditions will be explored in order to gain insight on the self-healing mechanism dependence on environmental conditions. It is important to notice that the outcomes of this task may influence an environmental conditions selection on phase II of this study.

Task 4: Characterization of Healing Products

After allowing for 28 days of healing, the specimens will be cut with a diamond blade saw and directly analyzed in an ESEM equipped with EDS, in order to observe the morphology and investigate the chemical composition of the healing products formed in the cracks. Atomic ratio plots and EDS maps will be generated to identify the chemical nature of healing products. This will provide significant insight into the healing mechanism, as the chemical nature of healing products is a consequence of the underlying chemical process which takes place during healing.

Phase II: Evaluation of Self-Healing Efficiency of SMA and Steel Reinforced Beam Mortar Specimen with Varying Microcapsule Contents under Wet Conditions (Water Submerged Conditions and Wet & Dry Cycles).

Objectives addressed:

- Measure healing efficiency of reinforced mortar specimens with microcapsules.
- Healing products characterization of reinforced mortar specimens with microcapsules.
- Evaluation of crack size, microcapsule dosage, and environmental conditions for self-healing of reinforced mortar specimens with microcapsules.

Task 5: SMA and Steel Reinforced Mortar Beams Production

Prismatic mortar specimens with a 0.4 water to cement ratio (w/c) will be cast with dimensions of 40 mm x 40 mm x 160 mm. Two wires, 2 mm in diameter, will be placed 1 cm from the bottom of the beam, with 2 cm spacing for both SMA and steel reinforcement configurations as shown in Figure 1.1. The mortar mix will be prepared with Type I Portland Cement, sand, tap water and microcapsules at dosages of 0 (control), 0.5, 1, and 2% by weight of cement. Finally, specimens will be demolded after 24 h of casting and cured for 28 days in a moist room subjected to (23 ± 2°C, > 95% Relative Humidity [RH]). Mix design proportions are detailed on Table 1.2.

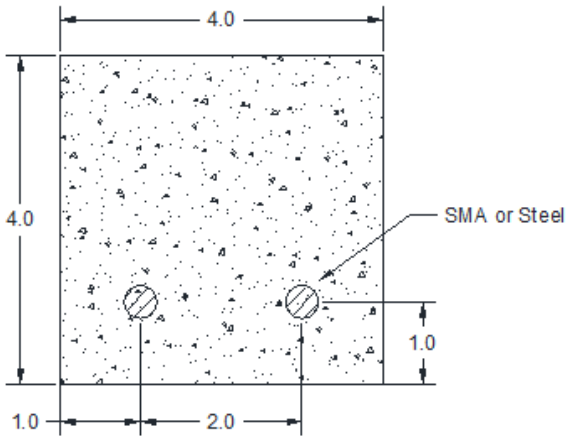

Figure 1.1 Reinforcement Layout (Units are in cm)

Table 1.2. Mortar Mix Proportions

Material Description	Proportions (kg/m^3)
Sand	1500
Cement, Type I	600
Water	210
Water Cement Ratio (W/C) = 0.4	

Task 6: SMA and Steel Reinforced Mortar Testing

Specimens will be tested by three-point bending test (ASTM C348) in order to induce cracks for a self-healing evaluation of mortar specimens. Crack width will be controlled through a strain-controlled load application at a rate of 0.01 mm/min to keep cracks in the micro range, where effective self-healing can take place. Sacrificial specimens will be

tested to failure in order to determine the stress-strain curves for comparison with specimens, which will be re-tested after healing.

Task 7: Evaluation of Healing Efficiency over Time

In order to quantify crack healing efficiency over time, a digital image analysis of light microscopy images will be utilized. The area of the cracks will be measured from images taken directly after flexural testing (day 0) and throughout the healing period at 3, 7, 14, and 28 days. This will allow the study to quantify self-healing efficiency as the ratio of healed crack area over initial crack area. To promote self-healing after cracking, test specimens will be exposed to wet conditions (water submerged conditions and wet & dry cycles) while heating the reinforcement with electric current in order to activate the shape memory effect of SMA and thereby reduce crack width. Sealed containers will be utilized to reduce carbonation, due to dissolution of CO_2 into the water, which will be replaced at days 3, 7, 14, and 28 of the healing period.

Task 8: Characterization of Healing Products

After allowing for 28 days of healing, the specimens will be cut with a diamond blade saw and directly analyzed in an ESEM equipped with EDS in order to observe the morphology and investigate the chemical composition of the healing products formed in the crack. Atomic ratio plots and EDS maps will be generated to identify the chemical nature of healing products.

Phase III: SMA and Steel Reinforced Mortar Specimen with Microcapsules Evaluation of Healing Over Time through a Mechanical Properties Recovery Approach

Objectives addressed:

- Measure healing efficiency of reinforced mortar specimen with calcium nitrate microcapsules.

Task 9: Analyze crack healing over time by Ultrasonic Pulse Velocity Test (UPV) at 0, 3, 7, 14, and 28 days and thus evaluate evolution of the dynamic modulus of elasticity over time. This task will allow us to investigate healing efficiency in a mechanical perspective. An increasing dynamic modulus of elasticity will be indicative of recovery of mechanical properties and thus, healing.

Task 10: Re-test beam specimens by three point bending test (ASTM C348) after 28 days of healing and evaluate the recovery of mechanical properties. Re-test of mortar beam specimens will provide valuable complementary information regarding the recovery of mechanical properties, which combined with UPV data, could provide a robust assessment of healing in a mechanical perspective.

1.4 References

Huang Haoliang and Ye Guang, Application of sodium silicate solution as self-healing agent in cementitious materials, International RILEM Conference on Advances in Construction Materials Through Science and Engineering, Vol. 1, 2011, 530-535.

Kaes M., Van Tittelboom K., and N. De Belie. The efficiency of self-healing cementitious materials by means of encapsulated polyurethane in chloride containing environments. Construction and Building Materials, Vol. 71, 2014, 528-537.

Karagöl, F., Demirboga, R., Kaygusuz M.A., Yadollahi, M.M., Polat, R.The influence of calcium nitrate as antifreeze admixture on the compressive strength of concrete exposed to low temperatures, Cold Regions and Technology 89 (2013) 30-35.

Li Victor C., Hebert Emily, Robust Self-Healing Concrete for Sustainable Infrastructure, Journal of Advanced Concrete Technology, volume 10 (2012), pp207-218.

Li W, Jiang Z, Yang Z, Zhao N, Yuan W (2013) Self-Healing Efficiency of Cementitious Materials Containing Microcapsules Filled with Healing Adhesive: Mechanical Restoration and Healing Process Monitored by Water Absorption. PLoS ONE 8(11): e81616. doi:10.1371/journal.pone.0081616.

Pelletier M., Brown R., Shukla A., and A. Bose, Self-healing concrete with a microencapsulated healing agent, Available online: http://energetics.chm.uri.edu/system/files/Self%20healing%20concrete%20-7-11.pdf (accessed 3 July 2015).

Ramachandran, V. S., 1995. Concrete Admixtures Handbook, Second edition. pp.740-756.

Van Tittelboom K., De Belie N., Van Loo D., and P. Jacobs, Self-healing efficiency of cementitious materials containing tubular capsules filled with healing agent, Cement and Concrete Composites, Vol. 33, 2011, 497–505.

Van Tittelboom K., and De Belie N., Self-Healing in Cementitious Materials – A Review. Materials, Vol.6, 2013, 2182-2217.

Wang J.Y., Soens H., Verstraete W., De Belie N., Self-healing concrete by use of microencapsulated bacterial spores, Cement and Concrete Research 56 (2014) 139-152.

White SR, Sottos NR, Geubelle PH, Moore JS, Kessler MR, Sriram SR, et al, Autonomic healing of polymer composites. Nature 2001; 409 (6822):794

Wu M.,Johannesson B., Geiker M., A review: Self-healing in cementitious materials and engineered cementitious composite as a self-healing material, Construction and Building Materials 28 (2012) 571-583.

Yang Z.X.,Hollar J., He X.D.,Shi X.M., A self-healing cementitious composite using oil core/silica gel shell microcapsulses, Cem.Concr.Compos 33 (2011) 506-512.

CHAPTER 2

LITERATURE REVIEW

2.1 Introduction

Concrete deterioration is of great concern due to safety and economic reasons. In 2013, the latest report card on US infrastructure, performed by the American Society of Civil Engineers, rated the US infrastructure with a D+ grade. This qualification, far from acceptable, demonstrates the urgent need for new technologies which address the deficient durability performance of construction materials.

Concrete, as the most widely utilized construction material in the US and the world, is a major stakeholder in the infrastructure deterioration crisis which the US now faces. It is well known that concrete deterioration can take place due to several environmental factors which can physically and chemically attack the material. However regardless of environment conditions, cracks are inevitable in concrete structures, yet allow for deteriorating mechanisms to be significantly enhanced.

As cracks have been identified as the major contributor to concrete deterioration, in recent years, many techniques have been proposed and investigated in order to produce concrete materials that can repair by themselves upon a cracking event. The approaches for self-healing concrete that have been proposed are: (a) chemical encapsulation, (b) bacterial encapsulation, (c) mineral admixtures, (d) chemical in glass tubing, and intrinsic self-healing with a self-controlled tight crack width (Li & Hebert 2012). These autonomic healing systems work by either enhancing the well-known self-healing properties of cementitious materials (autogenous healing), or by endowing them with new, self-healing mechanisms (Wu et al. 2012).

Throughout this chapter, important information with regards of self-healing technologies in cementitious materials will be discussed. From the fundamentals of cement behavior –key for understanding of self-healing mechanisms– to the available techniques for the assessment of self-healing in cementitious materials, a thorough review will be conducted.

2.2 Cement Hydration

Cement hydration is the fundamental process which transforms sand, gravel, cement, and water into a solid structural material. Cement hydration is a chemical process of extreme complexity, and to date is not fully resolved. However, great amounts of knowledge have been generated regarding this subject over the years, inclusive of chemical and physical processes in hydration, cement phases, and hydration products, which will be discussed in this section.

It is important to notice that in cement chemistry a special notation is utilized. This notation will be utilized throughout this document. A cement chemistry notation is presented in Tables 2.1 and 2.2.

Table 2.1. Abbreviated Notations Used in Cement Chemistry (Caldarone 2009)

	Chemical Formula	Notation
Lime	CaO	C
Silica	SiO_2	S
Alumina	Al_2O_3	A
Iron	Fe_2O_3	F
Titanium	TiO_2	T
Magnesia	MgO	M
Potassium	K_2O	K
Sodium	Na_2O	N
Sulfur	SO_3	$\bar{S}$
Water	H_2O	H

Table 2.2. Abbreviated notation of cement components (Caldarone 2009)

	Chemical Composition	Abbreviated Notation
Tricalcium Silicate	$3\ CaO \cdot SiO_2$	C_3S
Dicalcium Silicate	$2\ CaO \cdot SiO_2$	C_2S
Tricalcium Aluminate	$3\ CaO \cdot Al_2O_3$	C_3A
Tetracalcium Alumino Ferrite	$4\ CaO \cdot Al_2O_3 \cdot Fe_2O_3$	C_4AF

2.2.1 Chemical and Physical Processes in Cement Hydration

Cement hydration is a highly complex process which involves several coupled chemical processes, each of which occurs at a rate determined both by the nature of the process and by the state of the system at any given instant (Bullard et al. 2010). Processes involved in cement hydration are the following: (a) Dissolution/dissociation which involves the detachment of molecular units from solid surfaces with water contact; (b) Diffusion, which describes the transport of solution components through the pore volume of cement paste, or along solids surfaces in the adsorption layer; (c) Nucleation, which initiates the precipitation of solids heterogeneously on solid surfaces or homogeneously in solution, occurs when the bulk free energy driving force to form the solid exceeds the energetic penalty of forming the new solid-liquid interface; (d) Growth, which incorporates molecular units into the structure of a crystalline or amorphous solid within its self-adsorption layer; (e) Complexation, which allows the formation of ion complexes or adsorbed molecular complexes on the surfaces of solids by the reaction between simple ions; and (f) Adsorption which provides the accumulation of ions or

other molecular units at an interface such as the surface of a solid particle in a liquid (Bullard et al. 2010).

The above mentioned processes can operate in series, parallel, or in other complex combinations (Bullard et al. 2010). For instance, the case of a simple crystal growth from solution bring in diffusion of solute to the vicinity of an existing solid surface, adsorption of the solute onto the surface, complexation of some solute species into a molecular unit that can be integrated into the crystal structure, attachment, and equilibrium of that molecular unit into the structure (Bullard et al. 2010; Lasaga et al. 1981; Morel et al. 1983). When these steps operate in series, they are coupled in the sense that the products of one step are the reactants for following steps (Bullard et al. 2010). Most of the time, one step in the sequence will have a notably lower rate, so that all but this specific step can reach equilibrium conditions; this step is called the rate controlling step which by itself will be responsible for the observed kinetic rate equation, the rate constant and the temperature dependence (Bullard et al. 2010). Furthermore, when the rates of two or more fundamental steps are comparable, rate equations and their dependence on system variables can turn much more complex in order to form experimental determinations (Bullard et al. 2010; Morel et al. 1983). The application of these concepts to cement hydration remains difficult to achieve, due to the challenge of isolating individual chemical processes for detailed study (Bullard et al. 2010). Thus, at present, there exists only partial knowledge about the net kinetic effects of the multiple interacting processes in cement hydration (Bullard et al. 2010).

2.2.1 Portland Cement Phases and C_3S

Ordinary Portland cement is composed of the following phases: (a) Tricalcium silicate $3CaO \cdot SiO_2$ (C_3S), which is the main component responsible for early strength gain and contributes significantly to late strength development as well; (b) Dicalcium silicate $2CaO \cdot SiO_2$ (C_2S) which contributes importantly to late strength gain; (c) Tricalcium aluminate $3CaO \cdot Al_2O_3$ (C_3A); (d) Tetracalcium aluminoferrite $4CaO \cdot Al_2O_3 \cdot Fe_2O_3$ (C_4AF); and (e) Calcium sulfate dehydrate $CaSO_4 \cdot 2H_2O$ ($C\bar{S}H_2$) which is gypsum (Mindess et al. 2002).

In considering Portland cement phases, the most relevant is tricalcium silicate or C_3S, according to the conventional cement chemistry notation (Bullard et al. 2010). This phase is present in cement in the form of alite, an impure form of C_3S which accounts for 50% to 70% of Portland cement by mass (Bullard et al. 2010). Alite is the main component for the formation of the principle product of hydration, calcium silicate hydrate gel (CSH), and thus tends to dominate in the early stage of hydration, which compromise setting and early strength development (Bullard et al. 2010).

The rate of hydration of pure C_3S, alite, and Portland cement have long been known to vary with time in orders of magnitude, and therefore it has been historically divided into several stages, defined by somewhat arbitrary points on a plot of hydration rate versus time (Bullard et al. 2010; Gartner et al. 2002). Gartner et al. sections the C_3S hydration into six stages according to calorimetric curve shown in Figure 2.1.

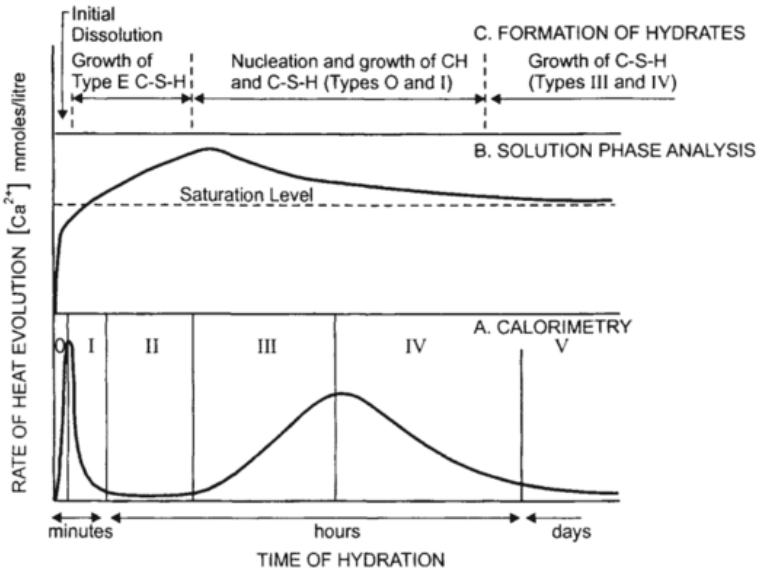

Figure 2.1 C_3S Pastes (W/S<1) Hydration Stages (Gartner et al. 2002)

The stages of hydration are as follows: (a) Stage 0 (initial fast reaction), which takes place very rapidly by means of the first wetting of C_3S, producing surface hydrolysis, and the release of ions into solution; (b) Stage I (first deceleration) which takes place regularly while concrete is being mixed and is characterized by the formation of a hydrate coating on the C_3S surface, which then retards dissolution; (c) Stage II (induction period) which takes place while concrete is transported, placed, and finished; this stage is characterized by a retarded nucleation of final hydrates and/or slow consumption of retarders; (d) Stage III (acceleration period) which corresponds to setting and initial curing; this stage is characterized by an accelerating growth of principal hydration products; (e) Stage IV (second deceleration) which corresponds to curing and demolding, and is characterized by the continued growth of hydration products into large empty spaces and is the beginning of diffusion control hydration; and (f) Stage V (final slow reaction) which corresponds to the continuous slow hardening (as long as moist curing is continued) and is characterized by gradual densification of microstructure around residual, unhydrated C_3S, which is a diffusion controlled process (Gartner et al. 2002).These stages are summarized in Table 2.3.

2.2.3 Portland Cement Hydration Products

Hydration of Portland cement produces many different components, which play an important role in concrete physical and chemical properties. The most significant hydration products are next described.

Calcium Silicate Hydrate (CSH or $C_3S_2H_8$) and Calcium Hydroxide (CH)

Calcium silicate hydrate, the principal hydration product, and Calcium hydroxide are formed from a C_2S and C_3S reaction with water, according to the following chemical reactions (Mindess et al. 2002):

$$2C_3S + 11H \rightarrow C_3S_2H_8 + 3CH$$

$$2C_2S + 9H \rightarrow C_3S_2H_8 + CH$$

Table 2.3 Typical Reaction Stages of C_3S Pastes at Low W/S (Gartner et al. 2002)

Reaction Stage	Corresponding Stages in Concrete-Making	Chemical Process	Overall Kinetic Behavior
0. Initial Fast Reaction	First wetting	Surface hydrolysis and release of ions into solution.	Very rapid, exothermic; can only be observed at very high w/s.
I. First Deceleration	Wetting, mixing	Formation of coating on C_3S surface, retarding dissolution.	Chemical control (probably by rate of heterogeneous nucleation)
II. Induction Period	Transporting, agitating, placing, and finishing (especially in presence of "retarders").	Retarded nucleation of final hydrates; slow consumption of "retarders".	Chemical control (by consumption of "retarders" and/or nucleation of hydrates)
III. Acceleration Period	Setting, initial curing	Accelerating growth of principal hydration products.	Auto-catalytic growth of principal hydrates (chemical control)
IV. Second Deceleration	Curing, demolding	Continued growth of hydration products into large empty spaces.	Onset of diffusion control; products otherwise similar to stage III
V. Final Slow Reaction	Continued slow hardening as long as moist curing is continued	Gradual densification of microstructure around residual unhydrated C_3S; CH recrystallization	Diffusion controlled but not necessarily by the same species as in IV. Slow changes in CSH?

It is important to note that $C_3S_2H_8$ is an approximate formula, as the actual composition of this hydrate is highly variable. Since water content varies widely, the value presented refers to water saturated conditions (Mindess et al. 2002). CSH is a poorly crystalline material, which forms as extremely small particles of less than 1μm in any direction. On the other hand, calcium hydroxide is a crystalline material with fixed composition (Mindess et al. 2002).

Ettringite ($C_6A\bar{S}_3H_{32}$) and Monosulfate ($C_4A\bar{S}H_{12}$)

Ettringite forms due to the hydration of tricalcium aluminate (C_3A) and the subsequent reaction with gypsum ($3C\bar{S}H_2$) according to the following chemical equation (Mindess et al. 2002):

$$C_3A + 3C\bar{S}H_2 + 26H \rightarrow C_6A\bar{S}_3H_{32}$$

Ettringite is a stable hydration product, providing there is an ample supply of sulfate available. If the sulfate is consumed before the full hydration of C_3A, then ettringite transforms to monosulfate, which contains less sulfate according to the following reaction (Mindess et al. 2002):

$$2C_3A + C_6A\bar{S}_3H_{32} + 4H \rightarrow 3C_4A\bar{S}H_{12}$$

2.3 Self-Healing Concrete

2.3.1 Autogenous Healing of Cementitious Materials

Autogenous healing of cementitious materials is a well-studied phenomenon. As early as 1836, the French Academy of Science had already noticed autogenous healing of concrete cracks in water retaining structures, culverts, and pipes (Wu et al. 2012). To date, many experimental studies have been conducted, as well as extensive practical experience gathered on the subject.

Autogenous healing in cementitious materials can take place due to physical and/or chemical processes, which can provide with transport and mechanical properties recovery of concrete materials. These mechanisms, illustrated by Figure 2.2, are the following: (a) calcium carbonate or calcium hydroxide formation; (b) crack blockage due to impurities in water and/or loose particles; (c) further hydration of unhydrated cement particles or cementitious materials; and (d) hydrated cementitious matrix expansion (Wu et al. 2012).

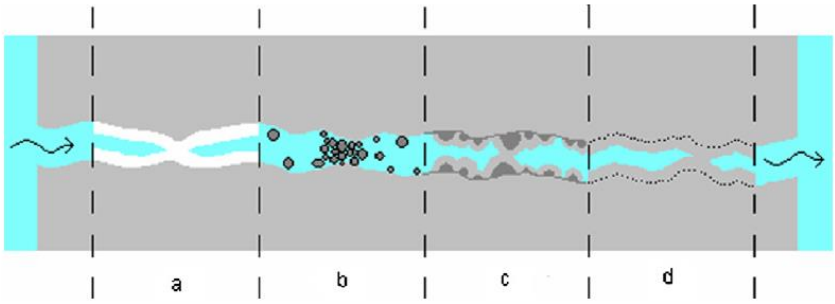

Figure 2.2 Autogenous Healing Mechanisms in Cementitious Materials (Wu et al. 2012)

Importantly, all these processes require water, either stationary or flowing, to trigger self-healing; further, the crack must be inundated in order for self-healing to be effective (Neville 2002). Lauer et al., for example, demonstrated that in air humidity as high as 95%, autogenous healing of cement paste became much lower than in water, and healing was inconsistent.

Crack width is another determinant factor for autogenous healing, since a robust healing will not take place above a certain crack width (Neville 2002). Several investigators have reported different maximum widths of cracks for self-healing, but conditions of testing as well as results tend to vary widely. Thus, generalizations about the maximum crack size that will heal are not possible (Neville 2002). Edvardsen reported that 1/4 to 1/2 of cracks 200 μm wide healed completely after 7 weeks of water exposure, depending on water pressure (Edvardsen 1999;

Neville 2002). Moreover, Lea stated in regard to a maximum crack width sealed by autogenous healing, that cracks up to 200 µm do not usually lead to any progressive corrosion in reinforcing steel (Lea 1970; Neville 2002). Furthermore, Li and Yang suggested that the requirement of crack width for robust autogenous healing should roughly be below 200 µm, possibly 50 µm (Li & Yang 2007).

From the several autogenous healing mechanisms mentioned, further hydration of cement and calcium carbonate formation are the most common and relevant processes for self-healing. However, further hydration is most relevant on very young concrete, where large amounts of unhydrated cement particles are available, while calcium carbonate formation becomes the predominant factor at a later time (Neville 2002). The formation of $CaCO_3$ in the form of calcite crystals is produced due to the interaction between calcium ions Ca^{2+} derived from $Ca(OH)_2$ or CSH phases from concrete and bicarbonates ${HCO_3}^{-2}$ or carbonates ${CO_3}^{-2}$, which are available in the water according to the following chemical reactions (Edvardsen 1999):

$$Ca^{2+} + {CO_3}^{-2} \Leftrightarrow CaCO_3 \ (pH_{water} > 8)$$

$$Ca^{2+} + {HCO_3}^{-2} \Leftrightarrow CaCO_3 + H^{+} \ (7.5 < pH_{water} < 8)$$

In addition, where and whether calcite formation will occur with a subsequent crystal growth depends besides from temperature, pH and CO_2 partial pressure; mainly on the saturation index Ω of calcite, which is a function of the concentration of Ca^{2+} and ${CO_3}^{-2}$ ions in the solution and the solubility product of calcite Kc, according to the following equation (Edvardsen 1999):

$$\Omega = \frac{(Ca^{2+})({CO_3}^{2-})}{K_c}$$

Experimental studies show that a Ω value of 20 is necessary to trigger calcite nucleation with subsequent crystal growth in a tube solution, but as crack surfaces in concrete can act as a catalyst to the nucleation process, it is believed that a far smaller Ω value should be required in such conditions (Edvardsen 1999). Additionally, thermodynamic considerations of $CaCO_3$ formation show that rising water pH and temperature, as well as falling CO_2 partial pressure in water are conditions which favor precipitation of calcite in cracks (Edvardsen 1999). A scheme of the calcite formation in concrete cracks is shown in Figure 2.3.

On the other hand, further hydration as an autogenous healing mechanism is a process in which unhydrated cement particles, when made available in a cracking event, produce crack recovery. As water penetrates into the crack, unhydrated cement particles made available in the surfaces of the crack can react with water, producing newly formed hydration products which subsequently heal the crack. Further hydration phenomenon differs from hydration occurring inside the bulk cement paste, due to the different conditions encountered in a crack environment (Huang et al. 2013). For instance, there is more water available in a crack than in the bulk cement paste; in fact, the space available for a growth process of hydration products is more abundant as well, thus influencing nucleation and the growth process of hydration products (Huang et al. 2013). Huang et al. reported that further hydration products in cracks are mainly composed of CH (Calcium Hydroxide) and CSH (Calcium Silicate Hydrate), with CH occurring in more significantly superior quantities than CSH, contrary to the cement hydration in the matrix. Furthermore, it was reported that in younger cement pastes, higher amounts of

unhydrated cement lead to greater self-healing, while on both young and older cement pastes, the self-healing mechanism slowed down significantly after 300 hours (Huang et al. 2013).

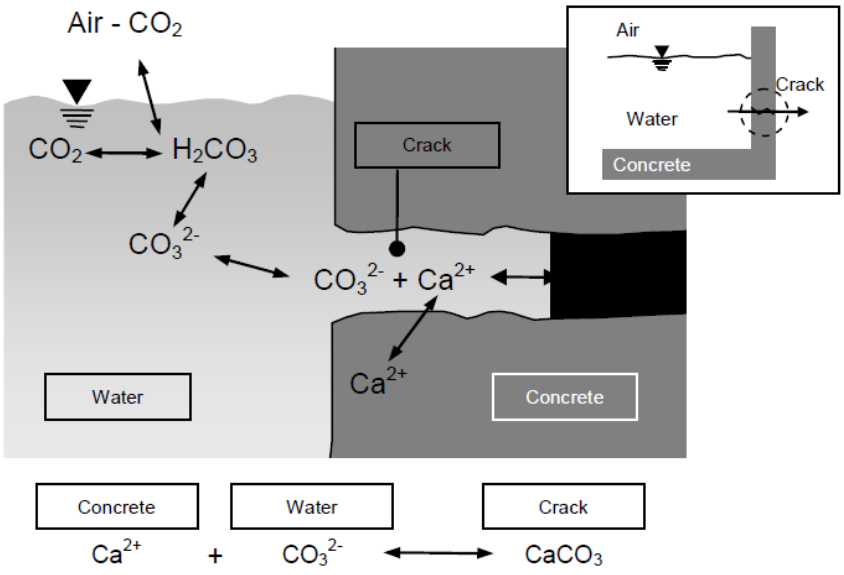

Figure 2.3 Media, Interfaces and Reactions in $CaCO_3$ – CO_2 – H_2O Systems (Edvardsen 1999) (Mihashi et al. 2012)

2.3.2 Engineering Cementitious Composites (ECC)

Engineered cementitious composites are a type of fiber-reinforced, cementitious, composite material which has been optimized through the use of micromechanics to behave in an ultra-ductile manner exhibiting a high-tensile ductility and a tight micro-crack width at moderate fiber contents of 2 percent by volume or less (Kan et al. 2010).

ECCs extreme tensile capacity (beyond 3%) is several hundred times that of regular concrete, while its toughness is similar to that of aluminum alloys (Kan et al. 2010). In contrast with conventional concrete, ECCs mechanical properties allow cracks in the material to remain consistently small (less than 60 µm) at even large deformations, thus allowing for self-healing mechanisms of cementitious materials (autogenous healing) to act more effectively, as shown in Figure 2.4 (Kan et al. 2010). Figure 2.5 shows the typical tensile stress-strain curve and crack width (CW) development of ECCs.

Kan et al. investigated the self-healing ability of ECCs under wet and dry cycles (Kan et al. 2010). In this investigation, ECC specimens were loaded by uniaxial tensile loading to several strain levels from 0.3% to up to 2% to generate cracks (Kan et al. 2010). Once the damage was induced, specimens were allowed to self-heal under wet and dry cycle conditions (Kan et al. 2010). Healing was assessed by resonant frequency (RF) recovery and ESEM observation, while EDS, TEM, FTIR and XRD were utilized to characterize healing products in the cracks (Kan et al. 2010). Experimental results showed that ECCs self-controlled CW characteristics contribute significantly to self-healing behavior (Kan et al. 2010). After 10 wet-dry cycles, RF recovery due

to self-healing exceeded 90% at even 2% imposed strain, while cracks smaller than 50 µm lead to a highly robust healing, as observed by ESEM images (Figure 2.5) (Kan et al. 2010). Furthermore, healing products were confirmed to be fiber-like CSH and stone-like $CaCO_3$, due to further hydration and formation of $CaCO_3$ crystals (Kan et al. 2010). Figure 2.6 shows the healing process of a 50 µm crack.

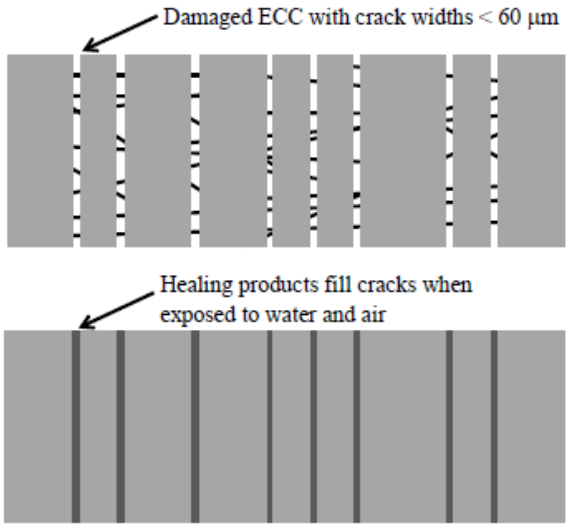

Figure 2.4 ECC Self-Controlled Tight Crack Width Self-Healing Approach (Li et al 2012)

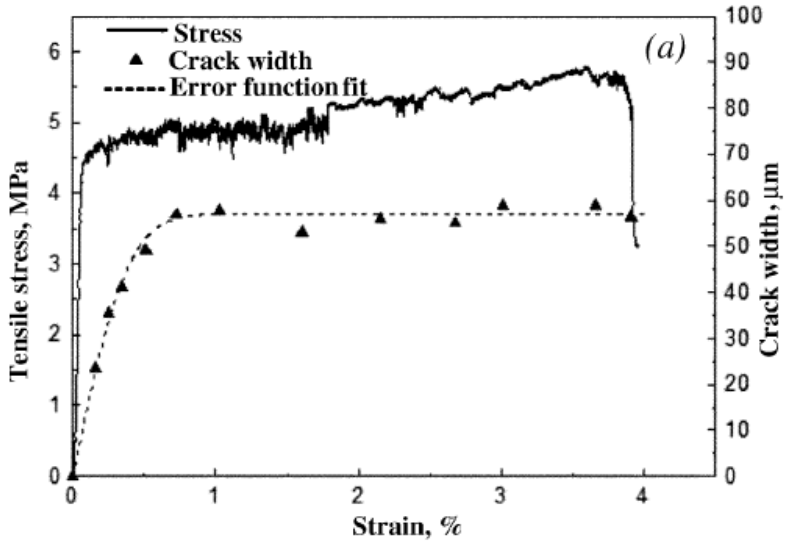

Figure 2.5 ECC Typical Tensile Stress-Strain Curve and Crack Width (CW) Development (Kan et al. 2010)

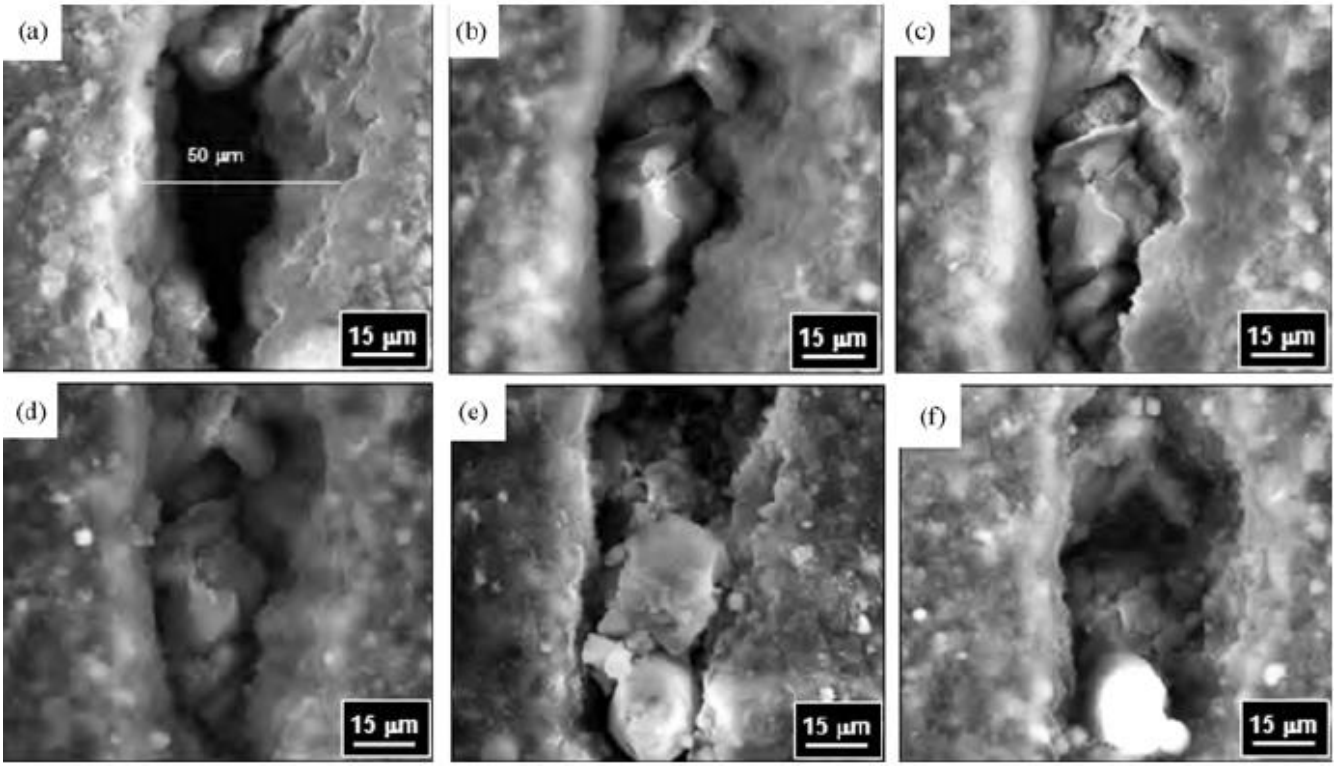

Figure 2.6 ECC Self-Healing Process of 50μm Crack: (a) Before Self-Healing, (b) After One Cycle, (c) After Three Cycles, (d) After 10 Cycles, (e) After 20 Cycles, and (f) After 49 Cycles (Kan et al. 2010).

2.3.3 Self-Healing with Expansive Agents and Mineral Admixtures

Mineral admixtures have been proposed as a self-healing approach for concrete materials by reducing permeability of concrete after cracking as shown in Figure 2.7 (Li & Herbert 2012). Kishi et al. investigated a mix of expansive agents ($C_4A_3\bar{S}$, $CaSO_4$ and CaO), swelling geo-materials (a combination of silicon dioxide, sodium aluminum silicate hydroxide, and morillonite clay), and various types of carbonates ($NaHCO_3$, Na_2CO_3 , and Li_2CO_3 among others) as partial replacement of cement (10% by weight), producing healing for cracks up to 0.22 mm in concrete with normal water to binder ratio (W/B=0.45) (Kishi et al. 2007; Li & Herbert 2012).

Mechanisms leading to crack self-healing were attributed to the combined effects of geo-materials swelling, expansive agent expansion, and precipitation of carbonates in the crack (Li & Herbert 2012). The self-healing action of cracks of mineral admixtures was evaluated by means of a water permeability test and optical microscopy, as shown in Figure 2.8; furthermore, healing products were characterized by SEM-EDS microanalysis, as shown in Figure 2.9 (Ahn et al. 2010) (Li & Herbert 2012).

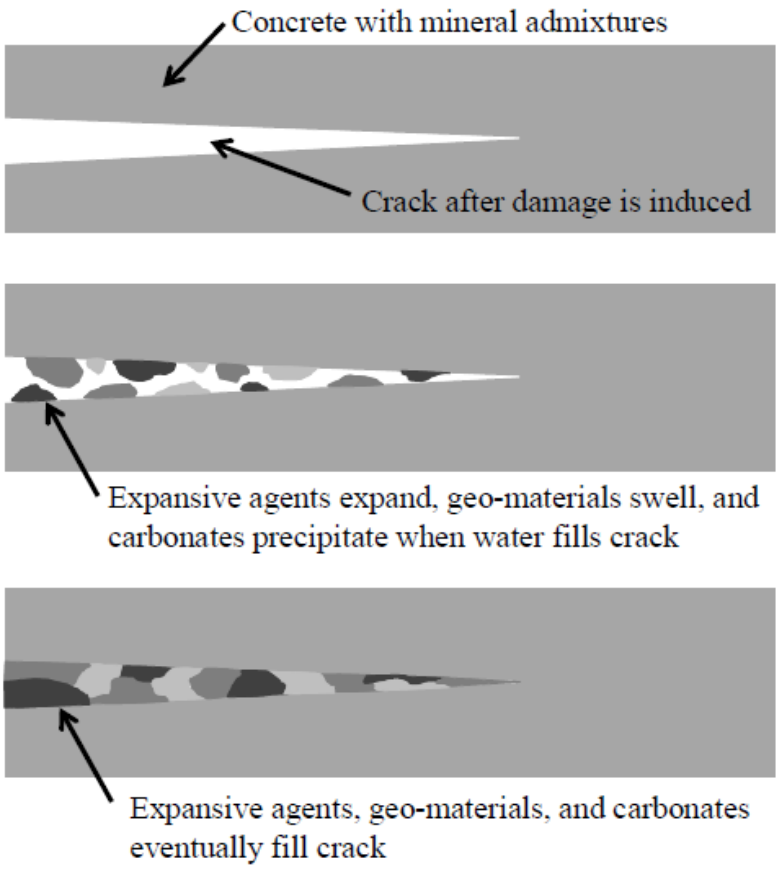

Figure 2.7 Mineral Admixture Self-Healing Approach (Li & Herbert 2012).

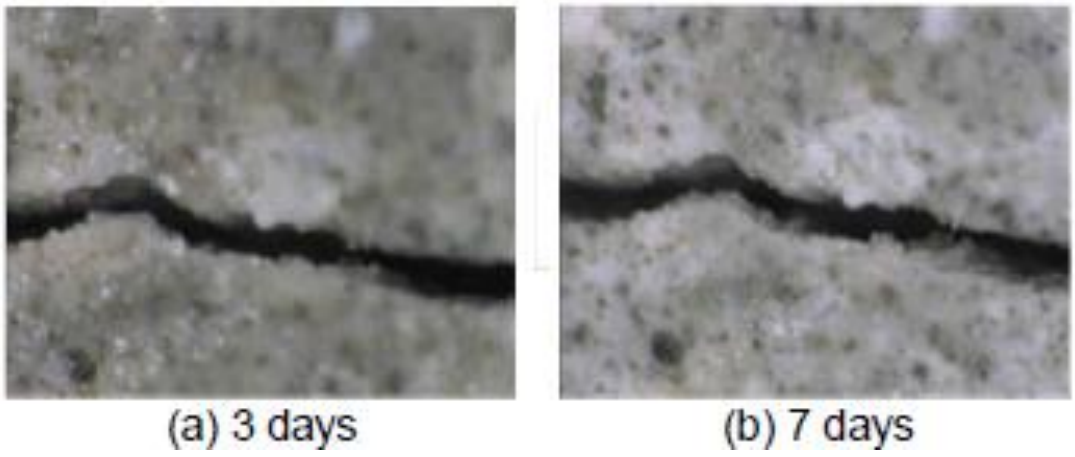

Figure 2.8 Optical Microscope Images of Self-Healing Process of a 0.2 mm Crack Over Time, due to Mineral Admixtures Action (Ahn et al. 2010) (*Continued*).

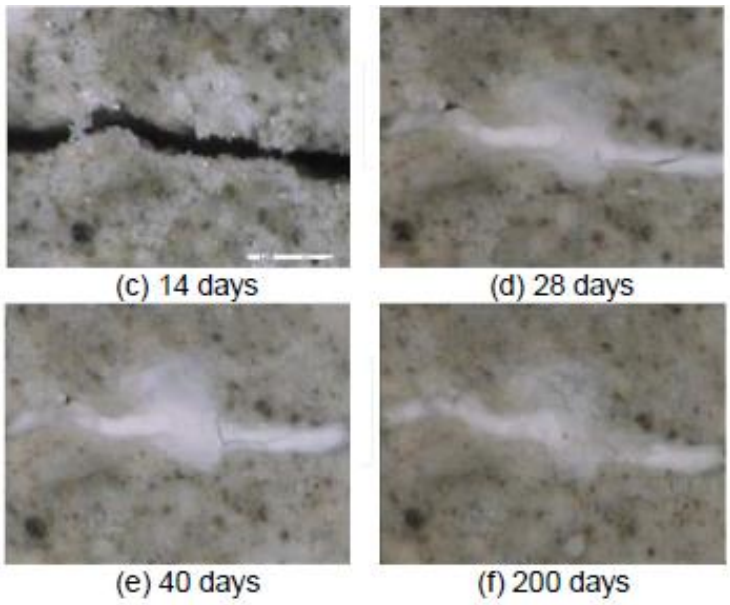

Figure 2.8 (*Continued*) Optical Microscope Images of Self-Healing Process of a 0.2 mm Crack Over Time, due to Mineral Admixtures Action (Ahn et al. 2010).

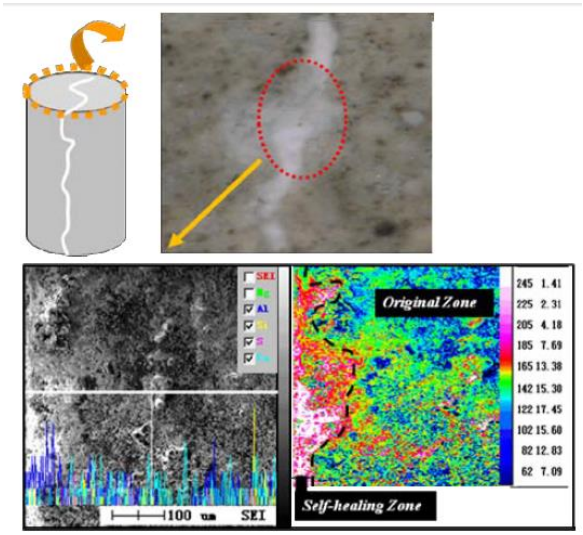

Figure 2.9 Characterization of Healing Products by SEM-EDS (Ahn et al. 2010).

2.3.4 Bacterial Concrete

Bacterial concrete self-healing approach makes use of alkali-resistant bacteria, which can precipitate calcite (calcium carbonate) through carbonate generation during bacteria metabolism, under a high calcium environment as shown in Figure 2.10 (Li & Herbert 2012) (Wiktor & Jonkers 2011) (Thijssen & Jonkers 2009). Specific bacteria selected for this approach must be able to survive conditions of high alkalinity and compressive pressure, as encountered inside

concrete microstructure (Li & Hebert 2012). Furthermore, nutrients must be provided to feed the bacteria, such as calcium lactate (Wiktor & Jonkers 2011) (Li & Hebert 2012).

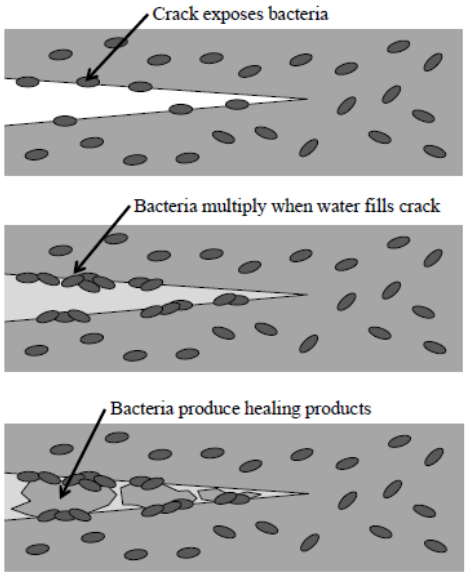

Figure 2.10 Bacterial Concrete Self-Healing Approach (Li & Herbert 2012).

Wiktor and Jonkers evaluated a two component, bio-chemical, self-healing agent consisting of a bacterial spore mixture and calcium lactate, embedded in expanded clay particles (Wiktor & Jonkers 2011). Self-healing results demonstrated that bacterial concrete displays superior self-healing capabilities, as compared to control, by doubling the maximum healable crack size as shown in Figure 2.11 (Wiktor & Jonkers 2011). Proposed healing mechanisms were the direct precipitation of calcium carbonate through metabolic conversion of calcium lactate and the indirect formation of calcium carbonate, due to the reaction of metabolically produced CO_2 , with available calcium hydroxide in the concrete matrix (Wiktor & Jonkers 2011).

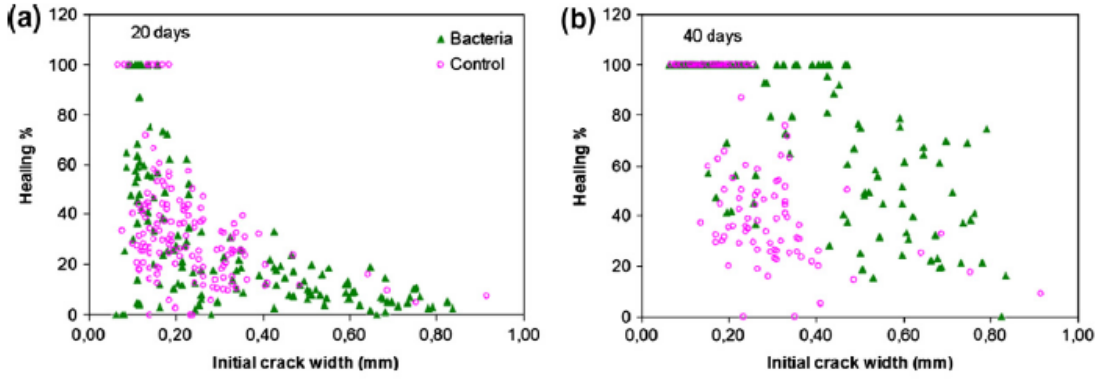

Figure 2.11 Bacterial Concrete Self-Healing Quantification after (a) 20 Days; (b) 40 Days. (Wiktor & Jonkers 2011) *(Continued).*

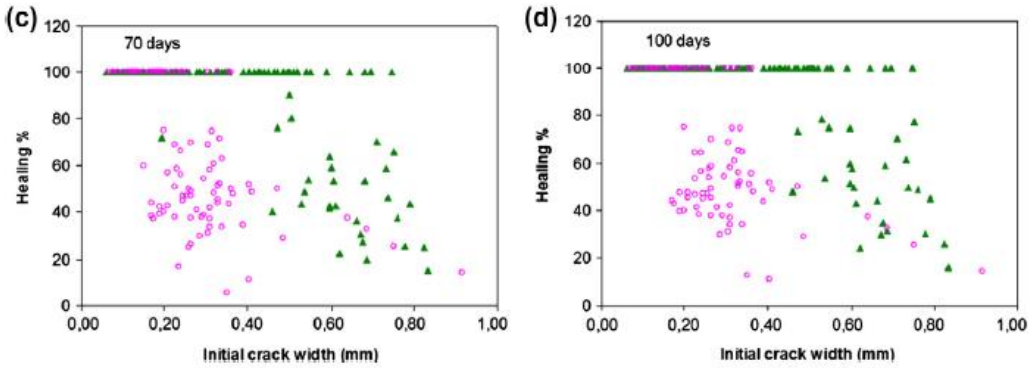

Figure 2.11 *(Continued)* Bacterial Concrete Self-Healing Quantification after: (c) 70 Days; and (d) 100 Days. (Wiktor & Jonkers 2011).

Chemical composition of healing products was confirmed to be calcium carbonate by SEM-EDS analysis where healing products exhibited a calcium, oxygen and carbon composition (indicative of calcium carbonate) and by Fourier-Transform Infrared (FTIR) spectra analysis, which were indicative of calcite and aragonite (crystalline forms of calcium carbonate) (Wiktor & Jonkers 2011).

2.4 Calcium Nitrate in Concrete

Calcium nitrate is a low cost solution, harmless to the environment chemical which serves for multiple purposes as a concrete admixture (Justnes 2005). Calcium nitrate may serve for the following purposes in concrete: (a) set accelerator, (b) counteraction of retardation effect by plasticizers while maintaining rheological properties, (c) long term strength enhancer, (d) anti-freeze admixture, and (e) inhibitor against chloride induced corrosion (Justnes 2005).

Calcium nitrate set acceleration and counteraction of retardation by plasticizers may be achieved by small dosages of (0.2-1% of dry admixture by mass of cement), enhancement of long term strength and anti-freeze effect may be achieved at moderate dosages (1-3%), and corrosion inhibition will require the highest dosages (3-4%) (Justnes 2005).

It is important to note that calcium nitrate is an effective set accelerator but less effective as a hardening accelerator (Oey et al. 2015). It has been reported that calcium nitrate may positively affect very early strength development of concrete (e.g., 8h) but has no significant effect at 1 day strength, thus highlighting the minor effect of calcium nitrate as a hardening accelerating admixture (Justnes 2005). Setting acceleration by calcium nitrate is strongly dependent on the chemical composition of cement and can be observed and analyzed by changes in the heat flow achieved during the induction period of cement hydration (Oey et al. 2015) (Justnes 1995).

2.4.1 Calcium Nitrate Effects on Early Hydration, Set and Strength Development

Abdelrazig et al. studied the effect of calcium nitrate in the early hydration of Portland cement by solution extraction and analysis of cement paste during the first three hours of hydration (Abdelrazig et al. 1999). Major ionic species concentrations were reported in control paste, as well as calcium nitrate admixed paste, as shown in Figures 2.12 and 2.13 (Abdelrazig et al. 1999). In a comparison of Figures 2.12 and 2.13, calcium ion levels increased as expected in calcium nitrate admixed paste, as well as sulphate and hydroxyl ions decreased (Abdelrazig et al. 1999). XRD analysis revealed that the decrease in sulphate and hydroxyl ions was related to an increase in gypsum and calcium hydroxide formation; as compared to control within the first five minutes of the hydration process (Abdelrazig et al. 1999). Abdelrazig et al. suggested that the addition of calcium ions to the system is responsible for sulphate and hydroxide precipitation, presumably to satisfy the solubility product criteria (Abdelrazig et al. 1999).

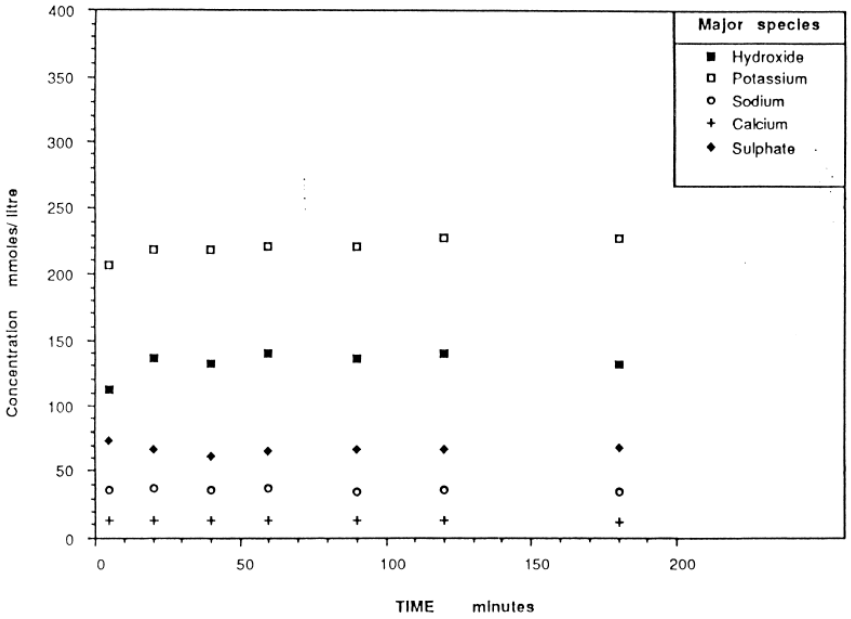

Figure 2.12 Concentration of Major Species in Control System (Abdelrazig et al. 1999)

The increase in the formation of gypsum and calcium hydroxide from solution is of great significance as gypsum plays an important role in ettringite formation, which affects the stiffening process and determines the extend of gypsum substitution in the CSH gel, which in turn influences strength development (Abdelrazig et al. 1999). Furthermore, additional formation of calcium hydroxide and gypsum provide an increase in heat evolution due to their hydration and precipitation, thus increasing temperature and further enhancing the hydration process (Abdelrazig et al. 1999). Importantly, there are many changes to the chemistry of liquid and solid phases of cement paste with the addition of calcium nitrate, but the additional gypsum and calcium hydroxide formation from solution in the first 5 min of hydration is of particular importance in regard to calcium nitrate effects on setting and strength development (Abdelrazig et al. 1999).

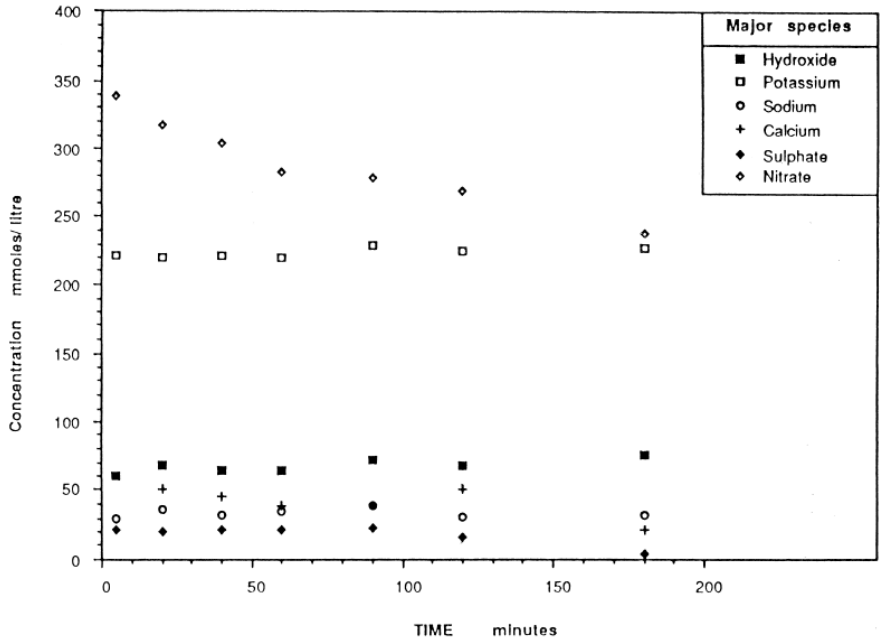

Figure 2.13 Concentration of Major Species in Nitrate System (Abdelrazig et al. 1999)

Justnes studied strength development changes on concrete due to a calcium nitrate admixture and determined that calcium nitrate affects very early strengths (e.g., 8 h) and long term strengths (from 28 days forward), but has no significant strength contribution at 1 day strengths (Justnes 2003). Figures 2.14 and 2.15 summarize Justnes' findings on strength development of concrete admixed with calcium nitrate, showing how strength development is generally affected in a positive fashion with the increase of calcium nitrate dosage at both very early (8h) and late (220 days) ages.

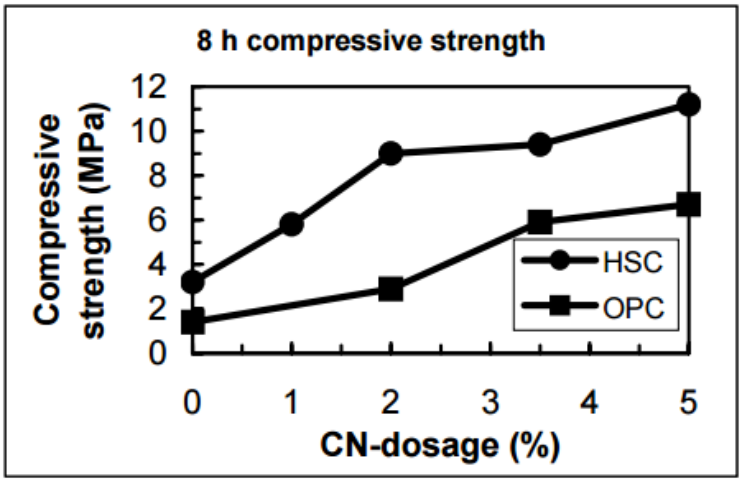

Figure 2.14 Early Compressive Strength (8h) for High Strength Portland Cement (HSC) and Ordinary Portland Cement (OPC) with Different Dosages of Calcium Nitrate (Justnes 2003)

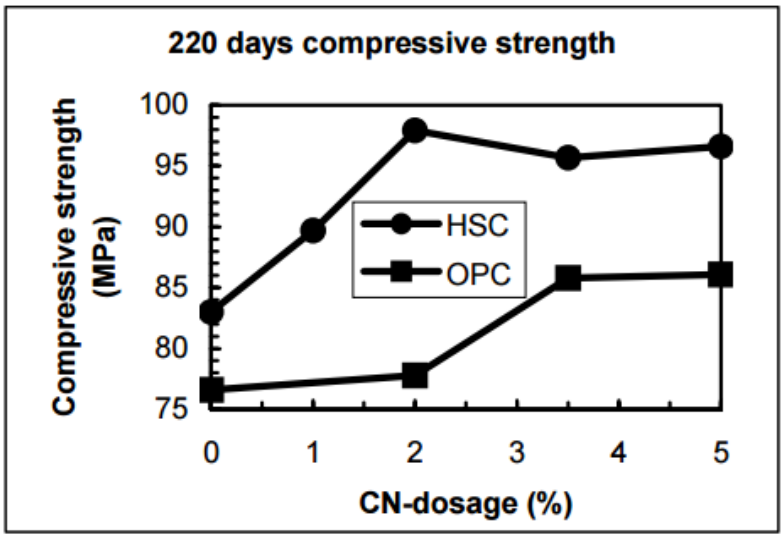

Figure 2.15 Compressive Strength at 220 Days for High Strength Portland Cement (HSC) and Ordinary Portland Cement (OPC) with Different Dosages of Calcium Nitrate (CN) (Justnes 2003)

2.4.2 Calcium Nitrate as Anti-Freeze Admixture

Concrete hydration is strongly affected by temperature, and therefore in cold weather conditions, the setting and hardening of concrete may be severely affected. As the temperature decreases, concrete sets more slowly and develops strength less quickly (Karagöl et al. 2013). It is important to note that concrete must be protected from freezing until it attains a minimum compressive strength of 3.5 MPa; otherwise, if concrete is allowed to freeze in the plastic state, its potential strength will be reduced by more than 50%, while its durability will be negatively affected (Karagöl et al. 2013).

Calcium nitrate functions as an anti-freeze admixture by depressing the freezing point of water and by accelerating setting and very early hardening of concrete (Karagöl et al. 2014). Depressing the freezing point of water protects concrete from an expansion into spaces between aggregate particles of solidifying water before the critical strength is achieved; while a rapid setting and very early hardening allows for a faster achievement of the critical strength (Karagöl et al. 2013) (Karagöl et al. 2014).

2.4.3 Calcium Nitrate as Corrosion Inhibitor Admixture

Justnes experimented with calcium nitrate as a corrosion inhibitor by comparing concrete cylindrical specimens with embedded steel rebar (Justnes 2005). Chlorides were added to the concrete mixes and the performance of calcium nitrate was compared to a more common corrosion inhibitor, calcium nitrite (Justnes 2005). Cylinders were stored in a 38°C and 90%RH environment and inspected over time for expansion cracks in the control specimen; upon the control specimen's cracking, bars were removed from all the specimens and inspected (Justnes 2005). Figure 2.16 shows a rebar removed from specimens after 3 years; the rebar, embedded in the control sample, was badly corroded, while the rebar embedded in concrete admixed with 2%

CN and 4%CN had only minor corrosion and no sign of corrosion respectively (Justnes 2005). It was concluded that calcium nitrate is at least equally efficient as a corrosion inhibitor than calcium nitrite while it is a more economical and less harmful chemical alternative (Justnes 2005).

Figure 2.16 Rebar Removed from Cylinders with 3.2% NaCl (Chlorides) Intermixed after 3 Years of Storage at 38°C and 90% RH. Upper, Middle and Bottom Bars are from Control, 2%CN Admixed and 4%CN Admixed Concrete Respectively (Justnes 2005).

2.5 Self-Healing by Microencapsulated Healing Agents

2.5.1 Microcapsules Material Selection

Microcapsule material selection holds a great significance for the proper implementation of self-healing through encapsulation of healing agents. Microcapsules must be strong enough to withstand the concrete mixing process and at the same time, weak enough so that breakage would take place upon a cracking event. Another important factor is the shelf-life of the microcapsules, which is strongly depend on microcapsule material. Several materials have been utilized to encapsulate healing agents for different types of self-healing concrete applications. Among these are glass, natural fibres, gelatine, paraffin, wax, polyurethane, and ceramics (Hilloulin et al. 2015). However, not all of these are able to resist the mixing process thus; these are not suitable as microencapsulating materials (Hilloulin et al. 2015).

Dry suggested the use of polymeric encapsulation in order to easily fine tune capsule properties, as well as to provide a material able to resist the mixing process (Hilloulin et al. 2015) (Dry 1994). Furthermore, Hilloulin et al. studied several polymeric materials as

alternatives for encapsulation of healing agents for self-healing concrete application obtaining promising results (Hilloulin et al. 2015).

2.5.2 Microcapsules in Cementitious Materials

Microencapsulation of healing agents approach for self-healing consists in incorporating cementitious materials with uniformly dispersed encapsulated chemical agents which upon their release due to capsule rupture in a crack can react with water, air, heat, components provided in the cementitious matrix (e.g. catalyzers), the cementitious matrix itself, or a combination of these (Van Tittelboom & De Belie 2013). Regardless of the nature of the reaction of healing agents, once released in the cracks these will generate newly formed components filling the cracks and thus repair the material.

The concept of self-healing through microencapsulation was first introduced by White et al. in polymer composites (White et al. 2001). White et al utilized a microencapsulated healing agent embedded in the composite matrix, which contained a catalyst capable of polymerizing the healing agent (White et al. 2001). As cracks formed in the matrix, microcapsules ruptured releasing the healing agent into the cracks through capillary action. Finally, the healing agent contacted the catalyst, triggering polymerization and thus, healing the cracks (White et al. 2001). White et al autonomic healing concept is shown in detail in Figure 2.17. Since the introduction of this novel autonomic healing system, the microencapsulation of chemical agents for self-healing application has been further developed in polymers and composites with a recent initiation as an application for concrete materials (Wang et al. 2013).

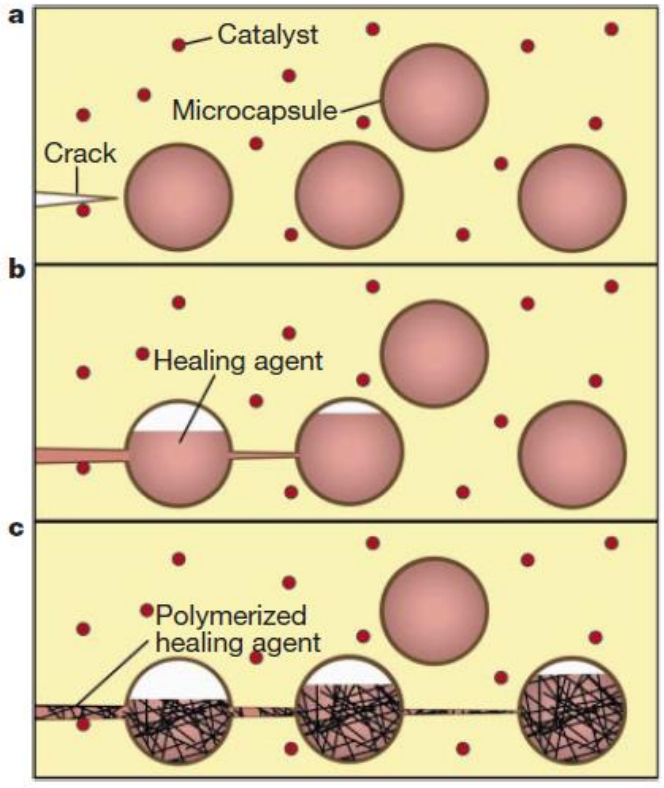

Figure 2.17 The Autonomic Healing Concept (White et al. 2001).

Encapsulation of healing agents to enhance or endow self-healing characteristics in cementitious materials presents a promising approach, due to: (a) The versatility of these systems, which allows for encapsulation of many different chemicals in a broad variety of sizes extending to the sub-micron size; (b) the potential for long shelf life, which may allow self-healing to remain active for long periods of time; and (c) the possibility of providing cementitious materials with self-healing mechanisms, regardless of environmental conditions (Li & Herbert 2012).

There are several factors which play a pivotal role for the proper functioning of self-healing through microencapsulation of healing agents. These factors are the following: (a) Adequate dosage and uniform distribution of microcapsules, so that sufficient healing agent is available throughout the cementitious matrix for effective self-healing; (b) adequate bond strength between the microcapsule external surface and the cementitious matrix so that rupture takes place upon a cracking event; and (c) a thigh crack width in order for robust healing to occur (Van Tittelboom & De Belie 2013).

In recent years, several healing agents were investigated including sodium silicate, polyurethane, epoxy, cyanoacrylates, and bacterial spores (Wang et al. 2014; Li et al. 2013; Huang & Ye 2011; Pelletier et al.; Kaes et al. 2014; Van Tittelboom et al. 2014). Furthermore, dual-component self-healing systems consisting of a healing agent and a catalyzer have also been explored (Yang et al. 2011).

Huang and Ye (2011) investigated a self-healing system consisting of wax shell capsules with sodium silicate as a healing agent in engineered cementitious composites (ECC). Beam specimens were tested by three point bending to 1mm deformation to induce cracks and then re-tested to failure after being allowed to self-heal. After re-test significant improvement of mechanical properties were reported as compared to control, as shown in Figure 2.18.

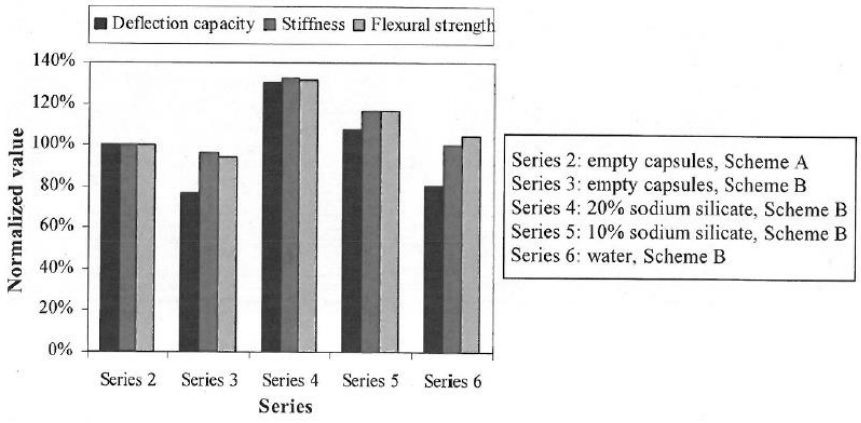

Figure 2.18 Comparison of Mechanical Properties Recovery (Huang & Ye 2011).

Yang et al. investigated self-healing of carbon microfiber reinforced mortar through a dual-component system consisting of oil core and silica shell microcapsules with methylmethacrylate (MMA) monomer and a triethylborane (TEB) solution as a healing agent and catalyst, respectively (Yang et al. 2011). Figure 2.19 illustrates the self-healing mechanism proposed by Yang et al.

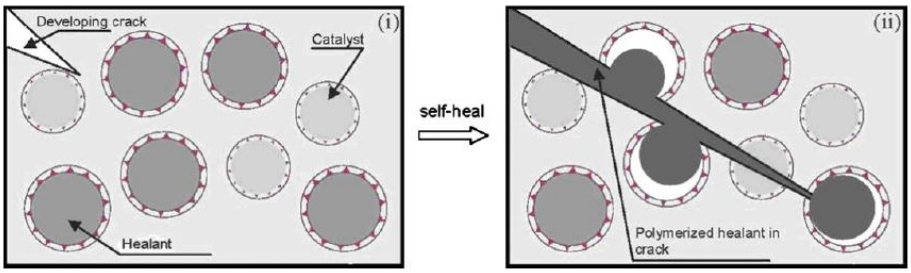

Figure 2.19 Illustration of Self-Healing Mechanism (Yang et al. 2011).

Reductions in the gas permeability coefficient, when compared to control was reported after loading specimens to 80% of ultimate compressive strength and allow them to heal for 24 hours, as shown in Figure 2.20 (Yang et al. 2011).

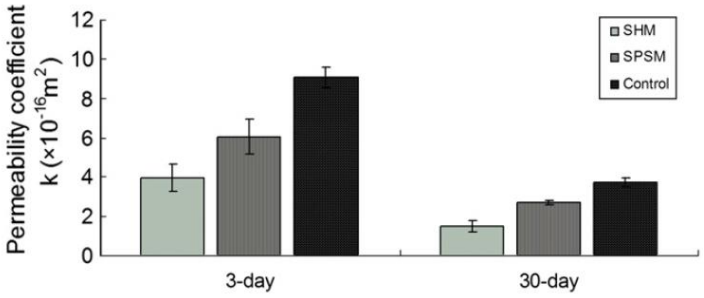

Figure 2.20 Permeability Coefficients of Cement Mortar Composite at 3-Day and 30-Day Curing Ages, Loaded under 80% of Ultimate Compressive Strength and Allowed to Heal for 24 Hours (Yang et al. 2011).

Further, a fatigue test under uniaxial compression cyclic loading was conducted on cylindrical specimens; results revealed improvements in crack resistance and toughness, compared to control specimens as shown in Figure 2.21 (Yang et al. 2011).

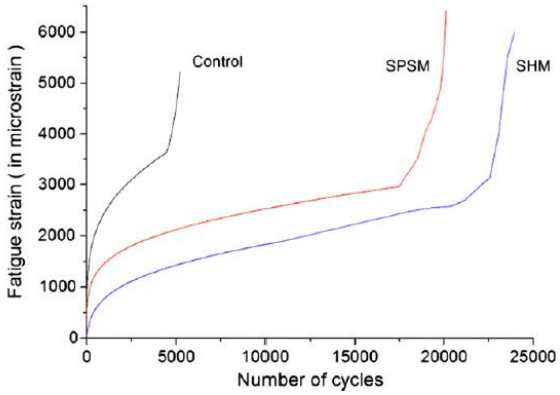

Figure 2.21 Fatigue Test Results under Uniaxial Compression Cyclic Loading (Yang et al. 2011).

Finally, healing products were investigated through FSEM-EDS microanalysis of a cylindrical specimen allowed to heal for 24 hours after being loaded to 80% of its ultimate compressive strength as shown in Figure 2.22 (Yang et al. 2011). FSEM-EDS microanalysis results revealed Carbon (C), Oxygen (O), and Silicon (Si) as the main components of the healing products, thus suggesting the presence of polymerized MMA in the cracks and thereby confirming the proper functioning of the healing mechanism (Yang et al. 2011).

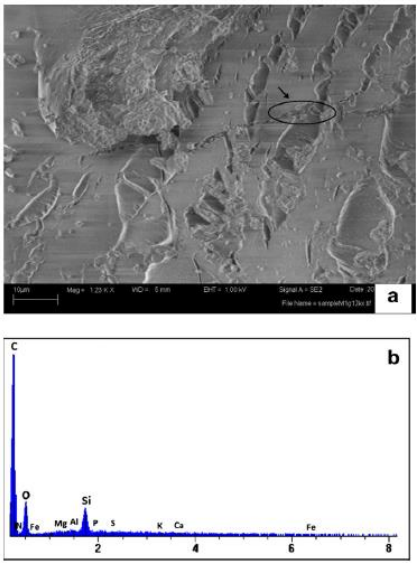

Figure 2.22 FSEM-EDS Analysis of Healing Products (Yang et al. 2011).

2.6 Shape Memory Alloy (SMA)

In 1932, the shape memory alloy (SMA) was first discovered by a Swedish physicist, Arne Ölander, who experimented with gold-cadmium (Au-Cd) alloys (Jani et al. 2013). Later in 1941, the term "shape-memory" was introduced by Vernon for his polymeric dental material (Jani et al. 2013). However, the importance of shape memory materials (SMMs) was not recognized until 1962, when William Buhler and Frederick Wang revealed the shape memory effect (SME) in nickel-titanium (NiTi) alloy, also known as nitinol (Jani et al. 2013).

Since Buhler and Wang's discovery, the demand for SMAs for engineering and technical applications has been increasing in a broad range of fields such as structures and composites, automotive, aerospace, biomedical, etc. (Jani et al. 2013). SMAs are metallic alloys that return to the original shape after being deformed by means of a transformation phenomenon known as shape memory effect (SME). SME may be activated by external stimuli such as heat or magnetic field for MSMAs (Jani et al. 2013).

2.6.1 Shape Memory Effect and Pseudoelasticity

SMAs present six possible phase transformations and can exist in two different phases: martensite and austenite, which display three different crystal structures, i.e., two for the martensite phase (twinned martensite and detwinned martensite), and one for the austenite phase, as shown in Figure 2.23 (Jani et al. 2013).

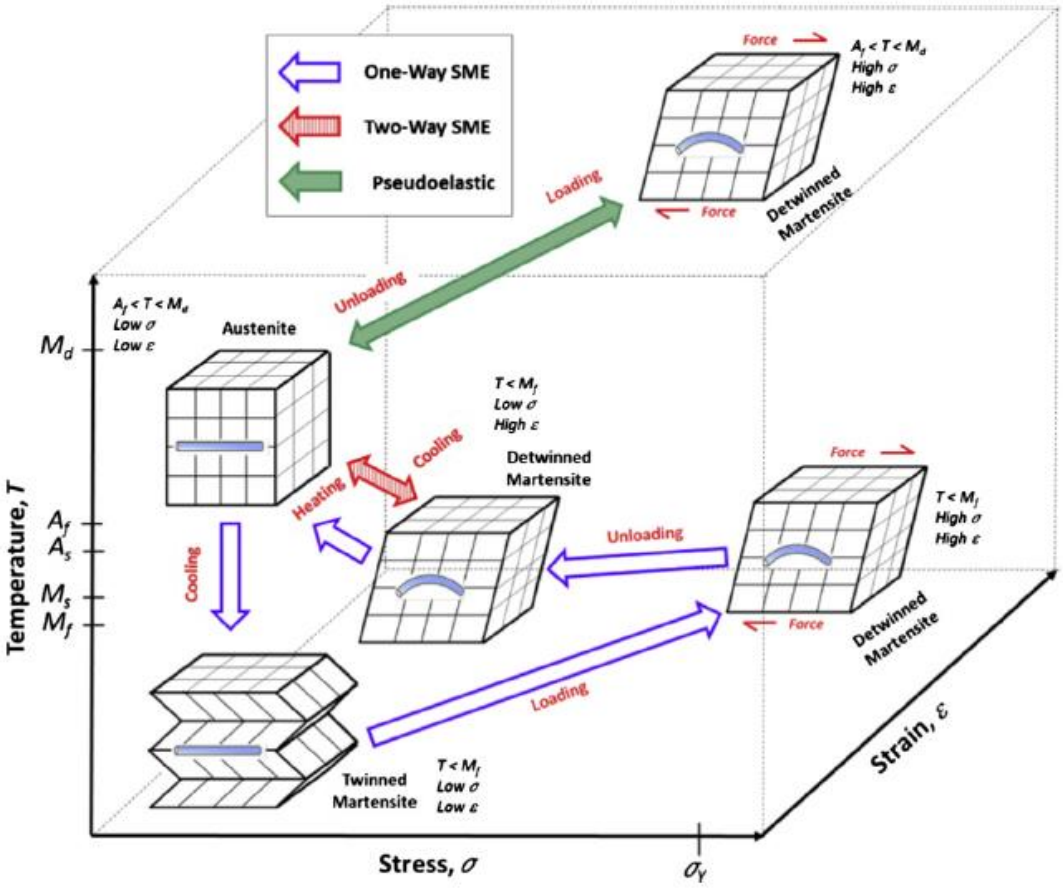

Figure 2.23 Phases in SMA and Crystal Structures (Jani et al. 2013).

The austenite and martensite structures are stable at high and low temperature respectively, thus when SMA is heated it transforms from martensite into the austenite phase (Jani et al. 2013). The transformation to austenite phase will start at the so-called austenite-start-temperature (A_s) and the material will complete its transition to the austenite phase once the austenite-finish-temperature (A_f) is achieved (Jani et al. 2013). When SMA is heated beyond A_s it starts contracting to recover its original shape while transforming into the austenite structure (Jani et al. 2013). When cooled, the phase transformation will start to revert at the martensite-start-temperature (M_s) and will be completed at the martensite-finish-temperature (M_f) (Jani et al. 2013). It is also important to notice that the highest temperature at which martensite can no longer be stress induced is known as M_d, and above this temperature the SMA will deform permanently like an ordinary metal (Jani et al. 2013).

The phenomena discussed above are known as shape memory effect and pseudoelasticity (or superelasticity) and can be categorized into three shape memory characteristics: (a) one-way shape memory effect (OWSME), where SMA retains a deformed state after the removal of a load and then recovers its original shape upon heating; (b) two-way shape memory effect (TWSME) in which SMA can remember its shape at both high and low temperatures; and (c) pseudoelasticity (PE) or superelasticity (SE) where SMA reverts to its original shape after

loading without the need of thermal activation at temperatures between A_f and M_d (Jani et al. 2013). Shape memory effect and superelasticity are illustrated in Figure 2.24.

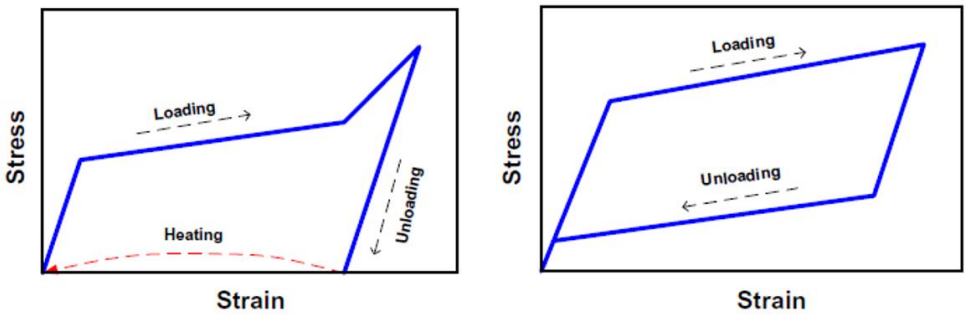

(a) (b)

Figure 2.24 SMA Stress vs. Strain Curves Illustration (a) Shape Memory Effect (b) Superelasticity (Sun et al. 2012).

Kuang and Ou investigated the application of SMA wires for crack closing action and the combination of SMA wires and hollow fibers containing adhesives for self-healing application in concrete as shown in Figure 2.25 (Kuang & Ou 2008).

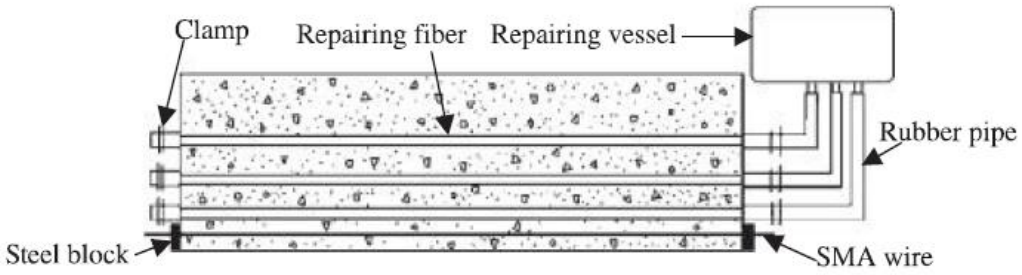

Figure 2.25 Self-Repairing Concrete using Fiber Containing Adhesives and SMA Wires (Kuang & Ou 2008).

Experimental results showed that superelastic SMA wires provided self-restoration capacity to concrete beams by reversing deflection and closing cracks almost completely after unloading as show in Figure 2.26 (Kuang & Ou 2008). Furthermore, adhesive released upon cracking by broken fibers were able to heal cracks and restore structural capacity of the crack site as shown in Figure 2.27 (Kuang & Ou 2008).

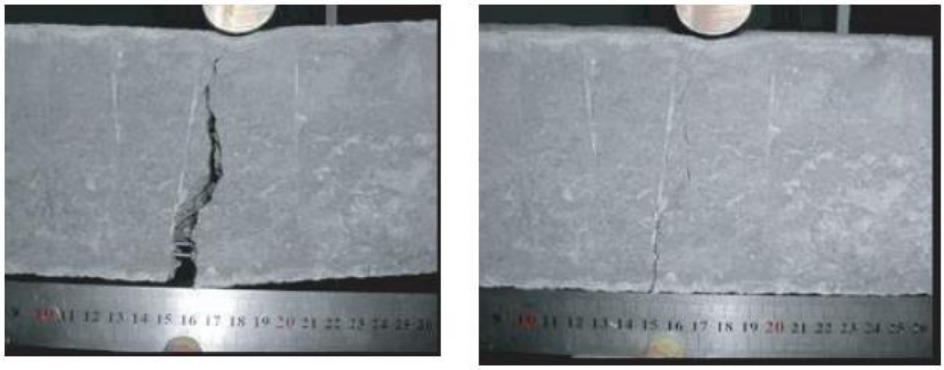

Figure 2.26 Crack Closing due to SMA (Kuang & Ou 2008).

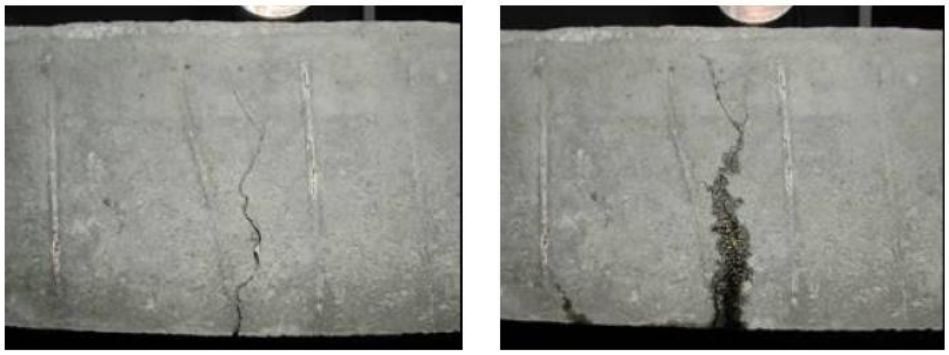

Figure 2.27 Crack Closing and Self-Healing due to Combined Action of SMA and Adhesive Released from Hollow Fibers (Kuang & Ou 2008).

Sun et al. studied factors affecting self-repair capability of SMA wires in composite materials for application in concrete structures. SMA wires were utilized as internal reinforcement, embedded in the material as well as external reinforcement outside the material as shown in Figure 2.28 (Sun et al. 2013).

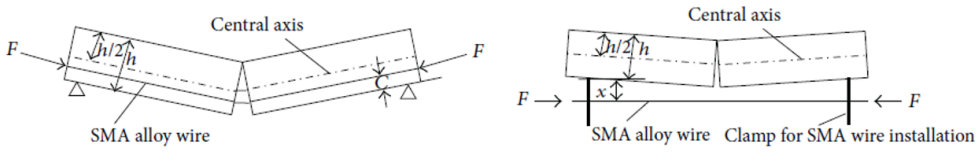

(a) (b)

Figure 2.28 Methods for Self-Repairing (a) Internal Embedment Repair Method (b) External Installation Repair Method (Sun et al. 2013).

Sun et al. concluded that while internal and external reinforcement have their own advantages and disadvantages both internal and external reinforcement methods are viable for crack closure application in concrete structures (Sun et al. 2013).

2.7 Evaluation of Self-Healing Concrete

2.7.1 Microscopy

Microscopy is one of the most widely utilized methods to evaluate cementitious materials (Tang et al. 2015). In this evaluation technique several types of microscopes are utilized to study the microstructure of specimens before and after healing (Tang et al. 2015). Microscopy methods largely utilized in concrete evaluation are petrography, optical microscopy, scanning electron microscopy (SEM) and environmental scanning electron microscopy (ESEM) (Tang et al. 2015).

In optical microscopy a digital microscope is utilized to observe crack surfaces, determine crack width and assess the progress of healing (Tang et al. 2015). Furthermore, SEM and ESEM techniques are based on the interaction between a sample and an electron beam which produces several signals that can be detected to form highly magnified images (Tang et al. 2015). Figure 2.29 illustrates SEM functioning. SEM and ESEM techniques allow to determine the morphology, shape and size of healing products as well as to obtain some crystallographic and chemical information of a specimen when coupled with backscattered electron imaging (BSEI) (Tang et al. 2015). BSEI provides atomic contrast (Z contrast) in images which is generated by the detection of backscattered electrons. Lastly, petrographic examination which is a method originally utilized to investigate the structure of rocks, consists in the exploration of microscopic thin sections of a specimen by a petrological microscope (Tang et al. 2015). This type of analysis can provide microstructural information of a specimen as well as visualization of cracks and healing products (Tang et al. 2015). ASTM C1723 “Examination of Hardened Concrete Using Scanning Electron Microscopy” and ASTM C856 “Standard Guide for Petrographic Examination of Hardened Concrete” are standards available to conduct SEM and Petrographic examination of concrete materials.

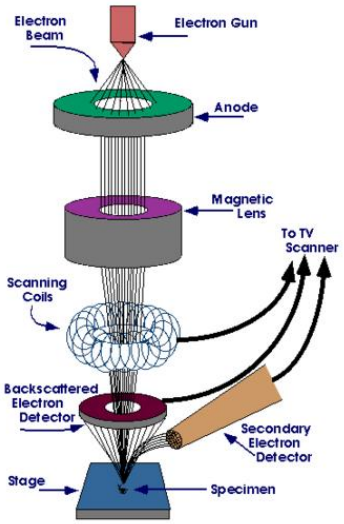

Figure 2.29 SEM Functioning (Purdue 2016).

2.7.2 Imaging

Imaging methods are often considered to examine cementitious materials before and after healing. However, visualization of healing agents released from embedded capsules or tubes and other quantification analysis are also possible with these techniques (Tang et al. 2015). Major imaging methods classified as imaging techniques include X-ray radiography/tomography, neutron radiography/tomography and digital image correlation (Tang et al. 2015). Radiography provides 2D images of the structure of the specimen while tomography provides 3D images generated by digital geometry processing from 2D images as shown in Figure 2.30 (Tang et al. 2015). Both radiography and tomography can utilize as a source of electromagnetic radiation, X-ray or neutron radiation (Tang et al. 2015). Figure 2.31 illustrate N-Ray and X-Ray radiographies.

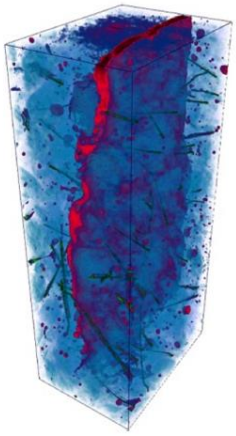

Figure 2.30 3D Image Generated by Tomography (Tang et al. 2015).

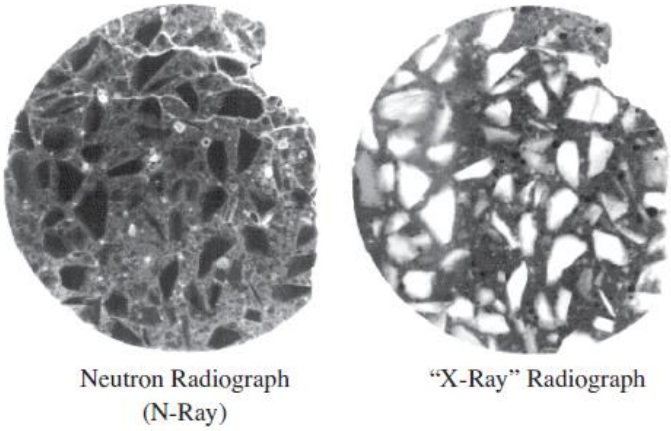

Figure 2.31 N-Ray and X-Ray Radiography Images of Concrete (Tang et al. 2015).

Lastly, digital image correlation is a technique to detect changes in 2D and 3D images by tracking and image registration methods (Tang et al. 2015). This technique can help to investigate crack development and closure as well as to provide deformations, displacements, and optical flow measurements (Tang et al. 2015).

2.7.3 Spectroscopy

Spectroscopy examination methods have been extensively utilized to characterize healing products in cracks for determination of their chemical composition (Tang et al. 2015). All spectroscopic techniques involve the interaction between a beam of electromagnetic radiation and a specimen (Tang et al. 2015). This interaction generates signals which can be subsequently analyzed (Tang et al. 2015). The position, shape and intensities of peaks of the spectrum generated by the detection of spectroscopic signals provide valuable information about the atomic and molecular structure of the specimen examined (Tang et al. 2015).

Major spectroscopy techniques are X-ray spectroscopy, infrared spectroscopy, Raman spectroscopy and X-ray diffraction. X-ray spectroscopy utilizes the X-ray spectrum of light while infrared analysis deals with the infrared region of light (Tang et al. 2015). Both of these methods are helpful to detect healing products generated in cracks and obtain information about their chemical nature (Tang et al. 2015). Furthermore, Raman spectroscopy depends on scattering of monochromatic light and provides information of chemical composition of inspected components (Tang et al. 2015). Lastly, X-ray diffraction measures the properties of X-ray beams diffracted by the atomic structure of a specimen generating valuable information about the chemical composition and structure of the material examined (Tang et al. 2015). Spectroscopy techniques are illustrated in Figure 2.32.

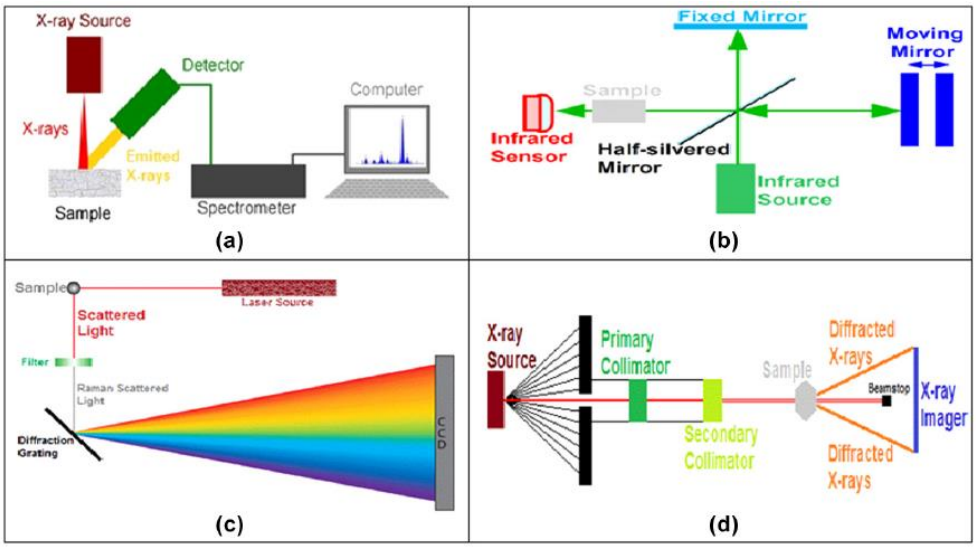

Figure 2.32 Spectroscopy Approaches: (a) X-ray Spectroscopy; (b) Infrared Spectroscopy; (c) Raman Spectroscopy and (d) X-ray Diffraction Analysis (Tang et al. 2015).

2.7.4 Ultrasonic Testing (UT)

Ultrasonic testing of concrete utilizes very short ultrasonic waves (50kHz) which are transmitted to concrete through a transducer and detected after the interaction with the material by the same or another transducer (Tang et al. 2015) (Özerkan & Yaman 2007). UT allows for the detection of internal flaws and discontinuities by the analysis of the emitted and received signals as shown in Figure 2.33 (Tang et al. 2015) (Özerkan & Yaman 2007).

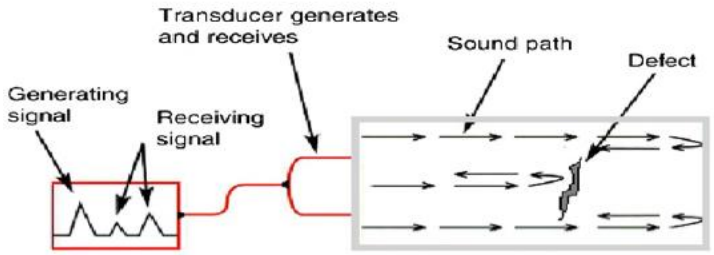

Figure 2.33 Ultrasonic Testing of Concrete (Tang et al. 2015).

Ultrasonic testing has been utilized to inspect concrete since 1940s with ultrasonic pulse velocity (UPV) being the most widely evaluated characteristic (Özerkan & Yaman 2007). UPV can be used for many applications in concrete materials among which, the determination of cracks uniformity, dynamic modulus of elasticity and estimated strength are of great relevance (Özerkan & Yaman 2007). Moreover ASTM C597 "Test Method for Pulse Velocity through Concrete" is an available standard for UT application in concrete materials.

2.8 References

Abdelrazig B.E.I., Bonner D.G., Nowell D.V., Dransfield J.M., Egan P.J., The solution chemistry and early hydration of ordinary Portland cement pastes with and without admixtures, Thermochimica, Acta 340-341, 1999, pages 417-430.

Ahn T.H. and Kishi T., Crack self-healing behavior of cementitious composites incorporating various mineral admixtures, Journal of Advanced Concrete Technology, Volume 8, No.2, 2010, pages 171-186.

Bullard Jeffrey W., Jennings Hamlin M., Livingston Richard A., Nonat Andre, Scherer George W., Schweitzer Jeffrey S., Scrivener Karen L., Thomas Jeffrey J., Mechanisms of cement hydration, Cement and Concrete Research, Volume 41, 2010, Pages 1208-1223.

Caldarone Michael A., High-Strength Concrete: A Practical Guide, Taylor & Francis, 2009.

Dry C. Smart multiphase composite materials that repair themselves by a release of liquids that becomes solids, SPIE Proc, 1994.

Edvardsen C., Water Permeability and Autogenous Healing of Cracks in Concrete. ACI Materials Journal, 1999, Title no. 96-M56.

Gartner E.M., Young J.F., Damidot D.A., Jawed I., Hydration of Portland cement, in: J.Bensted, P.Barnes (Eds.), Structure and Performance of Cements, 2nd Edition, Spon Press, New York, 2002, pages 57-113.

Haoliang Huang and Guang Ye, Application of sodium silicate solution as self-healing agent in cementitious materials, International RILEM Conference on Advances in Construction Materials Through Science and Engineering, Vol. 1, 2011, 530-535.

Hilloulin Benoit, Van Tittelboom Kim, Gruyaert Elke, De Belie Nele, Loukili Ahmed, Design of polymeric capsules for self-healing concrete, Cement & Concrete Composites, Volume 55, 2015, pages 298-307.

Huang Haoliang, Ye Guang, Damidot Denis, Characterization and quantification of self-healing behaviors of microcracks due to further hydration in cement paste, Cement and Concrete Research, Volume 52, 2013, pages 71-81.

Jani Jaronie Mohd, Leary Martin, Subic Aleksandar, Gibson Mark A., A review of shape memory alloy research, applications and opportunities, Materials and Design, Volume 56, 2013, pages 1078-1113.

Justnes Harald, Technical calcium nitrate as set accelerator for cement at low temperatures, Cement and Concrete Research, Volume 25, No.9, 1995, pages 1766-1774.

Justnes Harald, Calcium nitrate as a multifunctional concrete admixture, SINTEF Technology and Society, 2005.

Justnes Harald, Explanation of Long-Term Compressive Strength of Concrete Cause by the Set Accelerator Calcium Nitrate, Proceedings of the 11th International Congress on the Chemistry of Cement (ICCC), 2003, pages 475-484.

Justnes Harald, Corrosion Inhibitors for Concrete, Proceedings of the International Symposium on Durability of Concrete I Memory of Prof. Dr. Raymundo, Rivera, 2005, pages 179-199.

Kaes, M., Van Tittelboom, K., and N. De Belie. The efficiency of self-healing cementitious materials by means of encapsulated polyurethane in chloride containing environments. Construction and Building Materials, Vol. 71, 2014, 528-537.

Kan Li-Li, Shi Hui-Sheng, Sakulich Aaron R., Li Victor C., Self Healing Characterization of Engineered Cementitious Composite Materials, ACI Materials Journal, 2010.

Karagöl Fatma, Demirboga Ramazan, Kaygusuz Mehmet Akif, Yadollahi Mehrzad Mohabbi, Polat Riza, The influence of calcium nitrate as antifreeze admixture on the compressive strength of concrete exposed to low temperature, Cold Regions Science and Technology, Volume 89, 2013, pages 30-35.

Karagöl Fatma, Demirboga Ramazan, Khushefati Waleed H., Behavior of fresh and hardened concretes with antifreeze admixtures in deep-freeze low temperatures and exterior winter conditions, Construction and Building Materials, Volume 76, 2015, pages 388-395.

Kishi T., Ahn T., Hosoda A., Suzuki S., and Takaoka H., Self-healing behavior by cementitious recrystallization of cracked concrete incorporating expansive agent, In: 1st International Conference on Self-Healing Materials, 2007.

Kuang Yachuan, Ou Jinping, Self-repairing performance of concrete beams strengthened using superelastic SMA wires in combination with adhesives released from hollow fibers, Smart Materials and Structures, 2008.

Lasaga A.C., Rate laws of chemical reactions, in: Lasaga A.C., Kirkpatrick R.J. (Eds.), Kinetics of Geochemical Processes, No. 8 in Reviews in Mineralogy, Mineralogical Society of America, 1981, pages 1-68.

Lauer Kenneth R. and Slate Floyd O., Autogenous Healing of Cement Paste, ACI Journal Proceedings, Volume 52, Issue 6, 1956, pages 1083-1098.

Lea F.M, The Chemistry of Cement and Concrete, Third Edition, Edward Arnold, 1970.

Li Victor C., Yang En-Hua, Self Healing in Concrete Materials, Springer Series in Material Science, Self Healing Materials, Volume 100, pages 161-193.

Li Victor C., Hebert Emily, Robust Self-Healing Concrete for sustainable Infrastructure, Journal of Advanced Concrete Technology, Volume 10, 2012, pages 207-218.

Li W, Jiang Z, Yang Z, Zhao N, Yuan W (2013) Self-Healing Efficiency of Cementitious Materials Containing Microcapsules Filled with Healing Adhesive: Mechanical Restoration and Healing Process Monitored by Water Absorption. PLoS ONE 8(11): e81616. doi:10.1371/journal.pone.0081616.

Mihashi Hirozo, Nishiwaki Tomoya, Development of Engineered Self-Healing and Self-Repairing Concrete, Journal of Advanced Concrete Technology, Volume 10, 2012, pages 170-184.

Mindess Sidney, Young J.Francis, Darwin David, Concrete, 2nd Edition, Pearson Education, 2002.

Morel F.M.M., Principles of Aquatic Chemistry, Wiley-Interscience, New York, 1983.

Neville Adam, Autogenous Healing - A Concrete Miracle?, Concrete International, Design & Construction, American Concrete Institute, Volume 24, Issue 11, 2002, pages 76-82.

Oey Tandre, Stoian Julyan, Li Jialin, Vong Cecillia, Balonis Magdalena, Kumar Aditya, Franke Wolfram, Sant Gaurav, Comparison of $Ca(NO_3)_2$ and $CaCl_2$ Admixtures on Reaction, Setting, and Strength Evolution in Plain and Blended Cementing Formulations, ASCE Journal of Materials in Civil Engineering, Volume 27, Issue 10, 2015.

Özerkan G.N., Yaman Ö., Evaluation of cement mortars by ultrasound, 4th Middle East NDT Conference and Exhibition, 2007.

Pelletier, M., Brown, R., Shukla, A., and A. Bose. Self-healing concrete with a microencapsulated healing agent. Available online: http://energetics.chm.uri.edu/system/files/ Self%20healing%20concrete%20-7-11.pdf (accessed 3 July 2015).

Purdue University, Scanning Electron Microscope, Radiological and Environmental Management, Accessed March 2016, https://www.purdue.edu/ehps/rem/rs/sem.htm.

Sun L., Huang W.M., Ding Z., Zhao Y., Wang C.C., Purnawali H., Tang C., Stimulus-responsive shape memory materials: A review, Materials and Design, Volume 33, 2012, pages 577-640.

Sun Li, Liang Dezhi, Gao Qianqian, Zhou Jianhong, Analysis on Factors Affecting the Self-Repair Capability of SMA Wire Concrete Beam, Hindawi Publishing Corporation, Mathematical Problems in Engineering, 2013.

Tang Waiching, Kardani Omid, Cui Hongzhi, Robust evaluation of self-healing efficiency in cementitious materials - A review, Construction and Building Materials, Volume 81, 2015, pages 233-247.

Thijssen Arjan and Jonkers Henk M., Microscopic analysis of calcium carbonate based crack-filling material produced by bacteria in novel type of self-healing concrete , 31th International Conference on Cement Microscopy, Volume 1, 2009, pages 199-205.

Van Tittelboom, K., De Belie, N., Van Loo, D., and P. Jacobs. Self-healing efficiency of cementitious materials containing tubular capsules filled with healing agent. Cement and Concrete Composites, Vol. 33, 2011, 497–505.

Van Tittelboom, K, and N. De Belie. Self-Healing in Cementitious Materials – A Review. Materials, Vol.6, 2013, 2182-2217.

Wang J.Y., Soens H., Verstraete W., De Belie N., Self-healing concrete by use of microencapsulated bacterial spores, Cement and Concrete Research 56 (2014) 139-152.

White SR, Sottos NR, Geubelle PH, Moore JS, Kessler MR, Sriram SR, et al. Autonomic healing of polymer composites. Nature 2001; 409 (6822):794.

Wiktor Virginie, Jonkers Henk M., Quantification of crack-healing in novel bacteria-based self-healing concrete, Cement & Concrete Composites, Volume 33, 2011, pages 763-770.

Wu Min, Johannesson Björn, Geiker Mette, A review: Self-healing in cementitious materials and engineered cementitious composite as a self-healing material, Construction and Building Materials, Volume 28, 2012, pages 571-583.

Yang Z.X., Hollar J., He X.D.,Shi X.M., A self-healing cementitious composite using oil core/silica gel shell microcapsulses, Cem.Concr.Compos 33 (2011) 506-512.

CHAPTER 3

CHARACTERIZATION OF SELF-HEALING PROCESSES INDUCED BY CALCIUM NITRATE MICROCAPSULES IN CEMENT MORTAR

3.1 Introduction

Infrastructure deterioration is a major challenge due to the large amounts of economic resources required to inspect, maintain, and repair in-service structures. Concrete structures are a major part of the world's infrastructure and therefore their deterioration is of great concern. Concrete can deteriorate due to several environmental factors, which can chemically or physically attack the material. Regardless of the type of environmental conditions that a concrete structure is exposed to, the development of cracks provides an effortless access to harmful substances into the structure, which in turn accelerates deterioration. For this reason, innovative solutions to control and reduce cracking in concrete structures are of great importance for the future of infrastructure resiliency and sustainability.

Several strategies have been proposed to improve cementitious materials durability and the resiliency of concrete structures through autonomic healing systems. These systems may be broadly sorted into five categories: (a) chemical encapsulation; (b) bacterial encapsulation; (c) mineral admixtures; (d) chemical in glass tubing; and (e) intrinsic self-healing with self-controlled tight crack width (Li et al. 2012). These alternatives focus on the development of engineered concrete materials capable of either enhancing the well-studied self-healing properties of cementitious materials or endowing new self-healing mechanisms (Wu et al. 2012).

Encapsulation of healing agents to promote self-healing is a promising alternative due to: (a) its versatility, which allows the encapsulation of several chemicals in a broad variety of sizes down to nano-size; (b) its capability for a long shelf life; and (c) the possibility to provide cementitious materials with a self-healing mechanism independent from environmental conditions, which may allow for its application in a broad type of infrastructure (Li et al. 2012). However, the evaluation and application of this technology to cementitious materials is still in its early stages (Wang et al. 2014).

Several healing agents have been evaluated in recent years including sodium silicate, polyurethane, epoxy, cyanoacrylates and bacterial spores (Wang et al. 2014; Li et al. 2013; Huang and Ye. 2013; Pelletier et al. 2015; Kaes et al. 2014; Van Tittelboom et al. 2011). Dual-component healing mechanisms consisting of healing agent and an initiator such as methylmethacrylate monomer and triethylborane have also been investigated (Yang et al. 2011). However, many of these healing agents are expensive and/or require a catalyst to trigger the self-healing mechanism.

3.2 Objectives

The objective of this study was to evaluate the self-healing effectiveness of urea-formaldehyde microcapsules with calcium nitrate as a healing agent. Calcium nitrate was selected as a healing agent due to: (a) Its ability to react with available unhydrated cement particles in crack surfaces contributing to the formation of new hydration products that may potentially heal the crack; and (b) Its low cost, which makes it appealing in industrial applications. Microcapsules self-healing

action was evaluated qualitatively as well as quantitatively through crack recovery of damaged mortar beam specimens under dry and wet conditions. Moreover, formation of healing products due to self-healing was investigated in order to identify the effectiveness of calcium nitrate microencapsulation in concrete applications.

3.3 Background

Microencapsulation of healing agents to promote autonomic healing of materials was demonstrated by White et al. in polymer composites (White et al. 2001). Since, self-healing technology with microencapsulated healing agents has been mainly developed in polymers and composites while the research on its application on cementitious materials has recently started (Wang et al. 2014).

Microencapsulation self-healing approach consists of encapsulating a healing agent in a microcapsule reservoir where it can remain in a passive state until its action is required. The self-healing mechanism is then triggered as microcapsules rupture upon a cracking event. Once released, healing agents are activated in many different forms to promote self-healing. Healing agents may react due to contact with the cementitious matrix, moisture, air, heat or a combination of these, while others may be activated with a second component present in the matrix or provided by additional capsules (Van Tittelboom et al. 2013).

Important factors for the successful functioning of microencapsulation self-healing technology are the following: (a) Adequate dosage and uniform distribution of microcapsules throughout the material in order to provide sufficient healing agent at any given location for the self-healing mechanism to be effective; (b) Bond strength between microcapsules external surface and the cementitious matrix must exceed that of the microcapsules wall for breakage and thus healing agent release to take place upon a cracking event; (c) Healing agent available in a crack must not be less than the crack volume in order for self-healing to be complete, which explains the importance of crack width for the successful use of microencapsulation self-healing technology (Van Tittelboom et al. 2013).

Yang et al. investigated a two-component system for self-healing carbon microfiber-reinforced mortar consisting of oil core/silica gel shell microcapsules with methylmethacrylate (MMA) monomer and triethylborane (TEB) solution as a healing agent and catalyst, respectively (Yang et al. 2011). Higher crack resistance and toughness under fatigue loading were reported due to the self-healing effect of microcapsules as well as a reduction in gas permeability coefficient after damage compared to control (Yang et al. 2011).

Huang et al. investigated a one-component system consisting of wax shell microcapsules with sodium silicate as a healing agent in engineering cementitious composites (ECC) (Huang and Ye. 2011). The study demonstrated the effectiveness of sodium silicate as a healing agent as significant mechanical properties improvement were reported compared to the control specimens after conducting a recover efficiency test by three-point bending (Huang and Ye. 2011). Furthermore, Pelletier et al. reported significant mechanical properties recovery as well as a corrosion inhibition effect compared to control while utilizing polyurethane microcapsules with sodium silicate as a self-healing agent in self-healing mortar (Pelletier et al. 2015).

3.4 Materials and Methods

3.4.1 Microcapsule Preparation and Properties

Microencapsulation procedure and optimization was presented by Hassan and co-workers (Hassan et al. 2016). The microcapsule shell material selected to encapsulate calcium nitrate was urea-formaldehyde resin applied using an in-situ polymerization technique under a water-in-oil emulsion chemical process (Hassan et al. 2016). It was reported that the encapsulation mechanisms was controlled by the following production parameters: (a) temperature at which emulsion is heated, (b) choice and concentration of catalyst, (c) time allotted for the reaction, (d) agitation rate, (e) water-oil ratio, and (f) the choice of core material (Hassan et al. 2016). Figure 3.1 presents SEM images of microcapsules synthetized at an 800 rpm agitation rate.

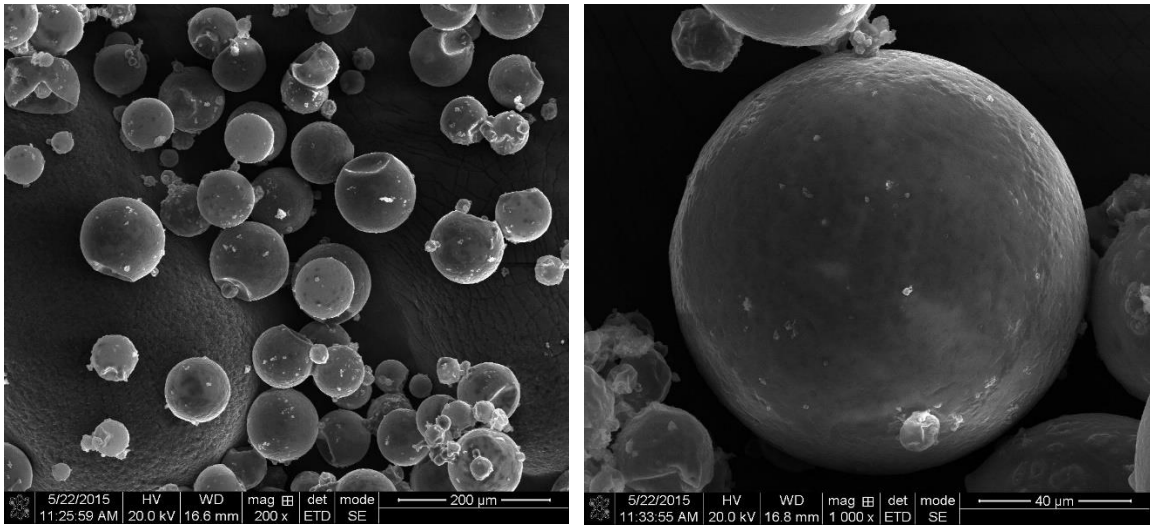

Figure 3.1 Secondary Electron Images of Microcapsules Synthetized at an 800 RPM Agitation Rate

Optimum fabrication parameters were obtained by heating at a temperature of 40°C for 1.5 hours, with 0.60 g of sulfonic acid (catalyst); the agitation rates were varied at three levels, 450, 800, and 1500 rpm in order to evaluate its effect on the microcapsule sizes as shown in Table 3.1 (Milla et al. 2016).

Table 3.1 Agitation Rate Effect on Microcapsule Size *(Milla et al. 2016)*

Agitation Rate (rpm)	Average Microcapsule Size (µm)
450	91.5
800	58.7
1500	45.2

3.4.2 Calcium Nitrate as Healing Agent

Calcium nitrate, which contains the same cations as C3S (tricalcium silicate) and C2S (dicalcium silicate), accelerates hydration due to the nucleating action of ions resulting in an enhancement of the processes of crystallization of hydrates (Karagöl et al. 2013; Ramachandran. 1995). Furthermore, in the presence of calcium nitrate, calcium hydroxide can react forming calcium hydroxynitrate, which is a double and basic salt capable to act as an initial structural skeleton for calcium hydrosilicates to form (Karagöl et al. 2013). While the main expected reaction of calcium nitrate is with unhydrated cement particles, it is important to notice that, calcium ions (Ca^{2+}) provided by calcium nitrate in cracks may also contribute to calcium carbonate precipitation by the increase of the saturation index Ω of calcite (Edvardsen, 1999). Based on these principles, calcium nitrate was utilized as a healing agent to fully exploit its ability to react with the cementitious matrix and to provide a potential intensification of autogenous healing due to further hydration and/or calcium carbonate formation on crack surfaces upon healing agent release.

It is important to notice that, while calcium nitrate reaction with Portland cement has been investigated by several authors (Abdelrazig et al. 1999; Justnes 1995; Justnes 2003; Justnes 2005; Ramachandran 1995) it is yet not fully resolved. Therefore, the development of thermodynamic and kinetic models for the chemical reaction between calcium nitrate and Portland cement is imperative to acquire a more in depth understanding of the healing process, and optimum conditions for self-healing. While the development of such models is of great complexity it offers the opportunity for further investigation.

3.4.3 Materials and Specimens

The material used in this study was cement mortar with a 0.48 water to cement ratio (w/c), which is typical of what is being used in Louisiana. This water to cement ratio was also selected to allow for comparative analysis with Milla et al. results (Milla et al. 2016). The mortar mix was prepared with Type I Portland Cement, Louisiana's graded sand with a maximum particle size of 4.76 mm, tap water, and microcapsules. The proportions of the base mortar mix are presented in Table 3.2(a).

A total of five different mortar mixes were produced at microcapsule dosages of 0 (control), 0.5, 0.85, 1.0, and 2.0% of cement content by weight. Microcapsule contents were selected based on similar studies with successful self-healing outcomes (Yang et al. 2011; Li et al. 2013; Gilford III et al. 2014; Wang et al. 2014; Milla et al. 2016). Furthermore Lv et al. work on probability model of spherical capsules healing ellipsoidal cracks in one-component self-healing matrix as well as Zemskov et al. work on analytical models of a crack hitting encapsulated particles were reviewed to gain insight on the relationship between microcapsule dosage and the probability of capsule breakage. It was noticed that for typical conditions encountered in this study (for 2% microcapsule content) the probability of a capsule being intercepted by a crack equated to nearly 20% for Yang et al. model and approximately 82 and 87% for Zemskov et al. models. However, these models are based on geometrical probability and stereology and do not take into consideration physical properties of the materials which significantly affects the probability of a crack hitting a microcapsule. As such, the probability yielded by these models will be low estimate of the actual probability as cracks will preferably develop through the weakest regions of the material which are the microcapsule sites (Lv et al. 2014; Zemskov et al. 2011).

Table 3.2 (a) Mortar Mix Proportions (b) Experimental Test Factorial

(a)

Material Description	Proportions (kg/m^3)
Sand, Denis Mills, LA	1375
Cement, Type I	500
Water	242
Water/Cement Ratio (W/C) = 0.48	

(b)

Specimen ID	Microcapsules Content (% of cement by weight)	Number of Specimens
1	0.5	6
2	0.85	6
3	1.0	6
4	2.0	6
Control	N/A	6

The details of the mixes and specimens produced are shown in the experimental matrix in Table 3.2(b). Six specimens were produced for each mortar mix, three to be exposed to air healing conditions and three to be exposed to water healing conditions after cracking. Specimens were cast in prisms with dimensions of 40 mm x 40 mm x 160 mm (as shown in Figure 3.2a), de-molded after 24 h, and cured for 40 days in a moist room (23 ± 2°C, > 95% Relative Humidity [RH]). Curing was performed for 40 days due to equipment availability constraints, which did not allow three-point bending tests to be conducted at 28 days.

(a) (b)

Figure 3.2 (a) Mortar Specimen ID Number 3 (1% Microcapsules Content) (b) Cut Mortar Specimen

3.4.4 Self-Healing Mortar Testing

Prismatic mortar specimens with dimensions of 40 mm x 40 mm x 160 mm were tested in three-point bending to induce cracks. Crack width was controlled through a strain-controlled load application at a slow rate of 0.01 mm/min, which allowed stopping the test right after the peak load was reached preventing sudden failure to take place. In the case of control specimens (from which wide cracks are reported), which had the highest strength and were significantly more brittle than specimen with microcapsules, it was extremely difficult to crack the specimens without complete failure to take place. For this reason, indirect tensile test were performed on Ø5 x10 cm cylindrical specimens (with the same mix design as the control prismatic specimens) to obtain the cracks.

In order to quantify the healing process of cracked specimens as a function of time, light microscopy was utilized. Different magnification rates were utilized for different crack sizes. Specimens were observed immediately after cracking and then subjected to a 28-day healing period under controlled environmental conditions. Specimens were observed at 3, 7, 14 and 28 days of the healing period. The crack width of each crack was measured by digital image analysis. Furthermore, Environmental Scanning Electron Microscopy (ESEM) with Energy Dispersive Spectroscopy (EDS) was employed to analyze and characterize the healing products after 28 days of healing.

3.4.5 Environmental Conditioning for Self-Healing

To promote self-healing after cracking, test specimens were exposed to air and water conditions. Specimens cured in air were placed in a 50 ± 4% relative humidity environment with a controlled temperature of 23 ± 2 °C. Water-cured specimens were submerged into tap water and kept at a temperature of 23 ± 2°C. Sealed containers were utilized to reduce carbonation due to dissolution of CO_2 into the curing water and water was replaced at days 3, 7, 14 and 28 of the healing period.

3.4.6 Quantification and Characterization of Self-Healing Products

Healing products formed as a function of time were quantified by digital analysis of light microscopy images. The area of each crack was measured before the healing process and the area of healing was measured at 14 and 28 days of the healing period in order to quantify self-healing as the ratio of healed area over the initial cracked area. Crack widths before healing were measured for all specimens as well. The light microscope utilized for data acquisition was a Zeiss SteREO Lumar.V12.

After 28-days of the healing period, the specimens were cut with a diamond blade saw to extract the midspan section of the specimen (were cracks were generated) as shown in Figure 3.2b. Two cuts were performed, each one at approximately 15 mm from the midspan of the beam extracting the small section of the specimen containing the cracks. After cutting the specimens, these were directly analyzed in an ESEM equipped with EDS in order to observe the morphology and investigate the chemical composition of the healing products. An atomic ratio plot and EDS maps were developed as part of the EDS microanalysis. The environmental scanning electron microscope utilized in this investigation was a FEI Quanta 3D Dual Beam SEM/FIB.

3.5 Results and Analysis

3.5.1 Identification of Healing Mechanism

As previously mentioned, a key factor for the success of self-healing microencapsulation technology is the ability of the microcapsules to break upon a cracking event in order to release the healing agent and to fill the crack through a capillarity mechanism. For this purpose, Figure 3.3 presents a microscopic image of a broken microcapsule found at the surface of a crack, which was inspected throughout this investigation. It is important to note that even though broken, the microcapsule preserved its spherical shape, which is a sign of strength and its ability in resisting the mixing process. It was also firmly attached to the crack surface, which is a sign of adequate bond between the microcapsule surface and the cementitious matrix.

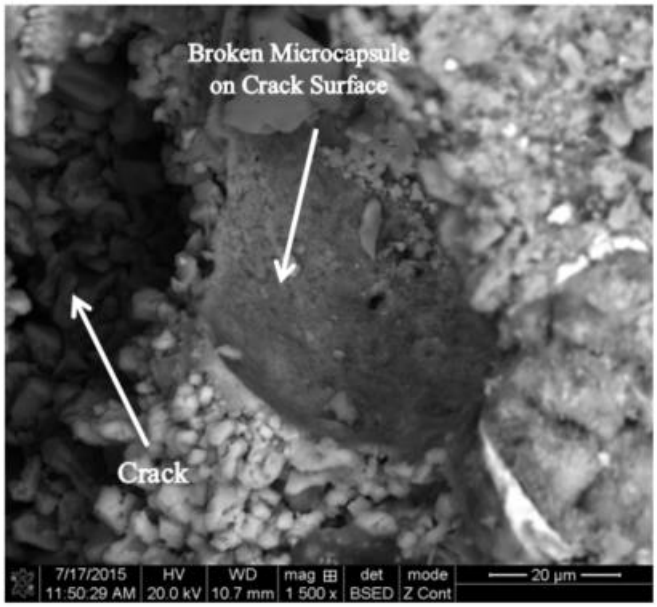

Figure 3.3 Broken Microcapsule on Crack Surface Mortar Specimen ID 1 (0.5% Microcapsules Content)

3.5.2 Crack Width

Immediately after cracking the mortar specimens, light microscopy images of the cracks were acquired. The six specimens available for each type of mortar mixture from Table 3.3 were divided into two groups, Group A for specimens that were subjected to air-healing conditions and Group B for specimens that were subjected to water-healing conditions. The initial average crack width obtained, as estimated by digital image analysis, for series A specimens ranged from 27.7 to 386.5 µm while for series B specimens crack width ranged from 27.0 to 231.9 µm. The details of the initial crack widths for air and water-cured specimens are presented in Tables 3.3 and 3.4.

Table 3.3 Air-Cured Specimens Initial Crack Width

Microcapsules		Crack Width (μm)											
		A1				A2				A3			
ID	Content (%)	n*	Mean	Std.Dev	CV	n	Mean	Std.Dev	CV	n	Mean	Std.Dev	CV
1	0.5	30	30.7	7.6	24.6	30	52.4	16.9	32.3	30	33.9	10.3	30.2
2	0.85	30	130.4	27.8	21.3	30	87.3	21.1	24.1	30	51.6	9.8	18.9
3	1.0	30	54.0	12.1	22.4	30	48.0	15.9	33.1	30	45.7	10.4	22.8
4	2.0	60	38.7	9.0	23.3	60	46.6	12.8	27.6	60	27.7	7.6	27.4
Control**	N/A	30	386.5	160.9	41.6	30	221.3	78.7	35.5				

*Number of measurements across the crack

**Control cracks from cylindrical specimens

Table 3.4 Water-Cured Specimens Initial Crack Width

Microcapsules		Crack Width (μm)											
		B1				B2				B3			
ID	Content (%)	n*	Mean	Std.Dev	CV	n	Mean	Std.Dev	CV	n	Mean	Std.Dev	CV
1	0.5	20	54.5	7.8	14.3	20	60.5	12.1	20.0	20	27.0	7.0	26.1
2	0.85	47	48.9	16.0	32.6	78	65.7	21.1	32.0	63	46.4	17.5	37.7
3	1.0	24	32.1	8.0	25.0	43	45.6	11.9	26.1	41	43.3	15.1	34.9
4	2.0	102	30.0	11.8	39.4	94	35.8	10.8	30.1	101	38.5	16.5	42.8
Control**	N/A	30	230.3	132.0	57.3	30	231.9	56.7	24.5				

* Number of measurements across the crack

**Control cracks from cylindrical specimens

It is important to note that even though indirect tensile tests were performed under strain-controlled conditions, the ability to control crack width was limited by the significantly superior strength of control specimens which in turn produced a highly brittle behavior in contrast to specimens with microcapsules. This highly brittle behavior exhibited by control specimens produced bigger cracks. Flexural Strength results of air-cured specimens are reported in Table 3.5.

Table 3.5 Air-Cured Specimens Flexural Strength

Microcapsules		Flexural Stress (MPa)					
ID	**Content (%)**	**A1**	**A2**	**A3**	**Avg.**	**Std. Dev.**	**CV**
1	0.5	3.43	3.44	3.96	3.61	0.30	8.4
2	1	4.13	4.07	4.05	4.09	0.04	1.1
3	2	2.72	3.11	3.07	2.97	0.22	7.3
4	0.85	5.57	6.36	4.79	5.57	0.78	14.1
Control	N/A	10.64	11.05	9.30	10.33	0.91	8.9

3.5.3 Healing Quantification

After cracking and acquiring the initial light microscopy images, the specimens were conditioned in a curing chamber. Throughout the healing process, light microscopy was utilized to acquire images of the specimens at 3, 7, 14, and 28 days. The analysis of these images revealed signs of healing in the form of small crystals-like features on the edge of the cracks on water-cured specimens after 7 days of healing. At 14 days of the healing process, the formation of healing products was distinguishable around the cracks of most water-cured specimens and the healing process continued to progress as a function of time until 28 days of healing were reached. No healing was observed on specimens exposed to air healing conditions after 28 days. This indicates that calcium nitrate solution released upon microcapsule breakage may not be able to provide enough moisture for significant hydration reaction to take place and/or calcium carbonate precipitation without an external source of moisture. Figure 3.4 presents images of the cracks before and after healing for specimens with 0.5, 0.85, and 1.0% microcapsule contents.

Digital image analysis was utilized in order to quantify self-healing after 14 and 28 days. Quantification was performed by comparing the area of the cracks at 14 and 28 days with the initial area of the cracks before healing to obtain the healing efficiency of the cracks as described by the following equation:

$$H_e = \frac{A_t}{A_0} x\ 100 \quad (1)$$

where,

H_e = Healing efficiency (%);
A_0 = initial area of the crack; and
A_t = the area of the crack at the time of analysis.

Day 1 **Day 28**

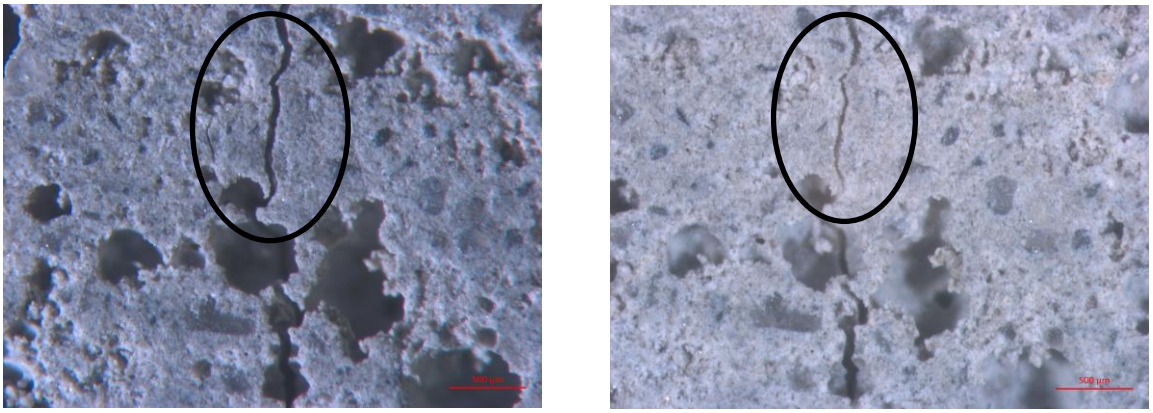

1 % Microcapsule Content

Day 1 **Day 28**

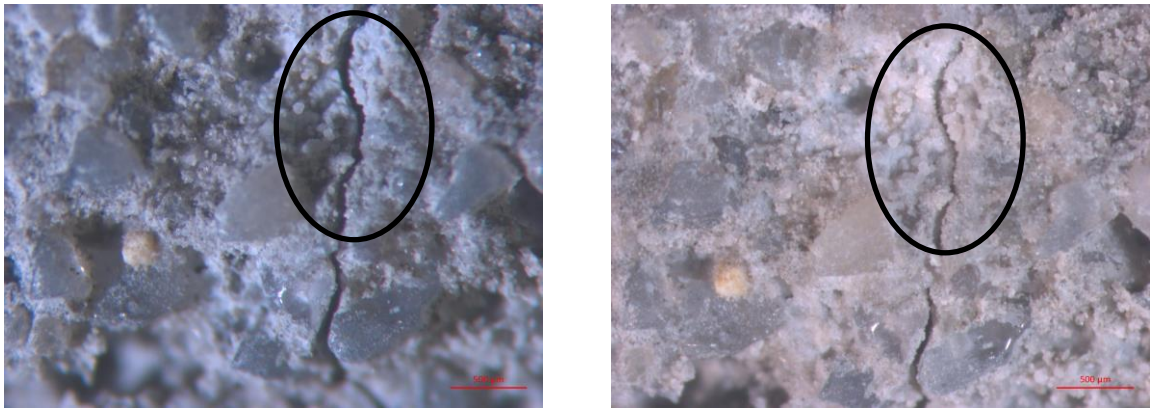

0.85% Microcapsule Content

Day 1 **Day 28**

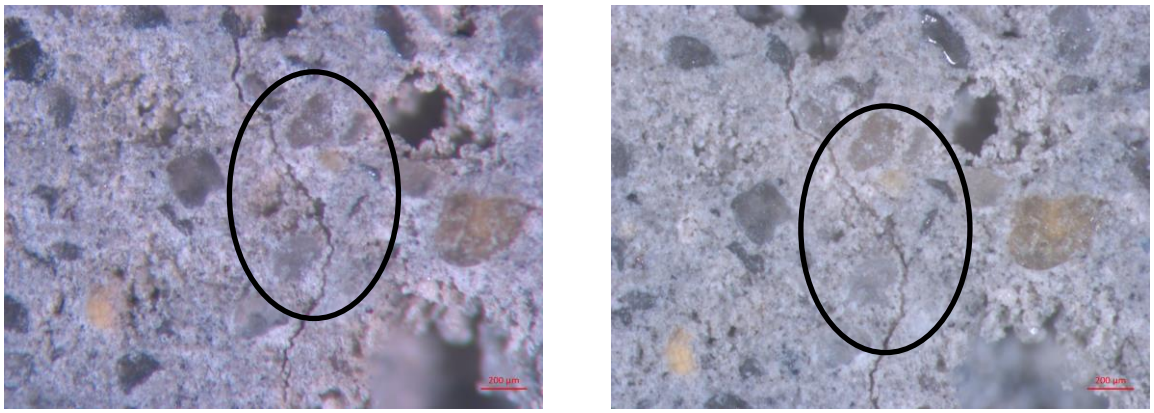

0.5% Microcapsule Content

Figure 3.4 Cracks Before and After Healing

Figure 3.5 show the healing quantification results. As shown in this figure, specimens with 0.85 and 1.0% microcapsule contents had the best self-healing performance after 14 days of healing. Recovery after healing process completion (28 days) for the 0.85 and 1.0% microcapsule content specimens were very similar to control (44%) with 44 and 42%, respectively. On the other hand, the lowest self-healing performance occurred at 2% microcapsule content where the healing efficiency after 28 days was 31%. These results indicate that an optimum content of microcapsule exists that would achieve the best healing efficiency.

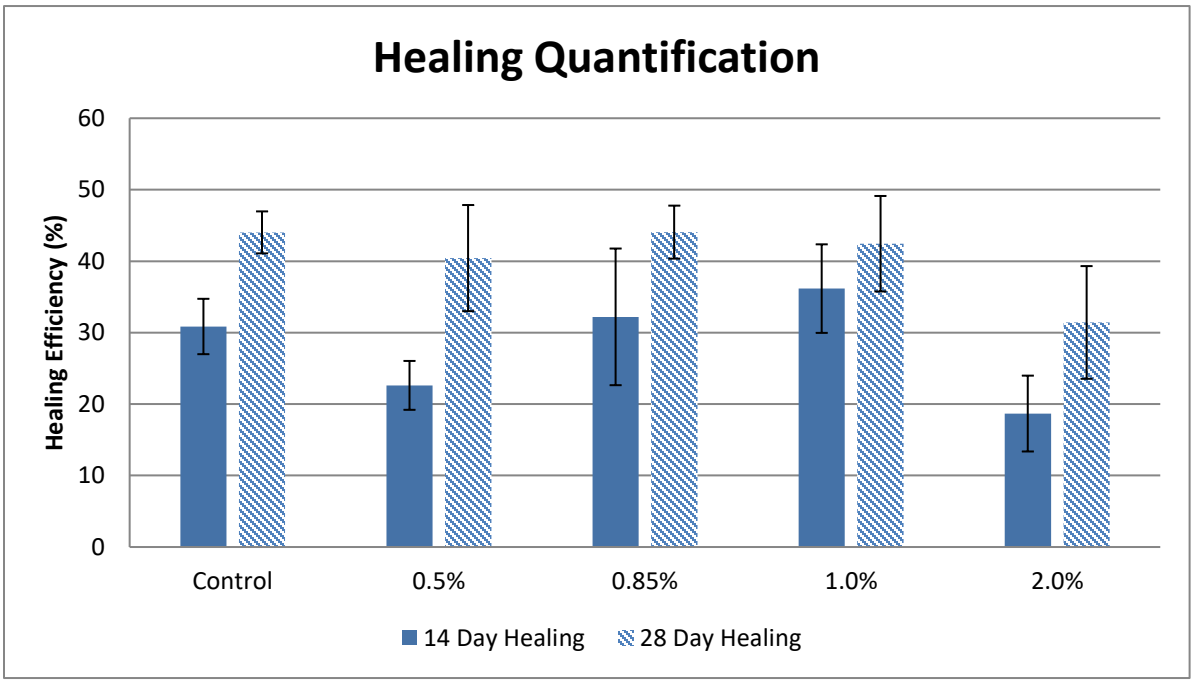

Figure 3.5 Variations of Healing Efficiency with Microcapsule Concentration at 14 and 28 Days

It is important to note that even though mortars with 0.85 and 1% microcapsules content had a better self-healing efficiency than the control at 14 days, the difference in healing efficiency at 14 days between the best performing mortar mix (at 1% microcapsule content) and the control was minor (around 5%). These results lead to question whether favorable conditions for further hydration in crack surfaces were met. Further investigation need to be conducted with lower water to cement ratio mortar mixes with microcapsules, which would lead to more unhydrated cement particles being available in the cementitous matrix. The availability of unhydrated cement particles would create a more favorable environment for the self-healing mechanism to be successful. Additionally, a standard curing time of 28 days or less should be implemented as it is likely that the 40 days of curing utilized in this study produced a higher degree of hydration in the cementitious matrix moderating the conditions for self-healing under the presence of calcium nitrate.

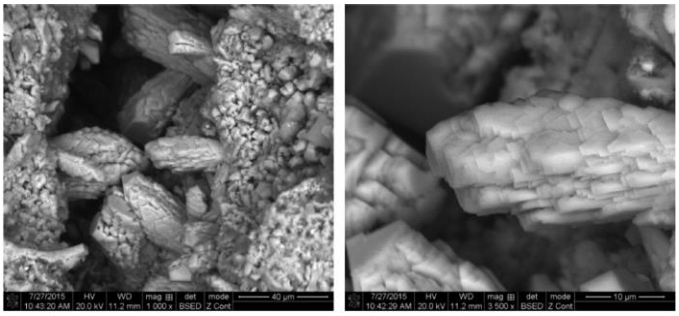

(a)

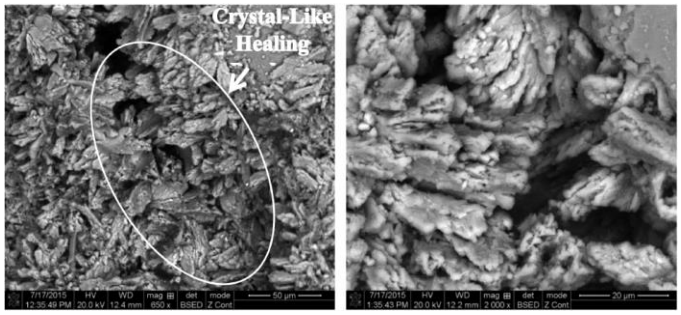

(b)

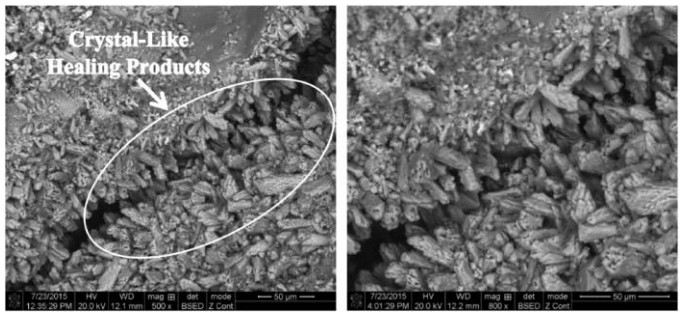

(c)

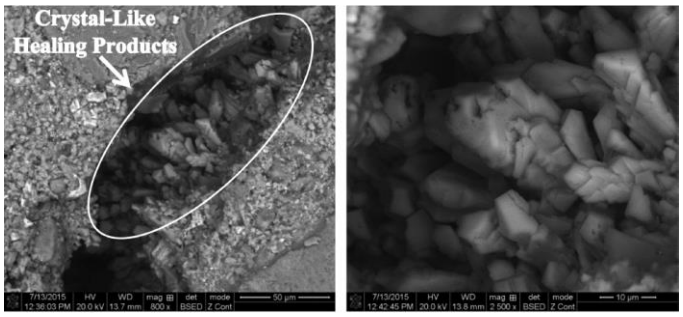

(d)

Figure 3.6 Healing Products in Mortar Specimen Crack for (a) Control, (b) 0.5% Microcapsules Content, (c) 0.85% Microcapsules Content (d) 2.0% Microcapsules Content.

3.5.4 Healing Products Characterization

After the 28 day healing period was completed, one specimen of each mortar type from Table 3.2(b) was cut and directly analyzed under ESEM. Back scatter electron (BSE) images of the healing products generated in the cracks were acquired. As shown in Figure 3.6 (a through d), ESEM images revealed the bulk of the healing products to have a similar morphology in all specimens investigated. Morphology was crystal-like similar to that of calcite crystals. In addition, gel-like healing products were occasionally found as shown in Figure 3.7.

Figure 3.7 Healing Products in Mortar Specimen Crack (Left: 1% Microcapsule Content - Right: Control)

In order to investigate the healing products, EDS microanalysis was conducted on one specimen of each type from Table 3.2(b). An environmental pressure of 0.6 mbar and an accelerating voltage of 20kV were utilized. EDS spectrums were collected at specific locations (under spot mode) throughout the cracks where healing products were formed. After acquiring the data of all specimens investigated, a total of 165 EDS spot spectrums were gathered and an Al/Ca vs. Si/Ca atomic ratio plot was generated as shown in Figure 3.8.

The atomic ratio plot revealed valuable information about the chemical nature of the healing products generated in the cracks. As seen in Figure 3.8, an overwhelming majority of the points were located close to the origin where calcium rich crystals-like CH (Calcium Hydroxide) or calcite ($CaCO_3$) should plot (Winter. 2012). It is important to note that most of the spot spectrums collected contained carbon thus making it highly likely that the chemical nature of the calcium rich crystals were calcium carbonate in the form of calcite crystals. Some points did also plot in a region characteristic of CSH, which is nearly between 0.45 to 0.55 Si/Ca and 0.04 to 0.08 Al/Ca atomic ratios for cement pastes made out of clinker and gypsum; different cement compositions will produce variation on this region (Winter. 2012). These findings indicated the plausible presence of hydration products as part of the healing products.

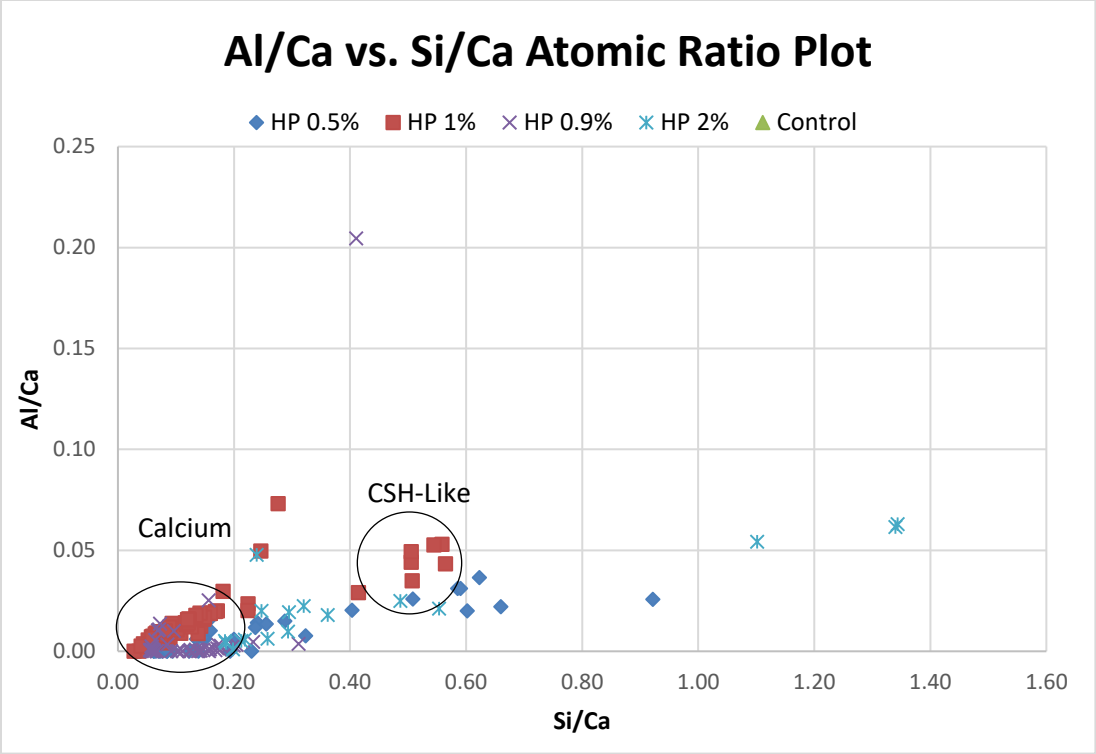

Figure 3.8 Healing Products Al/Ca vs. Si/Ca Atomic Ratio Plot

Moreover, points that were located between the origin and the CSH region were likely due to spectrums, which resulted in an X-ray contribution from both, calcium rich crystal and CSH phases due to the effect of the excitation volume and the scattering skirt (significant in ESEM). These effects made the resolution of the analysis larger than the individual phases of these components at those particular locations. CSH-like healing products presumably took place due to further hydration of unhydrated cement grains present in the cracks. Furthermore, points far away from the origin and the CSH-like region took place probably due X-rays contribution of silica sand particles (high Si/Ca ratio), which were sporadically observed in between the cracks (as shown in Figure 3.9), or high alumina phases like monosulfate, monocarbonate and ettringite (high Al/Ca ratio) phases associated with further hydration healing products in the cracks.

In addition to the EDS spot analysis, an EDS map was acquired in order to get more insight on the chemical composition of the healing products. Figure 3.9 presents an EDS map obtained from the same region of Figure 3.6c. As shown in Figure 3.9, it is distinguishable from the calcium and carbon elemental distribution maps that the presences of both elements are strongly correlated with the healing products present in the cracks. Moreover, one large silica sand particle in the cementitious matrix as well as a small silica sand particle in between the healing products were detected due to the high concentration of silicon present in those areas. The elemental distribution maps proved to be powerful tools to identify phases in the material and gave us valuable evidence supporting that the likely chemical composition of the crystal-like healing products encountered in the cracks were that of calcium carbonate in the form of calcite crystals.

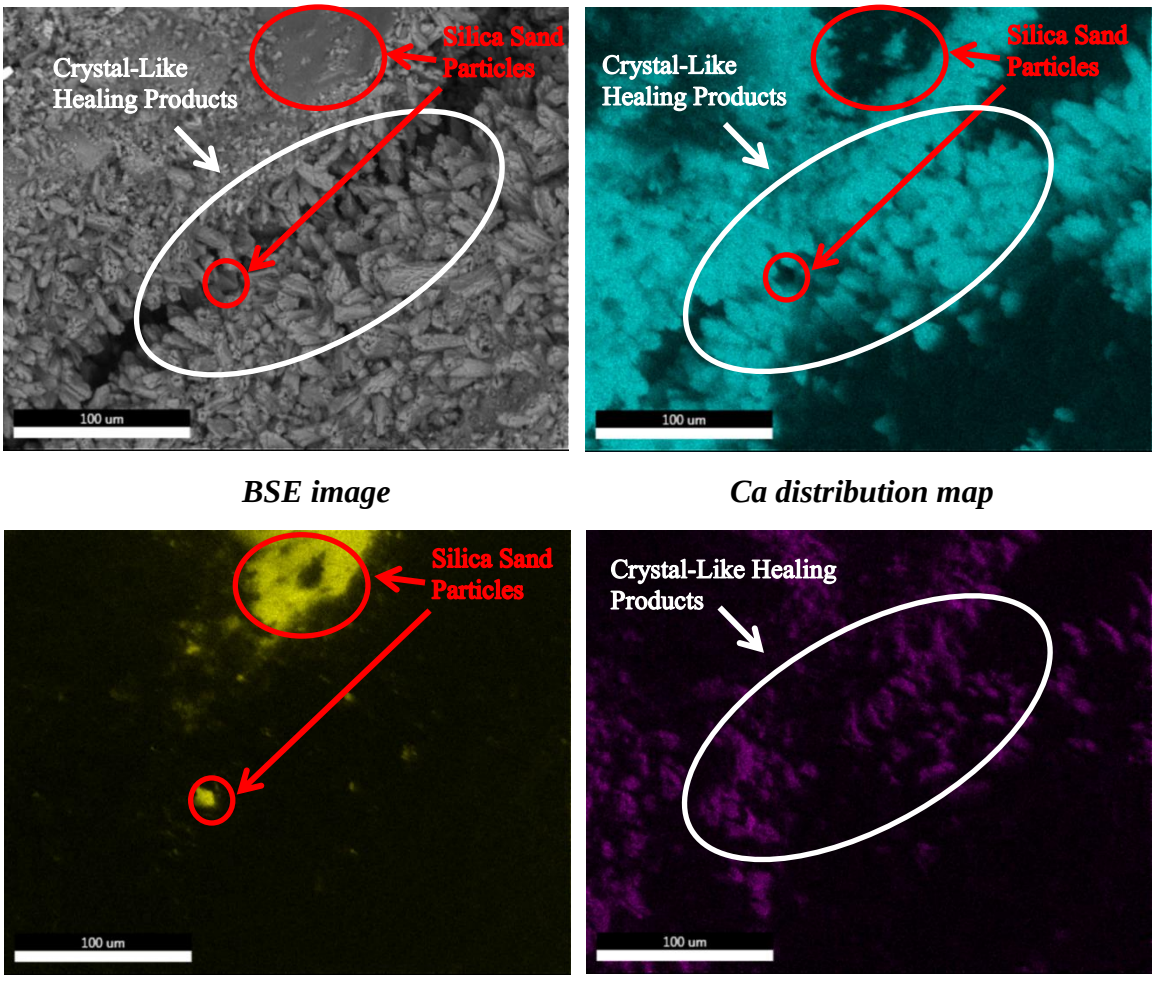

BSE image ***Ca distribution map***

Si distribution map ***C distribution map***

Figure 3.9 BSE Image of Crack after Healing With their Respective Ca, Si and C Distribution Maps

3.6 Summary and Conclusions

The objective of this study was to evaluate the self-healing effectiveness of urea-formaldehyde microcapsules with calcium nitrate as a healing agent. Analysis of captured images showed signs of healing in the form of small crystals-like features at the edge of the cracks of water-cured specimens after 7 days of healing. Furthermore, an improvement in self-healing efficiency was reported in specimens with microcapsule contents of 0.85, and 1.0% compared to the control after 14 days of the healing period. Yet, it is noted from these results that the selected test parameters did not create a favorable environment for the self-healing mechanism to be successful.

The Environmental Scanning Electron Microscopy (ESEM) coupled with Energy Dispersive Spectroscopy (EDS) was utilized to investigate the morphology and chemical nature

of the healing products. Crystal-like and gel-like healing products were found with the majority being crystal-like. Crystal-like healing products were likely calcium carbonate in the form of calcite crystals while gel-like healing products chemical nature was presumably CSH. Further research is needed with lower water to cement ratio mortars with microcapsules under standard curing time conditions in order to produce a favorable environment for self-healing mechanism to take place and to fully exploit the potential benefits of calcium nitrate as a healing agent.

3.7 Acknowledgment

The authors would like to acknowledge the financial support through a grant from Qatar National Research Foundation (QNRF)/ National Priorities Research Program (NPRP) as well as the laboratory support from Louisiana Transportation Research Center (LTRC).

3.8 References

Abdelrazig B.E.I., Bonner D.G., Nowell D.V., Dransfield J.M., Egan P.J., The solution chemistry and early hydration of ordinary Portland cement pastes with and without admixtures, Thermochimica, Acta 340-341, 1999, pages 417-430..

Edvardsen, C. (1999). "Water Permeability and Autogenous Healing of Cracks in Concrete." ACI Materials Journal, Title no. 96-M56.

Gilford III, J., Hassan, M., Rupnow, T., Barbato M., Okeil, A., Asadi S. (2014). "Dicyclopentadiene and Sodium Silicate Microencapsulation for Self-Healing of Concrete." J. Mater. Civ. Eng. 25 (5), 886-896.

Hassan, M., Milla, J., Rupnow, T., Al-Ansari, M., and B. Daly. (2016). "Micro-Encapsulation of Calcium Nitrate for Concrete Applications." Paper# 16-0421, submitted to the 95th Transportation Research Board Annual meeting, Washington, D.C., Under review.

Huang, H., and Guang, Y. (2011). "Application of sodium silicate solution as self-healing agent in cementitious materials." International RILEM Conference on Advances in Construction Materials Through Science and Engineering, Vol. 1, 530-535.

Justnes Harald, Technical calcium nitrate as set accelerator for cement at low temperatures, Cement and Concrete Research, Volume 25, No.9, 1995, pages 1766-1774.

Justnes Harald, Calcium nitrate as a multifunctional concrete admixture, SINTEF Technology and Society, 2005.

Justnes Harald, Explanation of Long-Term Compressive Strength of Concrete Cause by the Set Accelerator Calcium Nitrate, Proceedings of the 11th International Congress on the Chemistry of Cement (ICCC), 2003, pages 475-484.

Kaes, M., Van Tittelboom, K., and N. De Belie. (2014). "The efficiency of self-healing cementitious materials by means of encapsulated polyurethane in chloride containing environments." Construction and Building Materials, Vol. 71, 528-537.

Karagöl, F., Demirboga, R., Kaygusuz M.A., Yadollahi, M.M., Polat, R. (2013). "The influence of calcium nitrate as antifreeze admixture on the compressive strength of concrete exposed to low temperatures." Cold Regions and Technology 89, 30-35

Li, V. C., Hebert, E. (2012). "Robust Self-Healing Concrete for Sustainable Infrastructure." Journal of Advanced Concrete Technology, volume 10, pp207-218.

Li, W., Jiang, Z., Yang, Z., Zhao, N., Yuan, W. (2013) "Self-Healing Efficiency of Cementitious Materials Containing Microcapsules Filled with Healing Adhesive: Mechanical Restoration and Healing Process Monitored by Water Absorption." PLoS ONE 8(11): e81616. doi:10.1371/journal.pone.0081616.

Lv, Z., Chen, H. (2014). "A probabilistic method for determining the volume fraction of pre-embedded capsules in self-healing materials." Smart Mater. Struct. 23, 115009.

Milla, J., Hassan, M., Rupnow, T., Al-Ansari, M., and G.Arce. (2016). "Evaluation of the Effect of Self-Healing Calcium Nitrate Microcapsules on Concrete Properties." Paper# 16-0422, submitted to 95th Transportation Research Board Annual meeting, Washington, D.C., Under reviewIn press.

Pelletier, M., Brown, R., Shukla, A., and A. Bose. "Self-healing concrete with a microencapsulated healing agent." Available online: http://energetics.chm.uri.edu/system/files/Self%20healing%20concrete%20-7-11.pdf (accessed 3 July 2015).

Ramachandran, V. S. (1995). "Concrete Admixtures Handbook." Second edition. pp.740-756.

Van Tittelboom, K., and N. De Belie. (2013). "Self-Healing in Cementitious Materials – A Review." Materials, Vol.6, 2182-2217.

Van Tittelboom, K., De Belie, N., Van Loo, D., and P. Jacobs. (2011). "Self-healing efficiency of cementitious materials containing tubular capsules filled with healing agent." Cement and Concrete Composites, Vol. 33, 497–505.

Wang, J.Y., Soens, H., Verstraete, W., De Belie, N. (2014). "Self-healing concrete by use of microencapsulated bacterial spores." Cement and Concrete Research 56, 139-152.

White, S.R., Sottos, N.R., Geubelle, P.H., Moore, J.S., Kessler, M.R., Sriram, S.R., et al. (2001). "Autonomic healing of polymer composites." Nature; 409 (6822):794

Winter, N. B. (2012). "Scanning Electron Microscopy of Cement and Concrete." WHD Microanalysis Consultants Ltd

Wu, M., Johannesson, B., Geiker M. (2012). "A review: Self-healing in cementitious materials and engineered cementitious composite as a self-healing material." Construction and Building Materials 28, 571-583.

Yang, Z.X., Hollar, J., He, X.D., Shi, X.M. (2011). “A self-healing cementitious composite using oil core/silica gel shell microcapsulses.” Cem.Concr.Compos 33, 506-512.

Zemskov, S.V., Jonkers, H.M., Vermolen F.J. (2011). “Two analytical models for the probability characteristics of a crack hitting encapsulated particles: Application to self-healing materials.” Computational Material Science 50, 3323-3333.

CHAPTER 4

EVALUATION OF SELF-HEALING MECHANISMS ON SMA AND STEEL REINFORCED MORTAR WITH CALCIUM NITRATE MICROCAPSULES

4.1 Introduction

Concrete is a brittle material and as such, it is prone to cracking, which has serious implications on the durability of structures. Cracks provide an easy access to detrimental substances into structures, which promote deterioration and as a consequence of this the need of intensive repair and maintenance. In the US alone, around 18 to 21 billion dollars are spent annually on repair, maintenance and replacement of deteriorating structures annually (Li et al. 2012). This gigantic economic pressure generated by infrastructure deterioration has created a major challenge, which needs to be addressed in order to achieve a sustainable development.

Chemical encapsulation self-healing approach is an attractive strategy for robust autonomous healing of concrete due to several relevant factors, which makes this technology promising: (a) its versatility, which allows for a broad spectrum of chemicals to be encapsulated in a variety of sizes down to the nano-size; (b) its potential for long shelf life, depending on microcapsule composition and shell thickness; and (c) its capability to endow concrete with self-healing properties independent from environmental conditions (Li et al. 2012). While this strategy offers many possibilities for durability advancements in concrete materials, it is a fairly novel approach and few chemicals have been tested (Wang et al. 2014).

Several traditional techniques for limiting crack sizes also include rebar and many types of fibers; a novel approach to control and reduce crack sizes has been proposed by using Shape Memory Alloys (SMAs) as reinforcement in concrete elements. Sun et al. investigated self-repair capability of SMA wires as internal and external reinforcement in composite materials for application in concrete structure (Sun et al. 2013). It was concluded that both internal and external reinforcement methods are viable for crack closure application in concrete structures (Sun et al. 2013). Kuang and Ou studied the application of super-elastic SMA wires and hollow fibers containing adhesives in concrete for a combined self-closing and self-healing effect (Kuang and Ou 2008). Self-restoration capacity of concrete by reversing deflection and closing cracks almost completely was reported; furthermore, adhesives released upon cracking were able to heal the cracks and to restore structural capacity (Kuang and Ou 2008).

4.2 Objectives

The objective of this study was to evaluate the self-healing effectiveness of SMA and steel reinforced mortar prepared with urea-formaldehyde microcapsules containing calcium nitrate as a healing agent. Calcium nitrate was selected as a healing agent due to: (a) Its ability to react with available unhydrated cement particles in crack surfaces contributing to the formation of new hydration products to potentially heal the crack; (b) Its ability to provide cracks with additional calcium ions, which may support the formation of calcium carbonate for crack recovery; and (c) Its low cost, which makes it appealing in industrial applications. Microcapsules self-healing action, SMA self-closing effect, and the combination of both were evaluated qualitatively as well as quantitatively through the investigation of crack recovery of damaged reinforced mortar beam

specimens under wet conditions. Moreover, the formation of healing products due to self-healing was investigated using Energy Dispersive Spectroscopy (EDS).

4.3 Background

Endowing materials with self-healing properties by means of embedded self-healing microcapsules is a relatively novel technique, which was first demonstrated by White et al. in polymer composites (White et al. 2001). Since White et al. first contribution, self-healing strategies continue to develop in polymer composites and its adaptation to concrete materials has recently been suggested (Wang et al. 2014).

Autonomous healing of materials through the incorporation of self-healing microcapsules, which provide inert micro-containers (microcapsules) of a healing agent uniformly dispersed throughout its matrix. Microcapsules protect the healing agent from reacting until its action is required upon a cracking event. Cracks would propagate throughout the material intersecting microcapsules and causing its rupture and release of healing agent. Once the healing agent is released, it may react in many different ways to heal a crack. In concrete, healing agents may react with the cementitious matrix, moisture, air, heat, a catalyst or a combination of these (Tittelboom and Belie 2013). To date, healing agents, which have been evaluated in cementitious materials include sodium silicate, polyurethane, epoxy, cyanoacrylates, methylmethacrylate monomer, and bacterial spores (Gilford Iii et al. 2014; Huang and Ye 2011; Li et al. 2013; Maes et al. 2014; Pelletier et al. 2010; Van Tittelboom et al. 2011; Wang et al. 2014; Yang et al. 2011). Despite the success of several of these agents to provide concrete with enhanced self-healing properties, many of these chemicals are expensive and/or necessitates a catalyst to function.

SMAs are metallic alloys, which have the capacity to return to their original shape after being deformed, by means of external stimuli such as heat (Mohd Jani et al. 2014). SMAs utilized as reinforcement in concrete can provide this composite material with a crack closing mechanism as deformation, which opens the crack, may be reverted by stimulating SMAs shape memory effect. For this reason, self-healing microcapsules and Nitinol (Nickel Titanium alloy), which is the most widely utilized SMA, were combined in this study to provide a dual effect of crack closing and healing to yield superior self-healing results.

4.4 Experimental Program

4.4.1 Microcapsule Preparation and Properties

Calcium nitrate was encapsulated with urea-formaldehyde by an in-situ polymerization technique under a water-in-oil emulsion chemical process similar to the one presented by Hassan et al. (Hassan, M., Milla 2015). As reported by Hassan et al., microcapsule encapsulation is affected by the following production parameters: (a) temperature at which emulsion is heated, (b) choice and concentration of polymerization catalyst, (c) reaction time, (d) agitation rate, (e) water-oil ratio, and (d) core material choice (Hassan, M., Milla 2015). Fabrication parameters utilized for microcapsule synthesis in this study were 1 hour of heating at 40°C, 0.1 of sulfonic acid (catalyst), and an agitation rate of 800 rpm; agitation rate has a direct effect on microcapsule size. Figure 4.1 shows Scanning Electron Microcopy (SEM) images of the microcapsules utilized in this study.

4.4.2 Calcium Nitrate as Healing Agent

Calcium nitrate was selected as the healing agent to exploit its ability to react with the cementitious matrix and to provide with an enhancement of autogenous healing of concrete upon its release in a crack environment. Calcium nitrate as well as two most relevant phases in cement C_3S (tricalcium silicate) and C_2S (dicalcium silicate) share the same cations (Ca^{2+}), which accelerates hydration and enhances the crystallization of hydrates due to the nucleating action of these (Karagöl et al. 2013; Ramachandran 1974). Furthermore, calcium hydroxide has the capacity to react in presence of calcium nitrate to form calcium hydroxynitrate, a double basic salt, capable to provide an initial skeleton for calcium hydrosilicates to form (Karagöl et al. 2013). Additionally, calcium ions provided by calcium nitrate may also assist in the formation of calcium carbonate in cracks as such ions have the ability to drive up the saturation index of calcite generating a favorable environment for calcite crystal formation and growth(Edvardsen 1999).

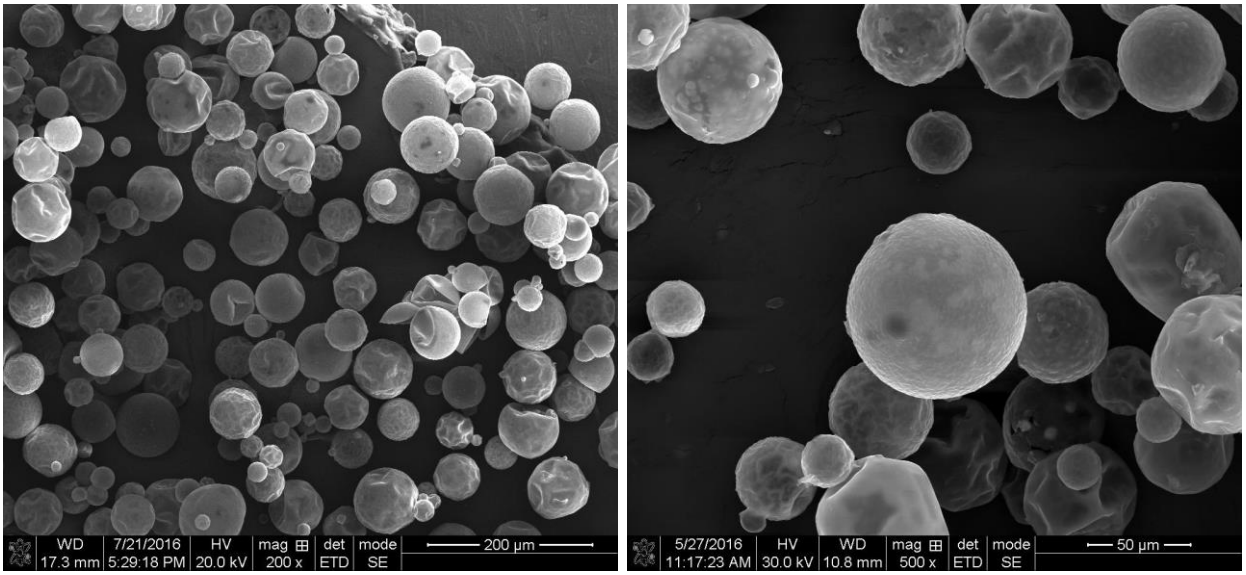

Figure 4.1. Secondary Electron Images of Microcapsules Synthetized at an Agitation Rate of 800 rpm

4.4.3 Materials and Specimens

The materials used in this study were SMA and steel reinforced cement mortar with a 0.40 water to cement ratio (w/c). The mortar mix was prepared with Type I Portland Cement, graded sand with a maximum particle size of 4.76 mm, microcapsules, plasticizer, defoaming agent, and potable water. The proportions of the base mortar mix are presented in Table 4.1a.

Table 4.1. (a) Mortar Mix Proportions and (b) Laboratory Test Matrix

(a)

Material Description	**Proportions**
Sand, Denis Mills, LA	1510 Kg/m^3
Cement, Type I	550 Kg/m^3
Water	220 Kg/m^3
Plasticizer	0.56% of cement content by weight
Defoamer	0.10% of cement content by weight
Water Cement Ratio (W/C)	0.40

(b)

Specimen ID	**Microcapsules Content (% by weight of cement)**	**Number of Specimens**
STEEL		
1	0.5	6
2	1.0	6
3	2.0	6
Control	N/A	6
SMA		
1	0.5	6
2	1.0	6
3	2.0	6
Control	N/A	6
TOTAL		**48**

A total of four different mortar mixes were produced at microcapsule dosages of 0 (control), 0.5, 1, and 2% of cement content by weight for both steel and SMA reinforced specimens. Six prismatic specimens with dimensions of 40 mm x 40 mm x 160 mm (as shown in Figure 4.2a) were cast at each microcapsule level for each reinforcement case. Reinforcement consisted of two 2 mm in diameter wires placed at one centimeter from the bottom and sides of the beam, spaced two centimeter from each other (as shown in Figure 4.2b). Specimens were de-molded after 24 h of casting, and cured for 28 days in a moist room (23 ± 2°C, > 95% Relative Humidity [RH]). The details of the mixes and prepared specimens are summarized in Table 4.1b. Out of the six specimens available for each group of samples, three were utilized for self-healing assessment by digital image analysis and the other three were tested using Ultrasonic Pulse Velocity (UPV) testing.

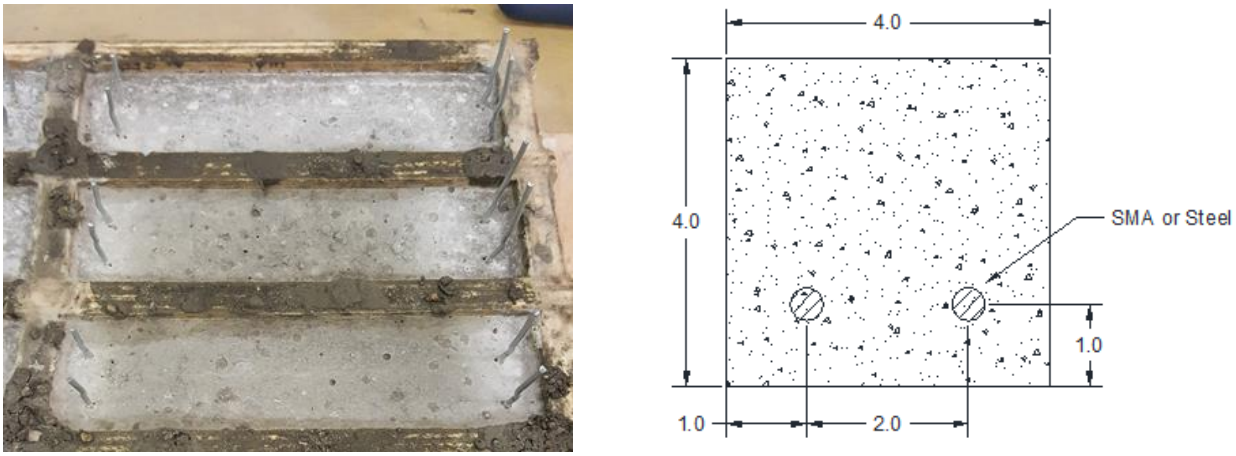

(a) (b)

Figure 4.2. (a) Steel Reinforced Mortar Specimen (b) Reinforcement cross section layout (units are in cm)

4.4.4 Self-Healing Mortar Testing

Specimens were tested in three-point bending; crack width was controlled through a strain-controlled load application. The rate of loading was 0.05 mm/min. In order to quantify the healing process of cracked specimens as a function of time, light microscopy was utilized. Specimens were observed right after cracking and were then subjected to a 14-day healing period under controlled environmental conditions. Specimens were observed at 3, 7 and 14 days of the healing period. The crack width of each crack was measured by digital image analysis. Furthermore, Environmental Scanning Electron Microscopy (ESEM) with Energy Dispersive Spectroscopy (EDS) was employed to analyze and characterize the healing products.

4.4.5 Ultrasonic Pulse Velocity Test (UPV)

Three specimens of each group of samples were subjected to UPV testing in order to assess the recovery of the dynamic modulus of elasticity over time. These specimens were allowed to dry for four days after completing each stage of healing (3, 7, and 14 days) at a temperature of 55 ± 5°C before UPV test was performed. Ten measurements were taken with the transducers placed at the extreme faces of the beams. The equipment utilized for this task was a Proceq Pundit PL-200 equipped with 150 kHz transducers.

4.4.6 Environmental Conditioning for Self-Healing

To promote self-healing after cracking, test specimens were exposed to water conditions. Specimens were submerged into distilled water and kept at a temperature of 55 ± 5°C; this temperature was selected to guarantee the activation of the shape memory effect of the SMA reinforcement, which was 45°C. Sealed containers were utilized to reduce carbonation due to dissolution of CO_2 into the curing water and water was replaced at days 3 and 7 of the healing period.

4.4.7 Quantification and Characterization of Self-Healing Products

Healing products formed as a function of time were quantified by digital analysis of light microscopy images. The width of each crack was measured before the beginning of the healing process and at days 3 and 7 of the healing period in order to quantify self-healing. The light microscope utilized for data acquisition was a Zeiss SteREO Lumar.V12. After completion of the healing period, one specimen of each group from Table 4.1b were cut with a diamond blade saw and were directly analyzed in an ESEM equipped with Energy-Dispersive Spectroscopy (EDS) in order to observe the morphology and investigate the chemical composition of the healing products. An atomic ratio plot was developed as part of the EDS microanalysis. The environmental scanning electron microscope utilized in this investigation was a FEI Quanta 3D Dual Beam SEM/FIB.

4.5 Results and Analysis

4.5.1 Identification of Healing Mechanisms

In order for self-healing to take place due to microencapsulation action, it is imperative the occurrence of microcapsule breakage upon a cracking event. Figure 4.3 showcases a broken microcapsule on the crack surface and the presence of healing products sealing the crack at that particular location. Figure 4.3 demonstrates the successful functioning of the microcapsule breakage mechanism as well as the presence of healing products in the vicinity of a broken microcapsule.

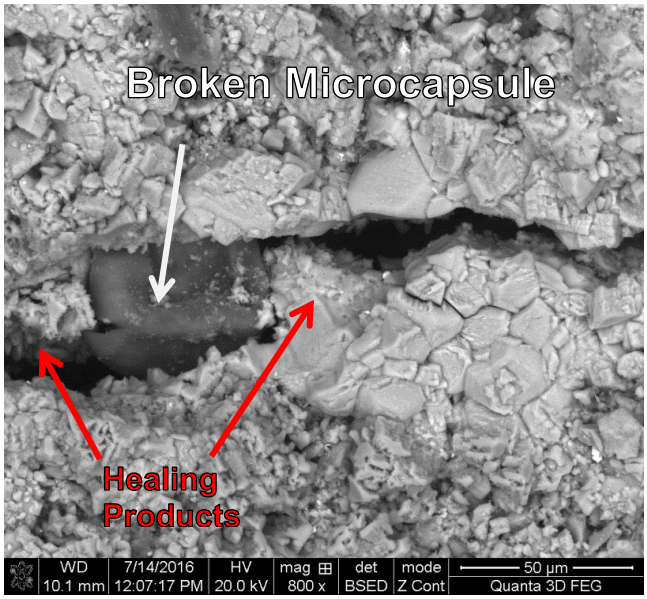

Figure 4.3. Broken Microcapsule in Cracked Area (0.5% Microcapsule Content Specimen with Steel Reinforcement)

4.5.2 Crack Width

Light microscopy images of mortar beams were collected right after cracking and were analyzed to measure the initial crack width. Specimens utilized in digital image analysis showed cracks

ranging from 13 to 152 μm. It is acknowledged that crack width plays a key factor in self-healing efficiency; Table 4.2 (a and b) presents the initial crack widths of both steel and SMA reinforced specimens. For each specimen, the widths from the narrowest side (closest to the beam neutral axis) and the widest side (bottom of the beam) of the cracks are provided to give a better sense of the degree of initial damage inflicted on each specimen prior healing.

Table 4.2. (a) Steel Reinforced Specimens Initial Crack Width and (b) SMA Reinforced Specimens Initial Crack Width

(a)

STEEL		**1**		**2**		**3**	
		Narrow	**Wide**	**Narrow**	**Wide**	**Narrow**	**Wide**
Control	**Mean**	35.7	90.8	40.5	111.1	46.3	115.9
	SD	9.5	21.8	4.6	20.0	8.0	18.9
0.50%	**Mean**	16.5	29.3	27.5	87.8	35.1	149.2
	SD	3.6	4.6	8.5	15.4	10.6	14.7
1%	**Mean**	13.0	42.3	39.9	146.8	16.5	64.4
	SD	3.3	9.3	8.9	34.1	2.3	9.1
2%	**Mean**	24.1	84.2	45.2	102.4	53.3	139.6
	SD	5.4	9.0	9.0	14.9	7.5	19.9

(b)

SMA		**1**		**2**		**3**	
		Narrow	**Wide**	**Narrow**	**Wide**	**Narrow**	**Wide**
Control	**Mean**	25.8	97.3	24.8	96.8	16.2	99.9
	SD	4.6	18.4	6.2	14.6	4.3	11.1
0.50%	**Mean**	30.0	121.0	31.4	125.0	35.7	127.1
	SD	7.1	21.5	7.6	9.7	5.3	14.5
1%	**Mean**	31.5	104.5	34.5	152.0	37.0	131.5
	SD	6.8	45.5	5.4	24.6	11.3	30.7
2%	**Mean**	33.0	103.1	18.5	89.4	48.4	94.8
	SD	8.8	21.7	4.4	16.7	8.2	19.2

4.5.3 Healing Quantification

After completing 14 days of healing, light microscopy images taken throughout the healing period at days 3 and 7 were digitally analyzed to assess the level of healing obtained at these particular early ages. It is noted that significant healing was achieved at 14 days on several samples thus limiting the ability to perform accurate assessment of crack size at such ages. Table 4.3 and Table 4.4 show images of cracks before and after healing for steel reinforced and SMA reinforced specimens, respectively.

Table 4.3. Cracks Before and After Healing for Steel Reinforced Specimens

Control (Initial CW= 35.7µm)		
Day 1	**Day 7**	**Day 14**
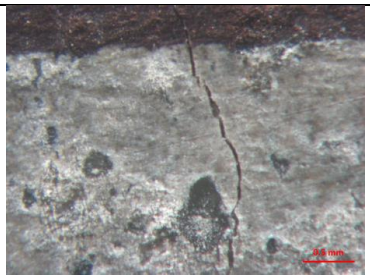	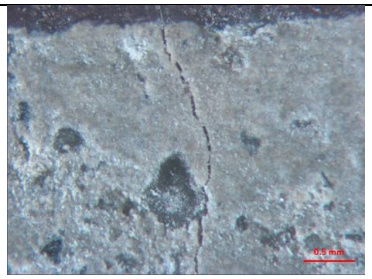	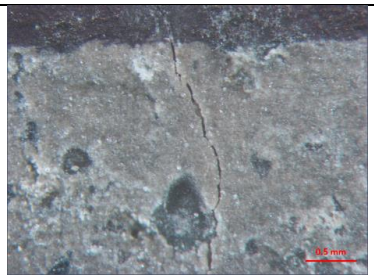
0.5% Microcapsule Content (Initial CW= 27.5 µm)		
Day 1	**Day 7**	**Day 14**
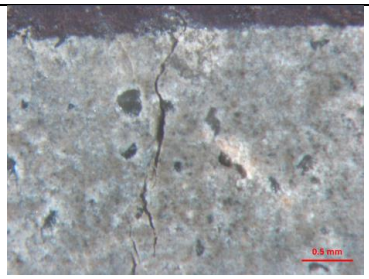	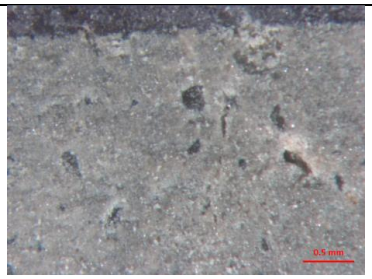	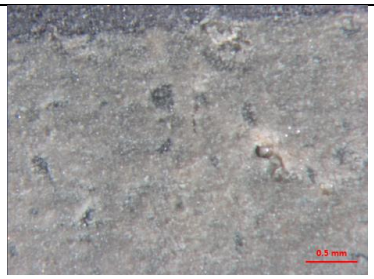
1% Microcapsule Content (Initial CW= 39.9 µm)		
Day 1	**Day 7**	**Day 14**
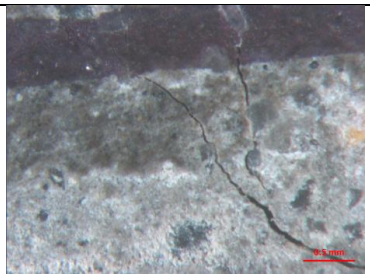	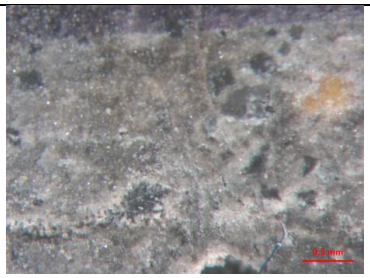	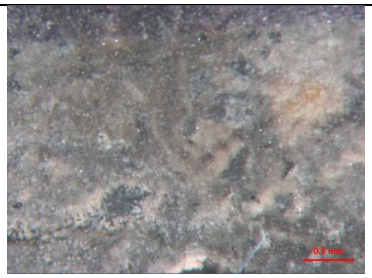
2% Microcapsule Content (Initial CW= 45.2 µm)		
Day 1	**Day 7**	**Day 14**
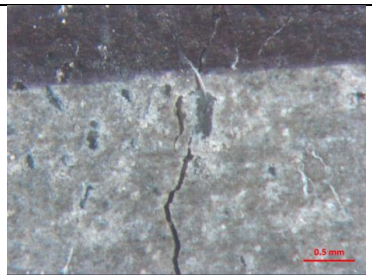	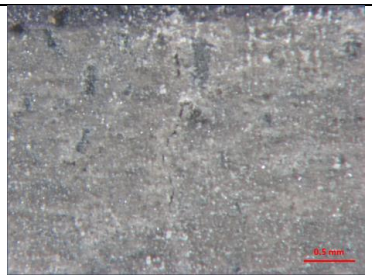	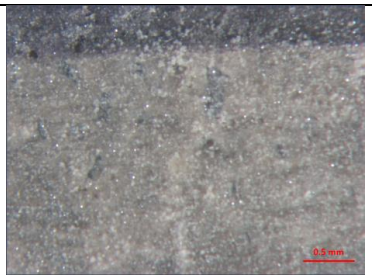

Table 4.4. Cracks Before and After Healing for SMA Reinforced Specimens

Control (Initial CW= 25.8 µm)		
Day 1	**Day 7**	**Day 14**
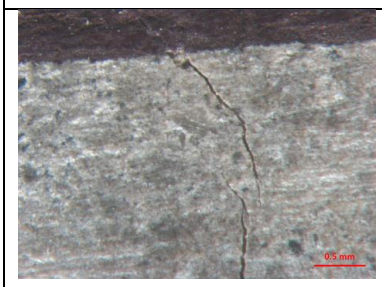	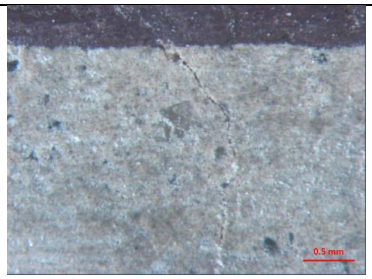	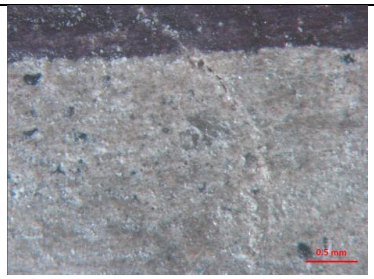
0.5% Microcapsule Content (Initial CW= 30.0 µm)		
Day 1	**Day 7**	**Day 14**
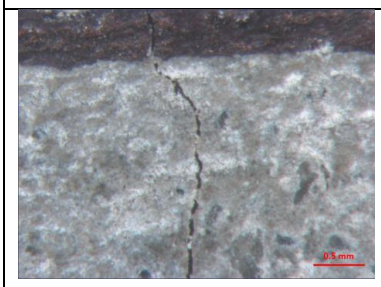	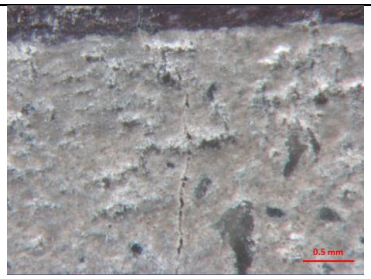	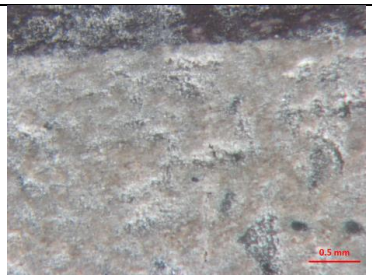
1% Microcapsule Content (Initial CW= 31.5 µm)		
Day 1	**Day 7**	**Day 14**
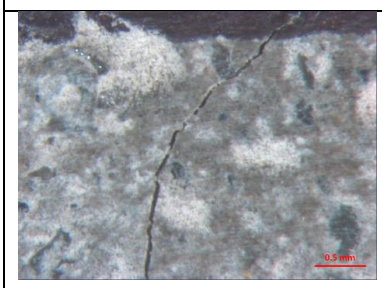	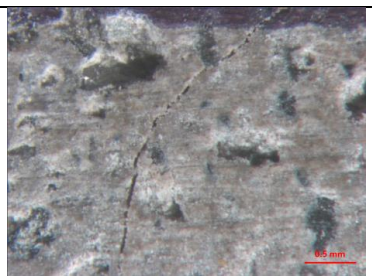	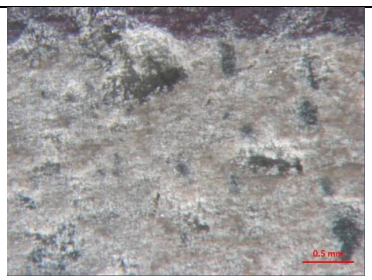
2% Microcapsule Content (Initial CW= 33.0 µm)		
Day 1	**Day 7**	**Day 14**
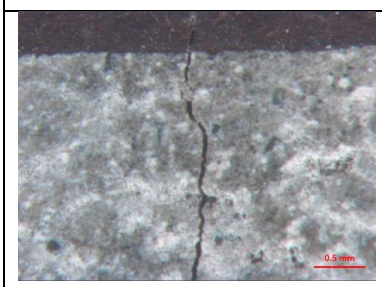	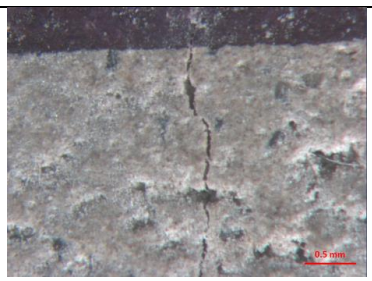	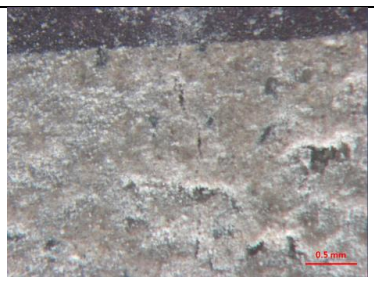

Quantification of the healing process was performed by comparing the size of the cracks at different healing stages with the initial crack width before healing to estimate the healing efficiency as described by the following equation:

$$H_e = \left(1 - \frac{CW_t}{CW_0}\right) x\ 100 \qquad (1)$$

where,

H_e = Healing efficiency (%);
CW_0 = Initial crack width; and
CW_t = Crack width at the time of analysis.

Figure 4.4 presents the normalized healing efficiency of both steel and SMA reinforced specimens. Healing efficiency was normalized to an equivalent 50 µm size crack according to the following equation:

$$NH_e = \left(\frac{H_e}{50\ \mu m}\right) x\ CW_0 \qquad (2)$$

where,

NH_e = Normalized Healing efficiency (%);
H_e = Healing efficiency (%); and
CW_0 = Initial crack width.

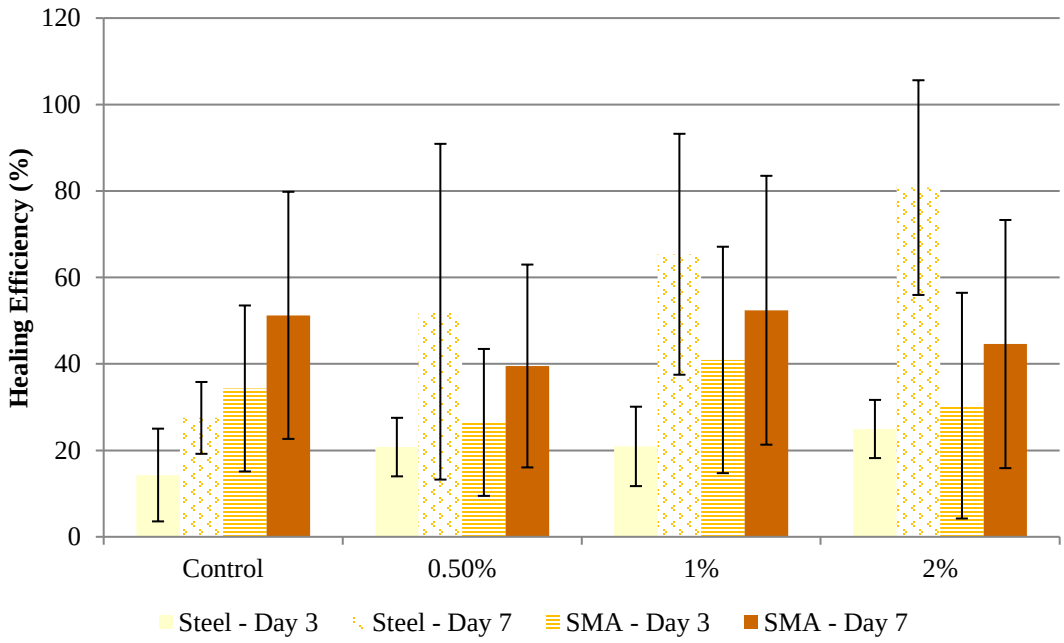

Figure 4.4. Normalized Healing Efficiency

Steel reinforced specimens exhibited an enhanced healing efficiency with microcapsules compared to control at both 3 and 7 days of the healing process and healing efficiency improved with the increase in microcapsule content. At 2% microcapsule content, which was the best performing case, healing efficiency improvement compared to control at 3 and 7 days of healing were 10.6% and 53.3% respectively. On the other hand, SMA reinforced specimens healing efficiency did not improve at 0.5% and 2% microcapsule content; however, a slight improvement compared to control is observed at 1% microcapsule content with a 6.6% and 1.2% increase in healing efficiency at 3 and 7 days of healing, respectively. It is important to note that the selection of microcapsule content should also consider the effects of microcapsules on the concrete physical properties. Previous studies by the authors showed an increase in microcapsule contents can lead to a reduction in concrete compressive strength due to the increase in air contents (Hassan, M., Milla 2015; Milla, J., Hassan 2015). Furthermore, an optimum microcapsule content exists to balance healing efficiency with its influence on concrete compressive strength.

SMA reinforced specimens were observed to perform better than steel reinforced specimens at 3 days of healing. This was explained by the crack closing effect generated by the SMA reinforcement after reaching the activation temperature of 45°C. The crack closing effect of SMA was identified in microscopy images, especially with wide cracks as shown in Table 4.4. Moreover, control SMA reinforced specimens exhibited a superior healing efficiency performance than control steel reinforced specimens at both 3 and 7 days of healing, which could be attributed for the most part to the crack closing effect of SMA.

4.5.4 Ultrasonic Pulse Velocity

UPV was used to assess the healing efficiency of cracks by analyzing the UPV recovery of the specimens throughout the healing process. To assist in interpretation, UPV recovery as compared to the day 0 (right after cracking) measurement was computed for all cases according to the following equation:

$$R_e = \left(\frac{UPV_t}{UPV_{Day0}} - 1\right) x\ 100 \quad (3)$$

where,

R_e = UPV recovery efficiency (%);

UPV_t = UPV at time of the analysis; and

UPV_{Day0} = UPV at Day 0.

Figure 4.5 presents the UPV recovery efficiency for both steel and SMA reinforced mortar specimens. As shown in Figure 4.5, there is a significant difference between UPV recovery of steel and SMA reinforced specimens, particularly at day 3. Steel reinforced specimens with and without microcapsules showed a negative recovery at day 3 of the healing process probably due to the thermal expansion of steel, which resisted healing. In contrast, all SMA reinforced specimens exhibited positive healing at Day 3 likely produced by both self-healing effect of microcapsules and crack-closing effect of SMA. Furthermore, it was observed that at 7 and 14

days of the healing process, microcapsules produced an improvement in UPV recovery as compared to control for both steel and SMA reinforced specimens. The best performing healing efficiency for both steel and SMA reinforced specimens at both 7 and 14 days of the healing occurred at 1% microcapsule content; yet, the 2% microcapsule content produced the optimum healing efficiency at 3 days of healing for SMA reinforced specimens. It is important to notice that UPV recovery efficiency of SMA with and without microcapsules was superior at all stages of healing to steel reinforced specimens likely due to crack-closing ability of SMA. Also, the combination of SMA reinforcement and microcapsules showed superior healing capability than the specimens with steel reinforcement without microcapsules.

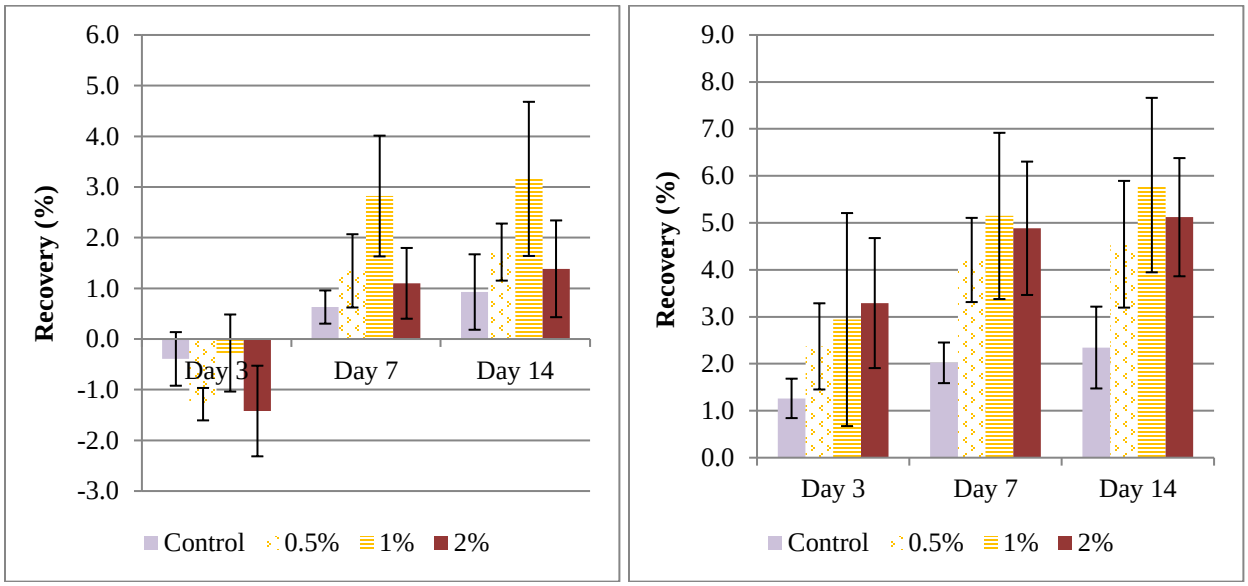

(a) (b)

Figure 4.5. SMA Reinforced Specimens UPV Recovery Efficiency (a) Steel Reinforced (b) SMA Reinforced

4.5.6 Healing Products Characterization

After the completion of the healing process, one specimen of each group shown on Table 4.1(b) was cut with a diamond blade saw to extract a small section of the beam containing the healed crack for direct analysis under ESEM-EDS. Cracks were examined and back scatter electron (BSE) images from healing products in cracks were collected. Figure 4.6 presents BSE images of healing products in cracks. It is important to notice that throughout all the specimens, two main type of morphologies were observed, crystal-like similar to calcite ($CaCO_3$) crystals and gel-like, with crystal like features being predominant.

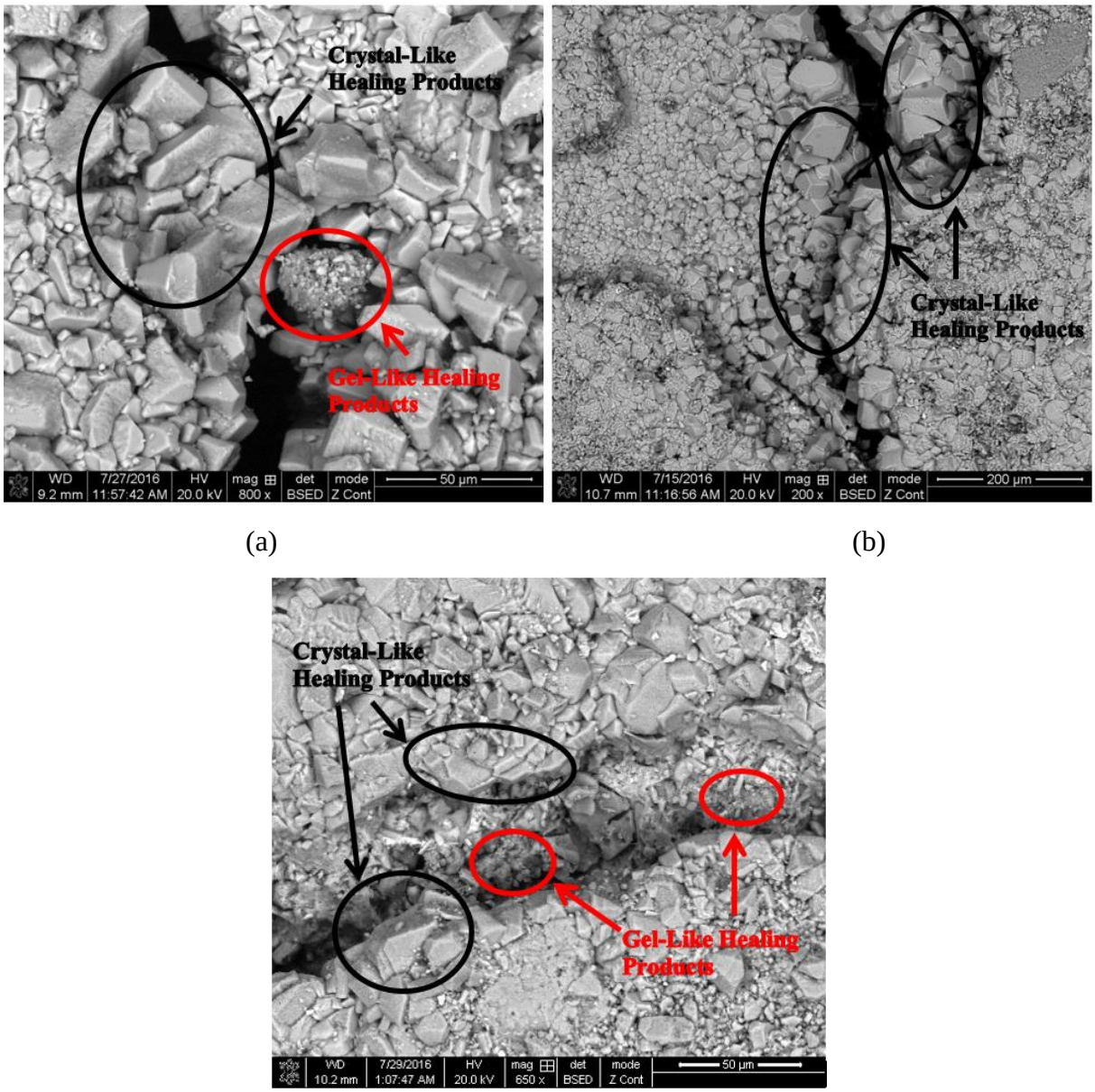

(a) (b)

(c)

Figure 4.6. Healing Products in Cracks (a) Control Specimen; (b) 1% Microcapsule Content Steel Reinforced Specimen (c) 0.5% Microcapsule Content Steel Reinforced Specimen

Energy dispersive spectroscopy spot spectrums were collected on each specimen at different locations in the cracks, targeting healing products. A total of 500 EDS spots were collected and analyzed to develop an Al/Ca vs. Si/Ca atomic ratio plot in order to gain insight on the chemical nature of the healing products encountered in the cracks as shown in Figure 4.7. The Al/Ca vs. Si/Ca atomic ratio plot presented in Figure 4.7 show the majority of points clustering close to the origin of the graph were calcium rich crystals such as calcium hydroxide (CH) and calcium carbonate ($CaCO_3$) should plot (Winter 2012).

It is important to notice that most of the EDS spot spectrums collected reported a significant amount of carbon, which is indicative that the nature of the healing products close to the origin is that of calcium carbonate in the form of calcite crystals. Moreover, some points plotted in a region characteristic of CSH (gel-like hydration product) which is approximately between 0.45 to 0.55 Si/Ca and 0.04 to 0.08 Al/Ca for pure cement pastes (clinker and gypsum), suggesting the presence of CSH-gel like healing products (Winter 2012). Furthermore, several points plotted in between the origin and the CSH region. This is common in ESEM-EDS micro-chemical analysis of concrete materials as many times the excitation volume from which X-rays are emitted exceeds the size of a single phase in the sample, thus providing with characteristic X-rays of more than one phase at a time (Winter 2012). Therefore, the points located between the origin and the pure CSH region represents a combination of both calcium rich crystals and CSH gel-like healing products. On the other hand, points located far from both the origin and the pure CSH region occur due to X-ray contributions from either high alumina phases like ettringite, monosulfate and monocarbonate (high Al/Ca ratios points) or sand particles (high Si/Ca ratios points) (Winter 2012).

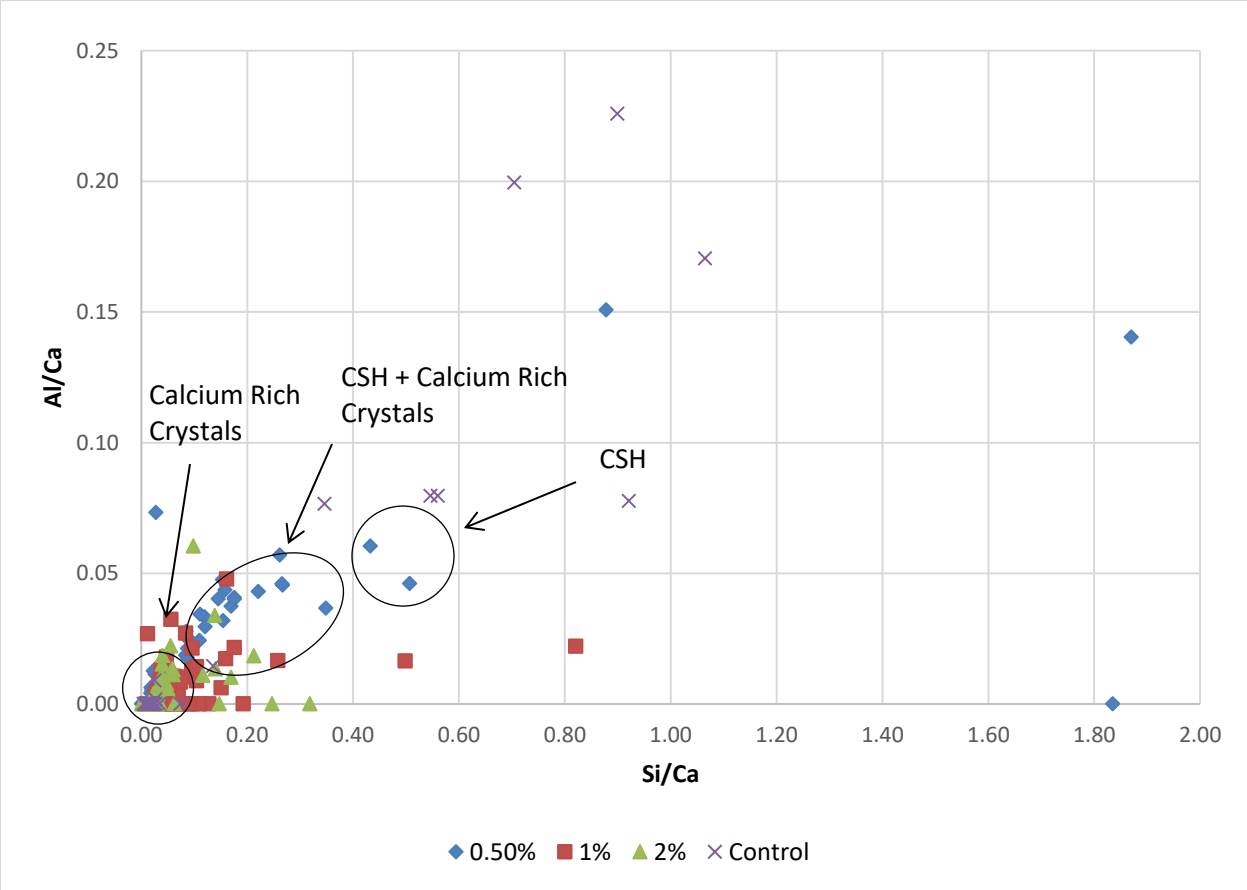

Figure 4.7. Al/Ca vs. Si/Ca Atomic Ratio Plot

4.6 Conclusions

The objective of this study was to evaluate the dual healing capabilities of self-healing microcapsules and shape memory alloys using mortar specimens. Based on the results of this study, it was determined that healing efficiency improved with the increase in microcapsule content at both 3 and 7 days of the healing process for steel reinforced mortar specimens. Furthermore, SMA reinforced specimens performed better than steel reinforced specimens at 3 days of healing likely due to crack-closing action of SMA.

UPV recovery efficiency of SMA with and without microcapsules was superior at all stages of healing to steel reinforced specimens. In addition, SMA reinforced specimens exhibited an improvement in UPV recovery with microcapsules compared to the control in all stages of healing. Best UPV recovery for SMA reinforced specimens was observed at 1% microcapsule content at days 7 and 14; however, optimum UPV recovery at day 3 was obtained at 2 % microcapsule content. Furthermore, steel reinforced specimens with microcapsules exhibited an improvement in UPV recovery at days 7 and 14 of the healing period with 1% microcapsule content being the best performing dosage.

The overwhelming majority of healing products encountered in cracks were of crystal like morphology and were identified as likely calcium carbonate in the form of calcite crystals. Furthermore, gel-like healing products were also identified and their chemical nature was likely that of CSH.

4.7 Acknowledgements

The authors would like to acknowledge the financial support through a grant from Qatar National Research Foundation (QNRF)/ National Priorities Research Program (NPRP) as well as the laboratory support from Louisiana Transportation Research Center (LTRC).

4.8 References

Edvardsen, C. (1999). “Water permeability and autogenous healing of cracks in concrete.” *ACI Materials Journal*.

Gilford Iii, J., Hassan, M. M., Rupnow, T., Barbato, M., Okeil, A., Asadi, S., Gilford, J., Hassan, M. M., Rupnow, T., Barbato, M., Okeil, A., and Asadi, S. (2014). “Dicyclopentadiene and sodium silicate microencapsulation for self-healing of concrete.” *Journal of Materials in Civil Engineering*, 26(5), 886–896.

Hassan, M., Milla, J. (2015). “Micro-Encapsulation of Calcium Nitrate for Concrete Applications.” *Transportation Research Board (In Press) , Washington (DC);*

Huang, H., and Ye, G. (2011). “Application of sodium silicate solution as self-healing agent in cementitious materials.” *International RILEM conference on advances in construction materials through science and engineering*, RILEM Publications SARL, 530–536.

Karagöl, F., Demirboğa, R., Kaygusuz, M. A., Yadollahi, M. M., and Polat, R. (2013). “The influence of calcium nitrate as antifreeze admixture on the compressive strength of concrete exposed to low temperatures.” *Cold Regions Science and Technology*, Elsevier, 89, 30–35.

Kuang, Y., and Ou, J. (2008). “Self-repairing performance of concrete beams strengthened using superelastic SMA wires in combination with adhesives released from hollow fibers.” *Smart Materials and Structures*, IOP Publishing, 17(2), 25020.

Li, V. C., Herbert, E., Senot, S., Schlangen, E., Li, V. C., and Herbert, E. (2012). “Robust Self-Healing Concrete for Sustainable Infrastructure Robust Self-Healing Concrete for Sustainable Infrastructure.” 10, 207–218.

Li, W., Jiang, Z., Yang, Z., Zhao, N., and Yuan, W. (2013). “Self-healing efficiency of cementitious materials containing microcapsules filled with healing adhesive: Mechanical restoration and healing process monitored by water absorption.” *PLoS ONE*, 8(11), 1–18.

Maes, M., Van Tittelboom, K., and De Belie, N. (2014). “The efficiency of self-healing cementitious materials by means of encapsulated polyurethane in chloride containing environments.” *Construction and Building Materials*, Elsevier Ltd, 71, 528–537.

Milla, J., Hassan, M. (2015). “Evaluation of the Effect of Self-Healing Calcium Nitrate Microcapsules on Concrete Properties.” *Transportation Research Board (In Press) , Washington (DC);*

Mohd Jani, J., Leary, M., Subic, A., and Gibson, M. A. (2014). “A review of shape memory alloy research, applications and opportunities.” *Materials and Design*, Elsevier Ltd, 56, 1078–1113.

Pelletier, M. M., Brown, R., Shukla, A., and Bose, A. (2010). “Self-healing concrete with a microencapsulated healing agent.” *University of Rhode Island, Kingston,USA*, (C).

Ramachandran, V. S. (1974). “Calcium chloride in concrete.”

Sun, L., Liang, D., Gao, Q., and Zhou, J. (2013). “Analysis on factors affecting the self-repair capability of SMA wire concrete beam.” *Mathematical Problems in Engineering*, 2013.

Tittelboom, K. Van, and Belie, N. De. (2013). *Self-Healing in Cementitious Materials—A Review*.

Van Tittelboom, K., De Belie, N., Van Loo, D., and Jacobs, P. (2011). “Self-healing efficiency of cementitious materials containing tubular capsules filled with healing agent.” *Cement and Concrete Composites*, Elsevier Ltd, 33(4), 497–505.

Wang, J. Y., Soens, H., Verstraete, W., and De Belie, N. (2014). “Self-healing concrete by use of microencapsulated bacterial spores.” *Cement and Concrete Research*, 56, 139–152.

White, S. R., Sottos, N. R., Geubelle, P. H., Moore, J. S., Kessler, M. R., Sriram, S. R., Brown, E. N., and Viswanathan, S. (2001). “Autonomic healing of polymer composites.” *Nature*, 409(6822), 794–797.

Winter, N. B. (2012). *Scanning Electron Microscopy of Cement and Concrete*. WHD Microanalysis Consultants Ltd., Rendlesham, Woodbridge, UK.

Yang, Z., Hollar, J., He, X., and Shi, X. (2011). “A self-healing cementitious composite using oil core/silica gel shell microcapsules.” *Cement and Concrete Composites*, 33(4), 506–512.

CHAPTER 5

SELF-HEALING EVALUATION OF SMA AND STEEL REINFORCED MORTAR WITH CALCIUM NITRATE MICROCAPSULES UNDER WET AND DRY CYCLES

5.1 Introduction

Reinforced concrete is a key material in the world infrastructure. Reinforced concrete durability largely depends on the permeability of concrete, which protects the integrity of the material against chemical and physical attacks as well as the embedded steel reinforcement against corrosion. Concrete is a brittle material and as such is prone to cracking, which can significantly increase its permeability and compromise the structure durability. Experimental evidence suggests that 100 μm represents a crack width threshold above which water flow through cracks is appreciable and thus detrimental for concrete structures (Li 2003). It is widely acknowledged that cementitious materials have the capacity to heal by an autogenous healing process in crack of less than 50 μm (Li and Yang 2008). However, crack widths can easily exceed 100 μm limiting autogenous healing effectiveness and providing an easy access for harmful substances into the structure. For this reason, efforts to control and reduce crack size in concrete structures are of great importance to enhance structures durability.

Methods to control crack width in the field include steel reinforcement and different type of fibers. Yet, Shape Memory Alloys (SMAs) have recently been proposed as an alternative to control and reduce crack size in concrete structures (Kuang and Ou 2008; Song et al. 2006; Sun et al. 2013). SMAs possess two valuable properties, which can provide with a crack closing effect when utilized as reinforcement in concrete, which are the Shape Memory Effect (SME) and superelasticity. The SME consists in the capacity of SMAs to return to a predetermined shape upon heating while superelasticity refers to the ability of SMAs to undergo large amounts of inelastic deformation recovering its shape after unloading (Song et al. 2006). These two unique properties, which are the result of a reversible phase transformations phenomenon of SMAs crystalline atomic structure, open the possibility to provide with reinforced concrete structures able to close cracks by the physical action of SMAs to a size suitable for proper functioning of engineered self-healing techniques or even autogenous healing of concrete (Song et al. 2006).

In this study the combination of the self-closing effect of SMA and the chemical encapsulation engineered self-healing technique are tested together to obtain an enhanced healing effect of both strategies working synergically. The healing agent selected for this study is calcium nitrate due to its potential to react with available unhydrated cement particles that can be encountered in crack surfaces, contributing to the formation of new hydration products to potentially heal the crack. Furthermore, calcium nitrate may provide with additional calcium ions in the crack environment, which may promote the formation of calcium carbonate for crack closing. Moreover, calcium nitrate possesses corrosion inhibition properties, which may allow for enhanced corrosion performance of structures even when a crack is not completely healed.

Lastly, the low cost of calcium nitrate could potentially make it suitable for industrial application.

5.2 Objectives

The objective of this study was to assess the self-healing capability of SMA and steel reinforced mortar with embedded urea-formaldehyde microcapsules containing calcium nitrate. Microcapsules self-healing effect in combination with SMA self-closing action were evaluated through crack recovery assessment of damaged reinforced mortar beam specimens under wet and dry cycles. Furthermore, healing products in cracks were investigated by Environmental Scanning Electron Microscopy (ESEM) and Energy Dispersive Spectroscopy (EDS).

5.3 Background

Engineered self-healing techniques include chemical encapsulation, bacterial encapsulation, mineral admixtures, chemical in glass tubing and intrinsic self-healing by self-controlled tight crack width with engineered cementitious composites (Li et al. 2012). Chemical encapsulation for self-healing application in cementitious materials is a relatively recent approach which was first implemented by White et al. in polymer composites (White et al. 2001). Chemical encapsulation technique for self-healing consists in providing the cementitious matrix with uniformly distributed reservoirs of a healing agent which remain in a passive state until its action is required upon a cracking event. The healing agent then reacts with the cementitious matrix, moisture, air, heat, a catalyst or a combination of these precipitating healing products in the cracks (Tittelboom and Belie 2013). Healing agents that have been evaluated to date include sodium silicate, polyurethane, epoxy, cyanoacrylates and methylmethacrylate monomer (Gilford Iii et al. 2014; Li et al. 2013; Maes et al. 2014; Pelletier et al. 2010; Van Tittelboom et al. 2011; Yang et al. 2011). However, many of these chemicals are expensive and/or require a catalyst to function.

Autonomous healing of concrete through encapsulation of healing agents is a highly versatile technique. For instance, several types of healing agents may be encapsulated through this approach in a broad variety of sizes down to the nano-range (Li et al. 2012). Furthermore, chemical encapsulation technique has a potential for long shelf life of the healing mechanism (depending on capsule shell thickness and composition) as well as the capacity to provide concrete with self-healing properties independent from environmental conditions (depending on the healing agents utilized) (Li et al. 2012).

Proper functioning of self-healing concrete through the application of microencapsulated healing agents require of some conditions in the design of the capsules and the material for successful implementation. For example, uniform dispersion and adequate dosage of microcapsules are key elements for proper operation of the healing mechanism as this will guarantee sufficient healing agent at any location for self-healing to take place(Tittelboom and Belie 2013). Moreover, the interface between the microcapsule shell and the cementitious matrix is of particular interest. The bond strength between the microcapsule shell and the cementitious matrix needs to be higher than the strength of the microcapsule shell so that rupture of the capsule and subsequent healing agent release can be assured after a cracking event(Tittelboom and Belie 2013). Lastly, crack size is a greatly significant factor for successful self-healing of concrete through microencapsulation approach as it is expected that crack volumes greater than the available healing agent volume may not heal robustly (Tittelboom and Belie 2013).

5.4 Experimental Program

5.4.1 Materials and Specimens

The base mortar mix used in this study to produce the cement mortar beam specimens utilized a 0.40 water to cement ratio (w/c), graded sand with a maximum particle size of 4.76 mm, microcapsules, plasticizer, defoaming agent, and potable water. Detailed proportions of the mortar mix are shown in Table 5.1a.

Table 5.1 (a) Mortar Mix Proportions and (b) Prepared Specimens

(a)

Materials	**Proportions**
Sand	1510 Kg/m^3
Cement (Type I)	550 Kg/m^3
Water	220 Kg/m^3
Plasticizer	0.56% (by weight of cement)
Defoamer	0.10% (by weight of cement)
Water Cement Ratio (W/C)	0.40

(b)

Microcapsules Content (by weight of cement)	**Number of Specimens**
STEEL Reinforced	
0.5%	6
1.0%	6
2.0%	6
Control	6
SMA Reinforced	
0.5%	6
1.0%	6
2.0%	6
Control	6
TOTAL	**48**

Four different mortar mixes were produced at 0% (control), 0.5%, 1%, and 2% microcapsule content by weight of cement for SMA and steel reinforced specimens. Six beam specimens (40 mm x 40 mm x 160 mm) were cast at each microcapsule level for each reinforcement case. Reinforcement layout, shown in Figure 5.1 consisted of two 2-mm in diameter wires placed at one centimeter from the bottom and sides of the beam (spaced two

centimeter from each other). Specimens were de-molded after 24 h of casting, and cured for 28 days in a moist room (23 ± 2°C, > 95% Relative Humidity [RH]). Mixes and specimens prepared are presented in Table 5.1b.

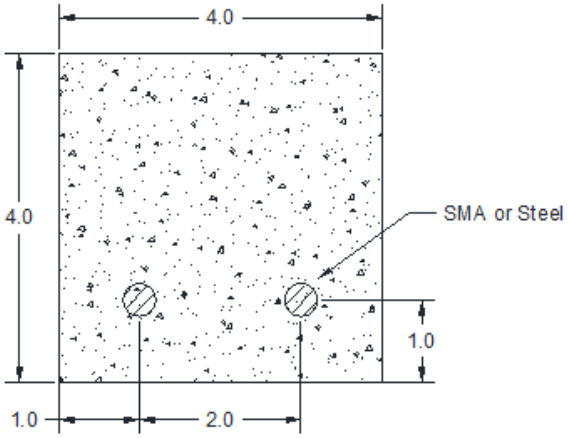

Figure 5.1. Reinforcement cross section layout (units are in cm)

5.4.2 Self-Healing Mortar Testing

Three-point bending test was conducted using a strain-controlled load application and was utilized to produce micro-cracks in beam specimens. To quantify healing of cracked specimens, light microscopy and UPV were used. Specimens were subjected to a total of 14 wet and dry cycles (healing period) under controlled environmental conditions and were observed and evaluated after 3, 7, and 14 cycles. Crack widths were measured at each stage of the healing process and Environmental Scanning Electron Microscopy (ESEM) with Energy Dispersive Spectroscopy (EDS) was employed to analyze and characterize the healing products encountered in the crack areas.

5.4.3 Ultrasonic Pulse Velocity Test (UPV)

Specimens were subjected to UPV testing in order to evaluate the evolution of the dynamic modulus of elasticity throughout the healing process. Specimens were examined right after completion of cycles 3, 7, and 14. Ten measurements were taken with the transducers placed at the opposite faces of the beams. A Proceq Pundit PL-200 ultrasonic testing apparatus equipped with 150 kHz transducers was utilized in the evaluation.

5.4.4 Environmental Conditioning for Self-Healing

Test specimens were exposed to wet and dry cycles to promote self-healing of cracks. Wet and dry cycles consisted of specimens being submerged into potable water for 24 hours at a temperature of 55 ± 5°C (this temperature was selected to guarantee the activation of the shape memory effect of the SMA reinforcement, which was 45°C) and then allow specimens to dry at room temperature for 24 hours.

5.4.5 Quantification and Characterization of Self-Healing Products

The formation of healing products were quantified by digital analysis of light microscopy images throughout the healing process. The width of each crack was measured right after cracking and after 3, 7 and 14 wet and dry cycles to quantify self-healing. A Zeiss SteREO Lumar V12 light microscope was utilized for acquisition of images. After completion of the healing process, one specimen of each type of mix (control, 0.5%, 1% and 2%) were cut with a diamond blade saw and directly analyzed under an ESEM equipped with Energy-Dispersive Spectroscopy to observe the morphology and investigate the chemical composition of the healing products. An atomic ratio plot was developed as part of the EDS micro-chemical analysis. The environmental scanning electron microscope utilized in this investigation was a FEI Quanta 3D Dual Beam SEM/FIB.

5.5 Results and Analysis

5.5.1 Flexural Testing and First-Crack Strength

Micro-cracks were successfully generated in mortar specimens by three-point bending test under strain control load application. Cracks ranging from 15 to 136 μm and 23 to 199 μm were induced in steel and SMA reinforced specimens, respectively. Yet, cracks evaluated in this study were limited to the range of 23 to 113 μm in size to provide with more uniformity in crack sizes and for reasonable comparison between steel and SMA reinforced specimens.

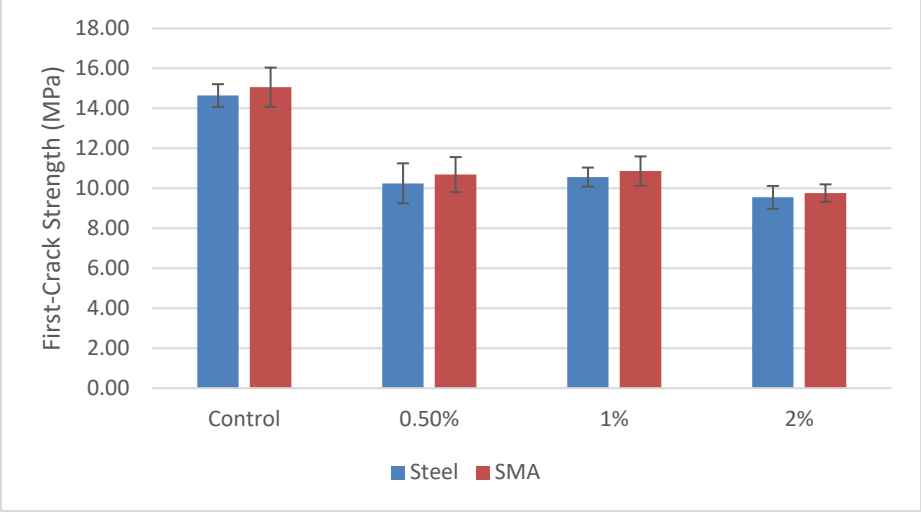

Figure 5.2. First-Crack Strength of Steel and SMA Reinforced (with and without Microcapsules)

The first-crack strength was assessed to gain insight on the effects of microcapsules on the mechanical properties of the materials. As shown in Figure 5.2, microcapsules produced a significant decrease in the first-crack strength of roughly 30% at 0.5% microcapsule content. However, further increase of microcapsule content of up to 2% did not significantly reduce the first-crack strength. This was demonstrated by performing an analysis of variances, which indicated a statistically significant difference between the means and a Tukey-Kramer HSD test demonstrating a significant difference between the control and 0.5%, 1%, and 2% microcapsule content. However, no statistically significant differences were found between 0.5%, 1% and 2% microcapsule content.

Table 5.2. Cracks Before and After Healing for Steel Reinforced Specimens

Control (Initial CW=44 µm)		
Before Healing	**7 Cycles**	**14 Cycles**
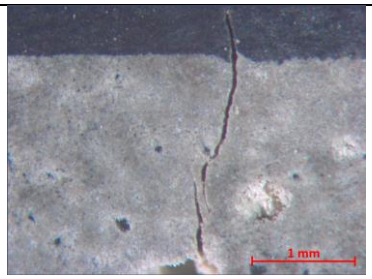	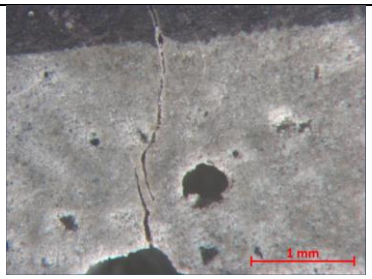	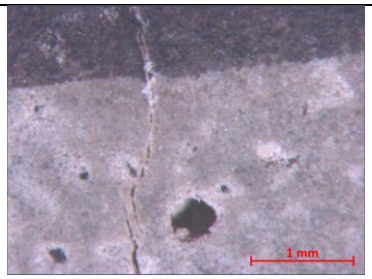
0.5% Microcapsule Content (Initial CW=31 µm)		
Before Healing	**7 Cycles**	**14 Cycles**
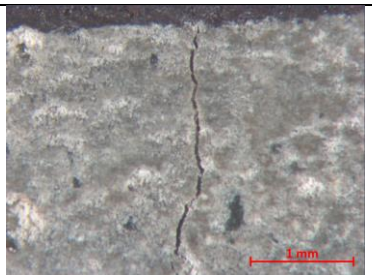	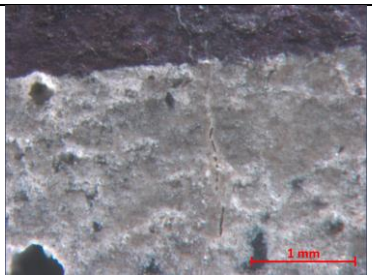	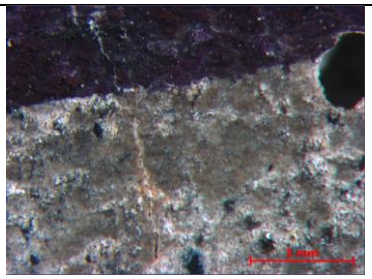
1% Microcapsule Content (Initial CW=59 µm)		
Before Healing	**7 Cycles**	**14 Cycles**
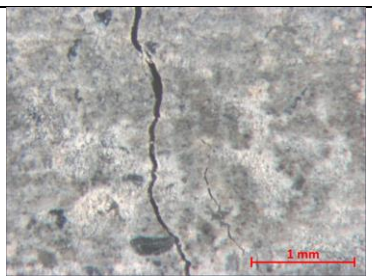	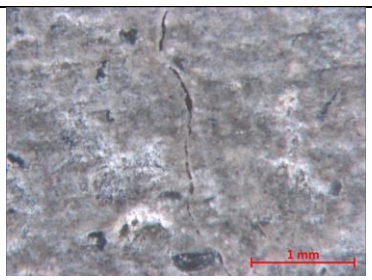	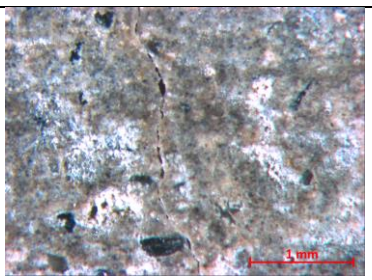
2% Microcapsule Content (Initial CW=32 µm)		
Before Healing	**7 Cycles**	**14 Cycles**
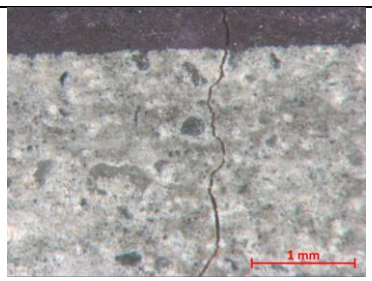	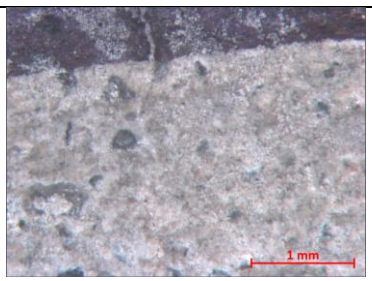	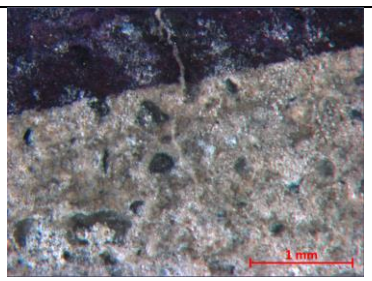

Table 5.3. Cracks Before and After Healing for SMA Reinforced Specimens

Control (Initial CW=47 µm)		
Before Healing	**7 Cycles**	**14 Cycles**
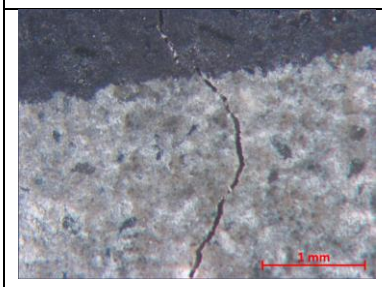	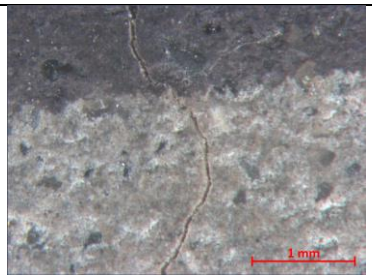	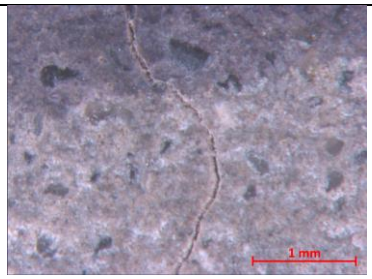
0.5% Microcapsule Content (Initial CW=45 µm)		
Before Healing	**7 Cycles**	**14 Cycles**
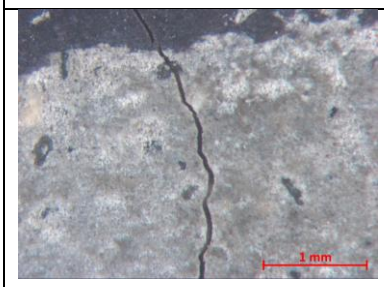	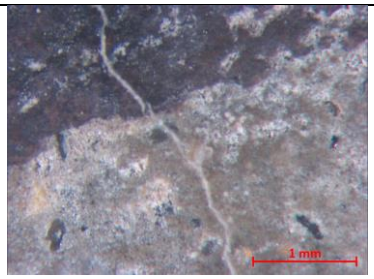	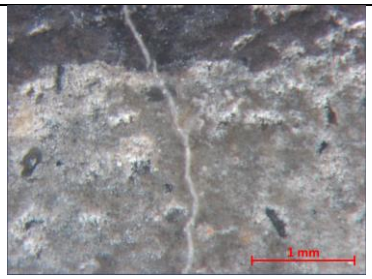
1% Microcapsule Content (Initial CW=58 µm)		
Before Healing	**7 Cycles**	**14 Cycles**
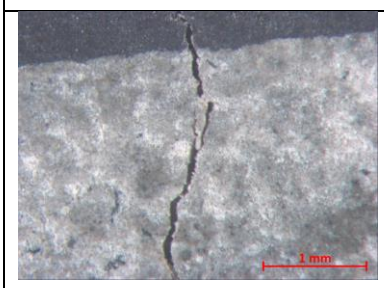	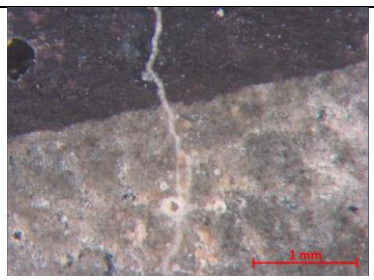	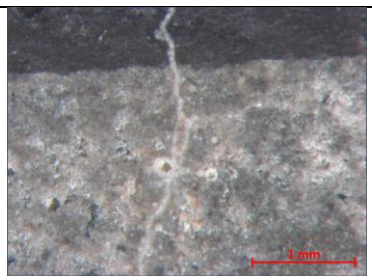
2% Microcapsule Content (Initial CW=37 µm)		
Before Healing	**7 Cycles**	**14 Cycles**
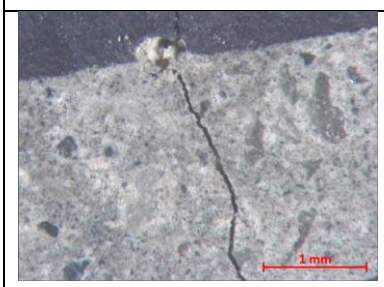		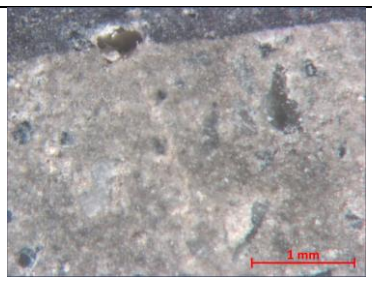

5.5.2 Healing Quantification

After completing the healing period (14 wet and dry cycles), digital analysis of the light microscopy images was performed in order to quantify healing after 3, 7 and 14 wet and dry cycles. Tables 5.2 and 5.3 present images of cracks before and after healing for steel and SMA reinforced specimens, respectively.

The quantification of healing was performed by comparing the size of the cracks at different stages of healing with the initial crack width (immediately after cracking) to obtain the healing efficiency as described by the following equation:

$$H_e = \left(1 - \frac{CW_t}{CW_0}\right) x\ 100 \qquad (1)$$

where,

H_e = Healing efficiency (%);
CW_0 = initial crack width; and
CW_t = crack width at the time of analysis.

Normalized healing efficiencies of steel and SMA reinforced specimens are presented in Figure 5.3. The healing efficiency was normalized to an equivalent 50 µm crack according to the following equation:

$$NH_e = \left(\frac{H_e}{50\ \mu m}\right) x\ CW_0 \qquad (2)$$

where,

NH_e = Normalized Healing efficiency (%);
H_e = Healing efficiency (%); and
CW_0 = initial crack width.

In steel reinforced specimens, 1% microcapsule content produced the best healing results at all stages of healing with a normalized healing efficiency of 32.2%, 32.8% and 33.2% after 3, 7 and 14 wet and dry cycles, respectively. Moreover, after 3 and 7 wet and dry cycles, the trend was the same with 0.5% microcapsule content being the second best healing performance, 2% microcapsule content the third and control the least performing group. On the other hand, after 14 wet and dry cycles, control, 0.5% and 1% microcapsule content groups exhibited a very similar healing efficiency while 2% microcapsule content performed worst. Analysis of variances (ANOVA) were performed on the normalized healing efficiency for steel reinforced specimens at every stage of the healing period, which found statistical significant difference between the means at 3 wet and dry cycles. Moreover, a comparison of all group pairs at 3 wet and dry cycles was conducted using a Tukey-Kramer HSD test showing statistically significant differences between Control and 1% microcapsule content as well as between 1% and 2% microcapsule content. Furthermore, an individual tailed t-Test was performed at 7 wet and dry

cycles obtaining a statically significant difference between normalized healing efficiency of 1% microcapsule content and control specimens.

The normalized healing efficiency of SMA-reinforced specimens exhibited the same trend after 3 and 7 wet and dry cycles with 1% microcapsule content being the best case, 2% the second best, 0.5% the third best, and control being the worst. Furthermore, similarly to the steel reinforced specimens 1% microcapsule content specimens performed better at every stage of the healing process exhibiting a 49.1%, 61.1% and 65.8% healing efficiency after 3, 7, and 14 wet and dry cycles respectively. Analysis of variances were conducted for SMA-reinforced specimens at every stage of healing. Yet, statistical significant differences between the means were not found possibly due to the large variability inherent of the healing process, which limited the ability of the statistical test to provide a difference at a 95% confidence level. Individual tailed t-test were performed comparing the best and worst healing performance cases at every stage of the healing process (1% to control in all cases). In this case, statistically-significant differences were found between 1% and control at all stages of healing.

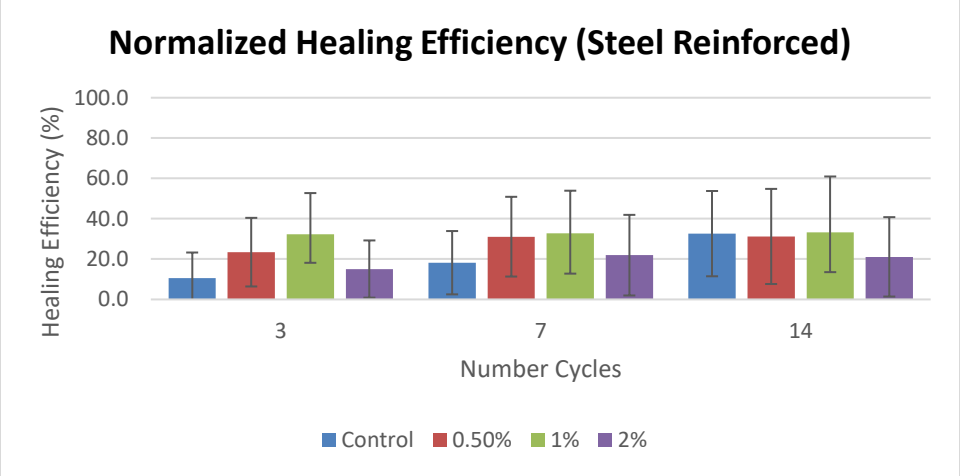

(a)

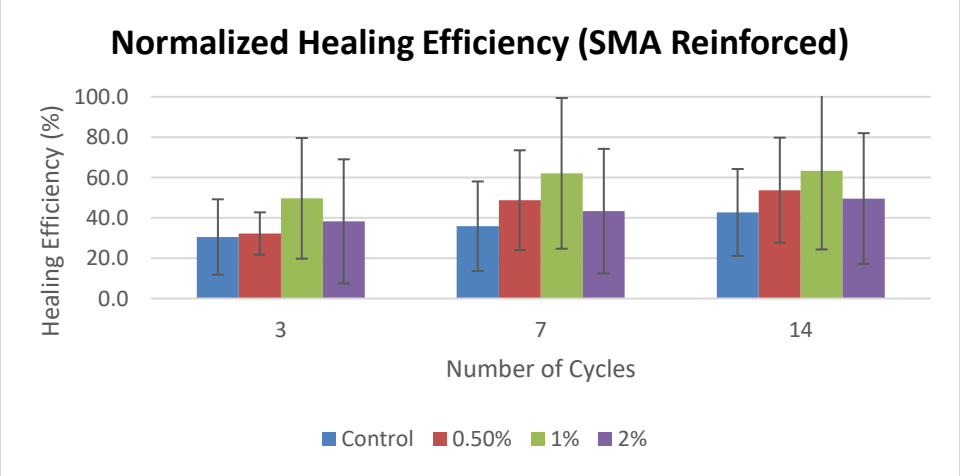

(b)

Figure 5.3. Normalized Healing Efficiency for (a) Steel Reinforced specimens (b) SMA Reinforced specimens

It is important to emphasize that while similar trends in healing efficiencies occur in steel and SMA reinforced specimens, SMA reinforced specimens had a noticeably higher (more than double in some cases) healing efficiency at all stages of healing for all cases, thus demonstrating the positive impact of SMA reinforcement in the healing of cracks. Furthermore, it is also important to notice that microcapsules have a clear tendency to enhance healing as healing efficiencies of specimens with microcapsule were greater than specimens without microcapsules (control) at all stages of healing for SMA and steel reinforced specimens (with the exception of 0.5% and 2% microcapsule content after 14 wet and dry cycles for steel reinforced specimens).

5.5.3 Ultrasonic Pulse Velocity

To further assess the healing efficiency of the cracks, UPV was measured throughout the healing process of all the specimens. UPV recovery was obtained by contrasting UPV measurements with the measurement right after cracking. UPV recovery was computed according to the following equation:

$$R_e = \left(\frac{UPV_t}{UPV_{Day0}} - 1\right) x\ 100 \quad (3)$$

where,

R_e = UPV recovery efficiency (%);
UPV_t = UPV at time of the analysis; and
UPV_{Day0} = UPV at Day 0.

UPV recovery on steel reinforced specimens displayed a similar tendency after 3, 7 and 14 wet and dry cycles. At all stages of healing, the 1% microcapsule content group had the best UPV recovery followed by 0.5% and 2% as shown in Figure 4. At all stages of healing, the control had the lowest UPV recovery.

On SMA reinforced specimens, small differences in UPV were observed after 3 and 7 wet and dry cycles. Yet, the 2% microcapsule content and the control displayed the best and second best recovery, respectively. On the other hand, after 14 cycles, a change in trend was observed with control having the best UPV recovery. However, no statistically-significant differences between the groups were observed after conducting the ANOVA. Furthermore, a tailed t-test also failed to identify statistical-significant differences between the control (best performing) and the 2% microcapsule content (second best performing) after 14 wet and dry cycles.

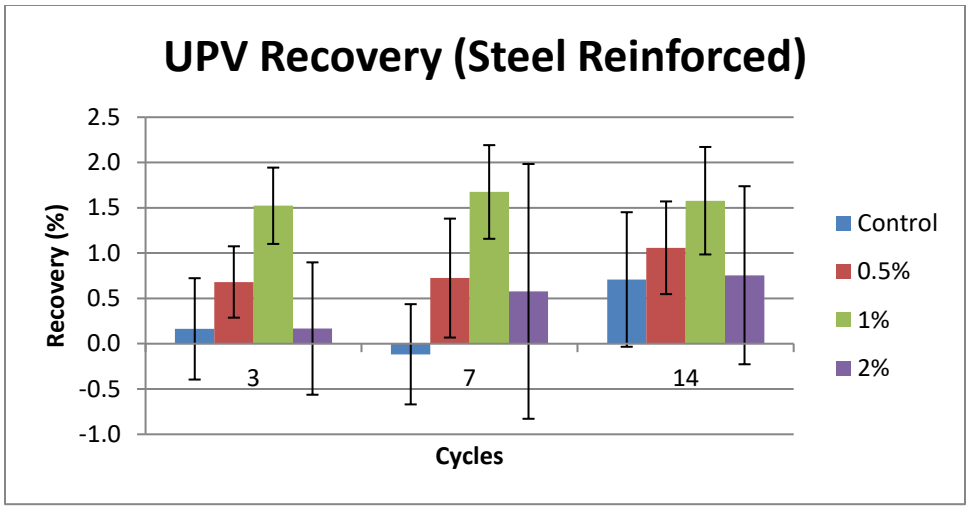

(a)

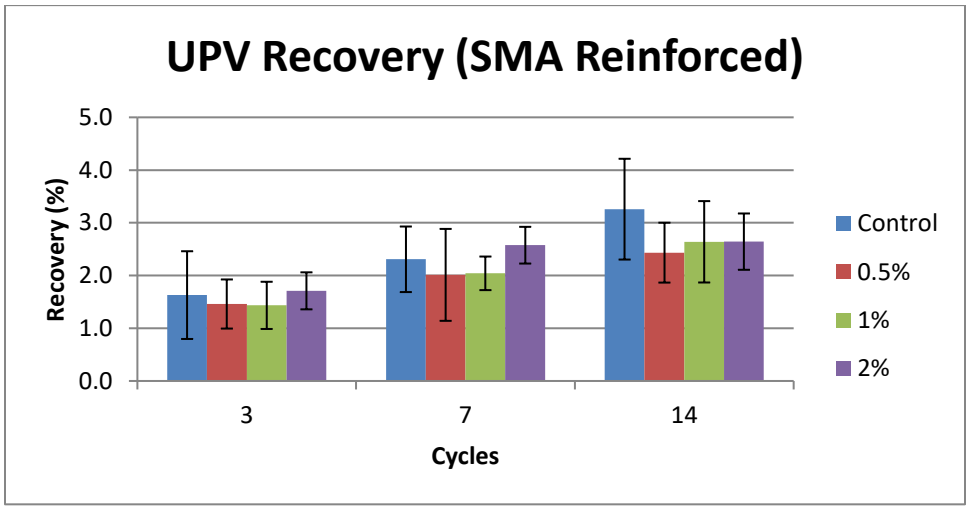

(b)

Figure 5.4. SMA Reinforced Specimens UPV Recovery Efficiency (a) Steel Reinforced Specimens (b) SMA Reinforced specimens

As it was the case with healing efficiency by crack image analysis, UPV recovery was notoriously influenced by the type of reinforcement utilized. SMA reinforcement had clearly a positive impact on UPV recovery at all stages of healing and all tested groups as it did on healing efficiency in crack image analysis.

5.5.4 Healing Products Characterization

Upon completion of the healing process, one specimen of each type of mix design (control, 0.5%, 1% and 2%) was cut with a diamond blade saw to extract a small section of the beam containing the healed crack for direct analysis under ESEM-EDS. Healing products in cracks were investigated and back scatter electron (BSE) images were collected. Figure 5.5 show BSE images of healing products in cracks. During the analysis, the main type of morphology observed was crystal-like similar to calcite ($CaCO_3$) crystals. Furthermore, gel-like healing products were rarely encountered.

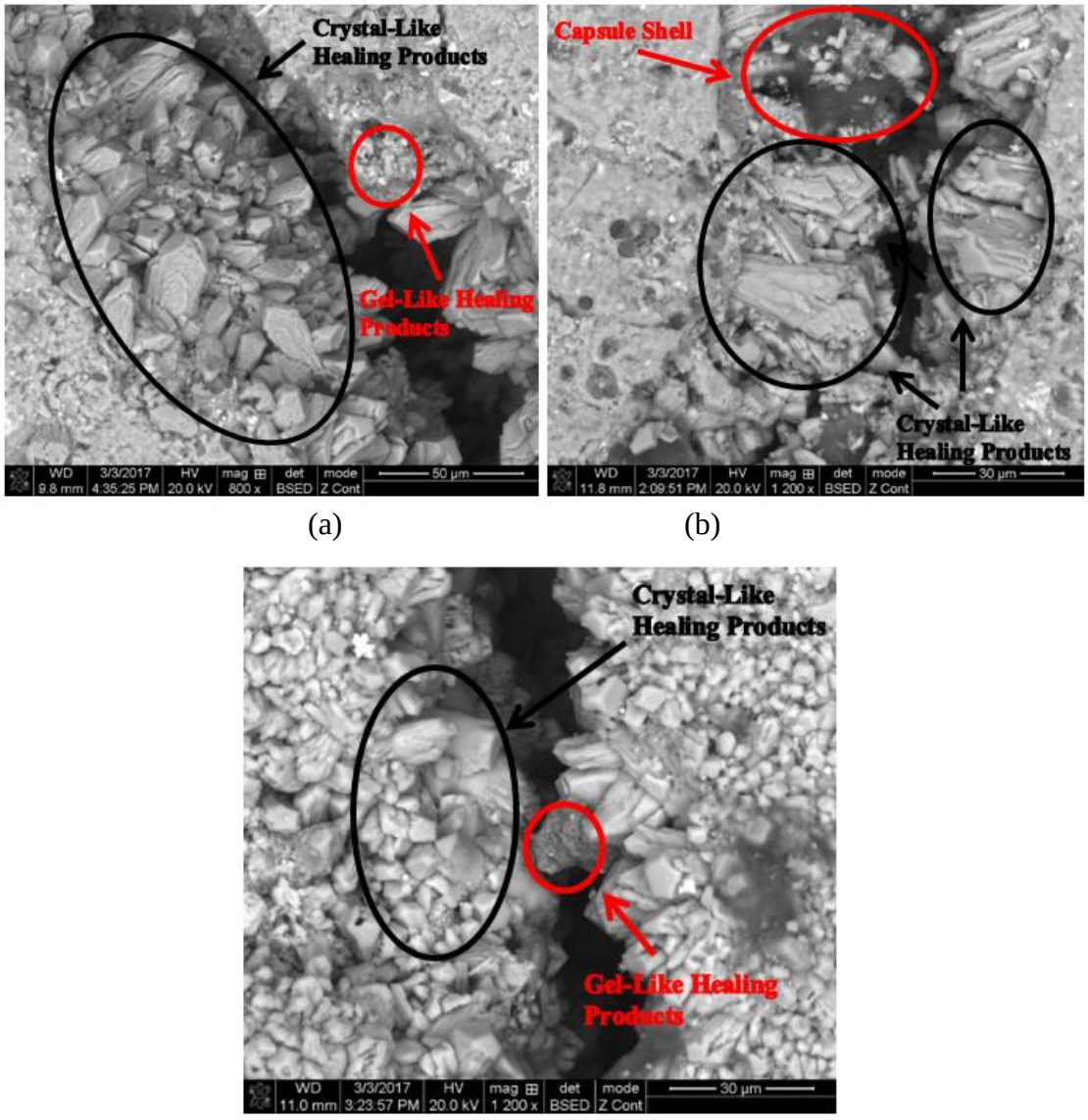

(a) (b)

(c)

Figure 5.5. Healing Products in Cracks (a) Control Specimen (b) 1% Microcapsule Content SMA Reinforced Specimen (c) 2% Microcapsule Content SMA Reinforced Specimen

EDS (Energy Dispersive Spectroscopy) spectrums were collected at different places in cracks where healing products were encountered utilizing the spot spectrum option of the ESEM-EDS equipment. Roughly160 spot spectrums were collected and plotted utilizing Al/Ca and Si/Ca atomic ratios from the spectrum data. Figure 5.6 presents the Al/Ca vs. Si/Ca atomic ratio plot developed. In the plot, there is a clear tendency for points to cluster in the origin, which is indicative of a significant presence of either calcium hydroxide (CH) or calcium carbonate ($CaCO_3$). Pure calcium carbonate or calcium hydroxide would ideally plot at the origin due to the lack of Al and Si in its chemical composition (Winter 2012). However, contributions of X-rays emitted by nearby features (due to excitation volume phenomena) in the cementitious matrix produces some distancing of these points to the origin (Winter 2012). Moreover, it is important

to notice that significant amounts of carbon were present in almost all spectrums collected providing evidence that the nature of the majority of healing products were that of calcium carbonate in the form of calcite crystals.

A region, which is approximately between 0.45 to 0.55 Si/Ca and 0.04 to 0.08 Al/Ca, is indicative of CSH gel of pure cement pastes (clinker and gypsum) (Winter 2012). Furthermore, the zone in between the pure CSH region and the origin is labeled as the region where contribution from calcium rich crystals and CSH features is encountered; the closer a point is to any of these regions the more likely it is that a larger portion of the analyzed volume is of this materials chemical nature (Winter 2012). Even though no point did directly plot on the CSH region, a couple of points were encountered in the combined region. Yet, the tendency was for points to be closer to the origin than to pure CSH region providing evidence of a limited quantity of CSH in the healing products.

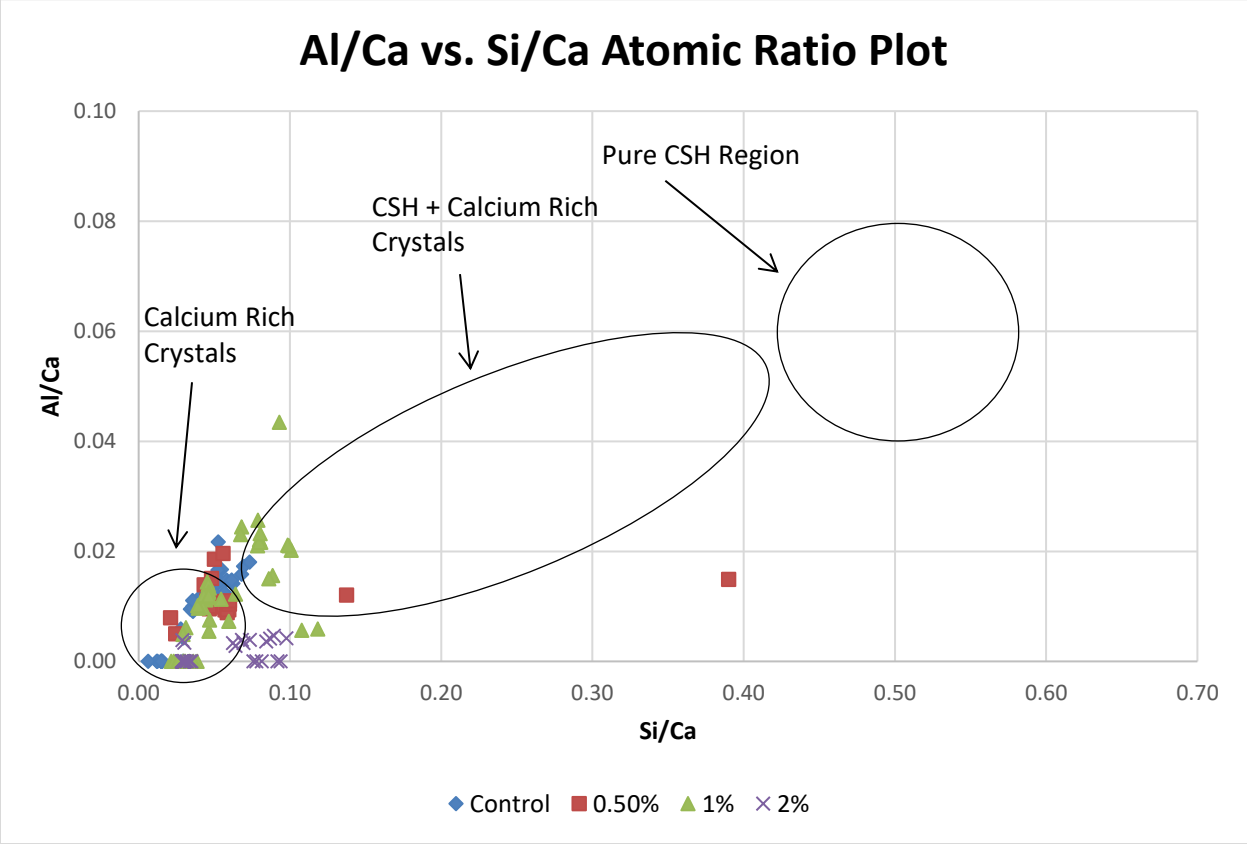

Figure 5.6. Al/Ca vs. Si/Ca Atomic Ratio Plot

5.6 Conclusions

After the experimental evaluation of self-healing performance of steel and SMA reinforced mortar with calcium nitrate microcapsules under wet and dry cycles, the following conclusions may be drawn:

- Specimens with 1% microcapsule content produced the best healing efficiency by digital image analysis at all stages of healing (after 3,7 and 14 cycles) for steel (statistically

significant at 3 and 7 cycles) and SMA (statistically significant at 3, 7 and 14 cycles) reinforced specimens. Moreover, except for steel reinforced specimens after 14 wet and dry cycles, specimens containing any dosage microcapsules produced a better healing efficiency than control at all stages of healing for steel and SMA reinforced specimen.

- Specimens with microcapsules produced the best UPV recovery for all stages of healing in steel reinforced samples. Also, specimens with 1% microcapsule content exhibited the best UPV recovery after 3, 7 and 14 wet and dry cycles for steel reinforced samples. Moreover, specimens with 2% microcapsule content on SMA reinforced specimens yielded the best UPV recovery after 3 and 7 wet and dry cycles. However, at 14 cycles control had the best UPV recovery performance, yet not statistically significant.

- Healing efficiency by digital image analysis as well as UPV recovery were notoriously influenced by the type of reinforcement utilized. SMA reinforcement had a large and positive impact on healing efficiency and UPV recovery at all stages of healing for all microcapsule containing specimens and control.

- Experimental evidence suggests that the overwhelming majority of healing products encountered in cracks are likely calcium carbonate in the form of calcite crystals. Furthermore, limited amounts of CSH gel-like healing products were also identified.

5.7 Acknowledgements

The authors would like to acknowledge the financial support through a grant from Qatar National Research Foundation (QNRF)/ National Priorities Research Program (NPRP) as well as the laboratory support from Louisiana Transportation Research Center (LTRC).

5.8 References

Gilford Iii, J., Hassan, M. M., Rupnow, T., Barbato, M., Okeil, A., Asadi, S., Gilford, J., Hassan, M. M., Rupnow, T., Barbato, M., Okeil, A., and Asadi, S. (2014). "Dicyclopentadiene and sodium silicate microencapsulation for self-healing of concrete." *Journal of Materials in Civil Engineering*, 26(5), 886–896.

Kuang, Y., and Ou, J. (2008). "Self-repairing performance of concrete beams strengthened using superelastic SMA wires in combination with adhesives released from hollow fibers." *Smart Materials and Structures*, IOP Publishing, 17(2), 25020.

Li, V. C. (2003). "On engineered cementitious composites (ECC). A review of the material and its applications." *Journal of Advanced Concrete Technology*, 1(3), 215–230.

Li, V. C., Herbert, E., Senot, S., Schlangen, E., Li, V. C., and Herbert, E. (2012). "Robust Self-Healing Concrete for Sustainable Infrastructure Robust Self-Healing Concrete for Sustainable Infrastructure." 10, 207–218.

Li, V., and Yang, E.-H. (2008). "Self Healing in Concrete Materials." *Self Healing Materials SE - 8*, 100, 161–193.

Li, W., Jiang, Z., Yang, Z., Zhao, N., and Yuan, W. (2013). "Self-healing efficiency of cementitious materials containing microcapsules filled with healing adhesive: Mechanical restoration and healing process monitored by water absorption." *PLoS ONE*, 8(11), 1–18.

Maes, M., Van Tittelboom, K., and De Belie, N. (2014). “The efficiency of self-healing cementitious materials by means of encapsulated polyurethane in chloride containing environments.” *Construction and Building Materials*, Elsevier, 71, 528–537.

Pelletier, M. M., Brown, R., Shukla, A., and Bose, A. (2010). “Self-healing concrete with a microencapsulated healing agent.” *University of Rhode Island, Kingston,USA*, (C).

Song, G., Ma, N., and Li, H. N. (2006). “Applications of shape memory alloys in civil structures.” *Engineering Structures*, 28(9), 1266–1274.

Sun, L., Liang, D., Gao, Q., and Zhou, J. (2013). “Analysis on factors affecting the self-repair capability of SMA wire concrete beam.” *Mathematical Problems in Engineering*, 2013.

Tittelboom, K. Van, and Belie, N. De. (2013). *Self-Healing in Cementitious Materials—A Review*.

Van Tittelboom, K., De Belie, N., Van Loo, D., and Jacobs, P. (2011). “Self-healing efficiency of cementitious materials containing tubular capsules filled with healing agent.” *Cement and Concrete Composites*, Elsevier Ltd, 33(4), 497–505.

White, S. R., Sottos, N. R., Geubelle, P. H., Moore, J. S., Kessler, M. R., Sriram, S. R., Brown, E. N., and Viswanathan, S. (2001). “Autonomic healing of polymer composites.” *Nature*, 409(6822), 794–797.

Winter, N. B. (2012). *Scanning Electron Microscopy of Cement and Concrete*. WHD Microanalysis Consultants Ltd., Rendlesham, Woodbridge, UK.

Yang, Z., Hollar, J., He, X., and Shi, X. (2011). “A self-healing cementitious composite using oil core/silica gel shell microcapsules.” *Cement and Concrete Composites*, 33(4), 506–512.

CHAPTER 6

SUMMARY AND CONCLUSIONS

The main goal of this study was to investigate the self-healing mechanism of unreinforced and reinforced mortar specimens with calcium nitrate microcapsules by means of the following objectives:

- Measure short term healing efficiency of unreinforced and reinforced mortar specimens with calcium nitrate microcapsules.
- Characterize healing products of unreinforced and reinforced mortar specimens with calcium nitrate microcapsules.
- Quantify technology limitations of unreinforced and reinforced mortar specimens with calcium nitrate microcapsules.
  a) Evaluate crack size effect on self-healing efficiency.
  b) Evaluate environmental conditions effect on self-healing (wet and dry conditions).
  c) Evaluate microcapsule dosage effect on self-healing efficiency.

To accomplish this goal, short term healing efficiency (up to 28 days) was evaluated for unreinforced and reinforced (steel and SMA) mortar specimens with embedded urea-formaldehyde microcapsules containing calcium nitrate as healing agent (at different dosages). Assessment of healing under dry conditions as well as water submerged conditions for unreinforced specimens was performed by digital analysis of light microscopy images of cracks. Furthermore, healing evaluation of reinforced specimens was completed under water submerged conditions as well as under wet and dry cycles by digital analysis of light microscopy images of cracks and UPV recovery. Moreover, after completion of the healing process, reinforced specimens were re-tested by three-point bending, yet, no significant recovery of first cracking strength was observed. Finally, healing products were investigated under ESEM-EDS for determination of its chemical nature.

6.1 Short Term Healing Efficiency

6.1.1 Healing under Dry and Water Submerged Conditions (Unreinforced Specimens)

Improvement in healing efficiency by digital image analysis for unreinforced specimens with microcapsules was reported at 14 days of healing for 0.85% and 1% microcapsule content. Yet, the improvement was minor. Moreover, specimens under dry healing conditions did not exhibit any appreciable healing after completion of the healing process confirming the need of an external source of moisture for proper functioning of the healing mechanism.

6.1.2 Healing under Water Submerged Conditions (Reinforced Specimens)

For steel reinforced specimens with microcapsules under water submerged conditions, healing efficiency improved significantly with the increase in microcapsule content at all stages of healing. This improvement in self-healing performance of steel reinforced specimens with microcapsules as compared to unreinforced specimens with microcapsules can be attributed to the lower water to cement ratio used in reinforced specimens (0.40 in reinforced specimens compared to 0.48 in unreinforced) as well as on the improvement of the microcapsule preparation procedure for the capsules utilized in reinforced mortar specimens. Moreover, SMA

reinforced specimens under water submerged conditions performed better than steel reinforced specimens at 3 days of the healing process for all cases (control, 0.5%, 1% and 2%) likely due to the immediate self-closing action of SMA reinforcement which favored early healing.

As for the UPV recovery, SMA reinforced specimens with and without microcapsules were superior at all stages of healing compared to steel reinforced specimens. Also, SMA reinforced specimens with embedded microcapsules presented an improvement in UPV recovery compared to control at all stages of healing. The best UPV recovery performance for steel reinforced specimens occurred at 1 % microcapsule content for all stages of healing. Furthermore, the best performing case for SMA reinforcement was at 1% microcapsule content at 7 and 14 days of healing and 2% microcapsule content at 3 days of healing.

6.1.3 Healing under Wet and Dry Cycles (Reinforced Specimens)

Reinforced specimens under wet and dry cycles with 1% microcapsule content produced the best healing efficiency by digital image analysis at all stages of healing (3, 7 and 14 cycles) for steel and SMA reinforced specimens. Furthermore, except for steel reinforced specimens after 14 wet and dry cycles, all specimens with embedded microcapsules produced a better healing efficiency than control at all stages of healing for steel and SMA reinforced specimens.

As for UPV, specimens with microcapsules produced the best UPV recovery for all stages of healing in steel reinforced specimens with 1% being the best performing case. Moreover, in SMA reinforced specimens, 2% microcapsule content produced the best UPV recovery after 3 and 7 wet and dry cycles. However, at 14 cycles control yielded the best UPV recovery, yet not statistically significant. It is important to notice that SMA reinforcement had a large positive impact on healing efficiency and UPV recovery at all stages of healing for all specimen types demonstrating a strong capability of SMA reinforcement to help in the healing process of cracks.

6.2 Characterization of Healing Products

After completion of the healing process on all experiments, specimens were cut and small sections of the beams containing healed cracks were extracted for direct exploration under ESEM-EDS. EDS microchemical analysis as well as morphology exploration of the healing products was performed. Results were presented in the form of atomic ratio plots as well as EDS maps. In all cases the overwhelming majority of healing products encountered in cracks exhibited a crystal-like morphology and were determined to be likely calcium carbonate in the form of calcite crystals. Furthermore, limited amounts of gel-like healing products were also encountered in cracks and its chemical nature was likely that of CSH.

6.3 Technology Limitations

6.3.1 Crack Size

Crack sizes ranging from 13 to 387 μm were analyzed throughout the different experiments performed on this study. It was noticeable that crack size had a significant effect on healing efficiency. Usually, larger cracks produced incomplete healing after the completion of the healing process while smaller cracks were able to heal more robustly. Under wet and dry cycles healing conditions, the larger crack size able to heal completely was a 58 μm crack (SMA reinforced specimen with 1% microcapsule content) after 14 wet and dry cycles. However, a 108 μm crack (SMA reinforced specimen with 2% microcapsule content) was able to heal up to 91%

after 14 wet and dry cycles. Furthermore, the largest crack size that was able to heal completely after 7 days of water submerged healing conditions was a 43 μm crack (steel reinforced specimen with 1% microcapsule content). Yet, a 84 μm crack (steel reinforced specimen with 2% microcapsule content) was able to heal up to an 83% after 7 days under water submerged conditions.

6.3.2 Environmental Conditions and Microcapsule Dosage

Self-healing capacity of reinforced and unreinforced mortar specimens with different contents of embedded microcapsules were tested at different environmental conditions (dry conditions, water submerged conditions and wet and dry cycles) to gain insight on the dependence of the self-healing mechanism to environmental conditions and capsule dosage. After evaluation, it was determined that dry conditions did not produced any appreciable healing, thus confirming the need for an external source of moisture for the healing mechanism to work properly. Furthermore, water submerged conditions produced the best healing results in contrast to wet and dry cycles. For instance, the best average normalized healing efficiency reported after 14 wet and dry cycles for steel and SMA reinforced specimens yielded 33.2% (at 1% microcapsule content) and 63.0% (at 1% microcapsule content) respectively. Yet, the best average normalized healing efficiency reported after just 7 days under water submerged healing conditions for steel and SMA reinforced specimens yielded 80.8% (at 2% microcapsule content) and 52.4% (at 1% microcapsule content) respectively. In the same fashion, the best average UPV recovery after 14 wet and dry cycles for steel and SMA reinforced specimens exhibited 1.67% (at 1% microcapsule content) and 3.26% (at control) respectively. Meanwhile, the best average UPV recovery after 14 days under water submerged conditions for steel and SMA reinforced specimens yielded 3.2% (at 1% microcapsule content) and 5.8% (at 1% microcapsule content) respectively.

6.4 Future Work

Results from this study offer several opportunities for future research. Topics for future work include:

- Evaluation of Engineered Cementitious Composites (ECC) with embedded self-healing microcapsules.
- Evaluation of SMA reinforced Engineered Cementitious Composites (ECC) with SMA with embedded self-healing microcapsules.
- Investigation of corrosion inhibition potential of cementitious materials embedded with urea-formaldehyde microcapsules containing calcium nitrate.
- Evaluation of alternative healing agents for stronger healing product generation in cracks (stronger than cementitious matrix).
- Mechanisms for better microcapsules dispersion in the cementitious matrix.
- Life Cycle Assessment (LCA) of microcapsule self-healing technology on concrete materials.

- Life Cycle Cost Assessment (LCCA) of microcapsule self-healing technology on concrete materials.

- The effect of nano-size capsules in self-healing efficiency of cementitious materials.

- The effects of different types of fibers on self-healing properties of cementitious materials embedded with self-healing microcapsules.

APPENDIX A
COPYRIGHT PERMISSION

VITA

Gabriel Arce was born and raised in Guayaquil, Ecuador. In 2013, he completed his Bachelor of Science in Civil and Environmental Engineering from the University of New Orleans. After graduation, Gabriel worked eight months for HOHESA, a ready mix concrete company in Guayaquil. In HOHESA he worked as concrete materials engineer in the quality control department. Later, in August of 2014 he joined Louisiana State University to pursue his Master of Science degree in Construction Management and his PhD in Engineering Sciences. Gabriel's interests include concrete materials, self-healing concrete, Engineered Cementitious Composites (ECC) and nanotechnology in construction materials.